Interactions between remodeling, architecture and tissue properties in cancellous bone.

Wisselwerkingen tussen remodelering, architectuur
en weefseleigenschappen in trabeculair bot.

Proefschrift

ter verkrijging van de graad van doctor aan
de Erasmus Universiteit Rotterdam
op gezag van de
Rector Magnificus

Prof.dr.ir. J.H. van Bemmel

en volgens besluit van het college voor promoties.

De openbare verdediging zal plaatsvinden op

woensdag 8 januari 2003 om 13.45 uur

door

Jacoba Catharina van der Linden

geboren te Vlaardingen

Promotie commissie

Promotor:	Prof.dr. J.A.N. Verhaar
Overige leden:	Prof.dr. H.A.P. Pols
	Prof.dr.ir. N. Bom
	Dr. P. Lips
	Prof.dr.ir. F. van Keulen
	Prof.dr.ir. R. Huiskes
	Prof.dr. G.P. Krestin
Copromotor:	Dr.ir. H. Weinans

Printed by Ponsen & Looijen bv, Wageningen, The Netherlands
ISBN 90-9016259-3

The Research in this thesis was supported by Zon MW (grant 90236082)
The printing of this thesis was financially supported by
Stichting Anna-fonds te Leiden
Nederlandse Orthopaedische Vereniging

Contents

Chapter 1

Introduction

The skeleton enables the body to maintain its outer shape, it protects vulnerable organs like the heart and lungs and the long bones act as lever arms for the muscle forces. Furthermore, it serves as a reservoir of minerals. The skeleton consists of two types of bone: compact bone, which forms the outer shell of the bones (the cortex) and cancellous bone, a very porous bone structure made of mineralized plates and struts. Cancellous bone is found in the ends of the long bones, where it serves to transfer external forces from the bone surface in the joints to the cortex. This cancellous bone gives the bones a relatively low mass and a high stiffness. The architecture of the long bones is illustrated in figure 1.1, which shows the cortex surrounding the cancellous bone in a slice of a human femur. Cancellous bone is also found in the spine, in flat bones like the skull and the pelvis and in the hand and feet.

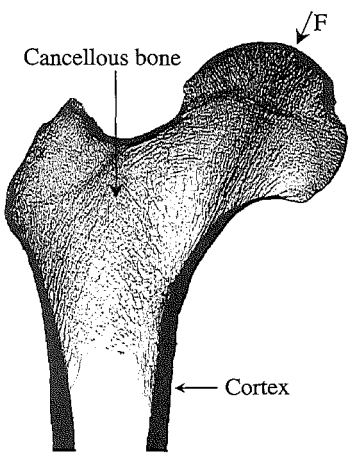

Figure 1.1: Slice of a human femur showing the cortex, the cancellous bone and the main load bearing direction (arrow in upper right corner) (Courtesy of Chris Jacobs, Stanford University.)

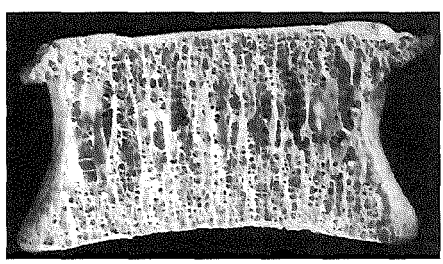

Figure 1.2: slice of a human vertebra, showing the alignment of the trabeculae in the vertical direction.

The architecture of the adult skeleton results from constant adaptation to the external forces applied to the skeleton. This is particularly clear in the cancellous bone. Most trabeculae (the plates and struts in the cancellous bone) are aligned to the main load bearing direction. These aligned trabeculae are supported by transversal trabeculae which are oriented in the plane perpendicular to the main load bearing direction. Together, these two types of trabeculae form a strong cancellous bone network with a low weight. The alignment of the trabeculae can be seen in the femur in figure 1.1 and the vertebra in figure 1.2. In the femoral head, trabeculae can be seen which transfer the forces applied to the femoral head to the cortex, in the vertebra most trabeculae are aligned vertically, in the main load bearing direction. More than a century ago, this alignment of trabeculae was already

observed by Roux [149] and Wolff [183]. Nowadays, the statement that the bone architecture adapts to external loads is generally known as Wolff's law [183].

In the cortex 95% of the volume is occupied by mineralized bone tissue, in cancellous bone the bone volume fraction is only 5% to 40%. Cortical bone accounts for approximately 80% of the weight of the skeleton, cancellous bone for the other 20% [124]. Bone tissue consists of organic and anorganic components. The anorganic component accounts for 65% of the dry weight of bone tissue and consists of calcium and hydroxide deficient hydroxyapatite. Besides this, numerous impurities are found in these crystals, such as carbonate, magnesium, potassium, fluoride, phosphate and citrate. Of the organic components, approximately 90% is formed by collagen, the other 10% consists of noncollagenous proteins, vascular elements and cells [14]. The collagen provides a high tensile strength, the mineral crystals give the bone tissue a high compression stiffness.

The skeleton can withstand forces higher than the forces that act on the skeleton during normal daily loading. By comparing the strains that occur in bone in vivo to the failure strain of cortical bone, the safety factor of bone to yield was calculated to be between 1.4 and 4.1 [6]. However, even the normal daily loads cause some damage in the bone tissue [5, 21]. This microdamage consists of small cracks in the bone tissue, which are far too small to cause failure of a whole bone or even a single trabecula. To prevent these cracks from growing and coalescing into bigger cracks, the damaged tissue must be replaced by new tissue. The replacement of the damaged tissue is performed by bone multicellular units (BMU's) in the so-called bone remodeling process. These BMU's consist of bone resorbing cells, osteoclasts, and bone building cells, osteoblasts [53].

In cancellous bone, the osteoclasts make resorption cavities in the surface of the trabeculae, as illustrated in figure 1.3. This bone resorption takes 3-6 weeks. After a resting period of approximately 9 days the osteoblasts refill the cavity with collagenous tissue, called osteoid. This tissue formation process takes 2-4 months [124, 125, 56]. Some days after formation of the collagenous tissue, the mineralization of this tissue starts. In the first two weeks, approximately 70% of the mineralization process is completed. After this initial fast mineralization, the growth of the mineral crystals continues slowly over the following years [64, 129]. In the cortex, osteoclasts dig tunnels in the longitudinal direction, which are filled by osteoblasts, as illustrated in figure 1.4.

During bone formation, some osteoblasts stay behind and are embedded in the bone matrix. These cells differentiate to osteocytes, which form a highly connected network in the bone tissue (see Fig.1.5). Because of their location in the tissue, their connection to other osteocytes and to bone lining cells on the surface, the osteocytes are assumed to play an important role in the maintenance process of the skeleton [114]. It is often hypothesized that osteocytes can detect stresses, strains and damage in the tissue. The network would enable the osteocytes to send signals to the bone surface to start bone remodeling.

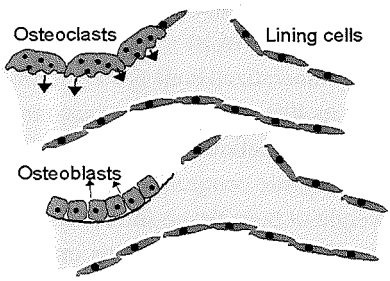

Figure 1.3: Schematical representation of bone remodeling in cancellous bone.

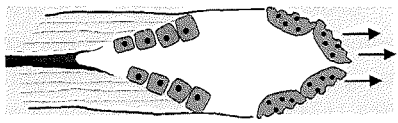

Figure 1.4: Schematical representation of bone remodeling in cortical bone.

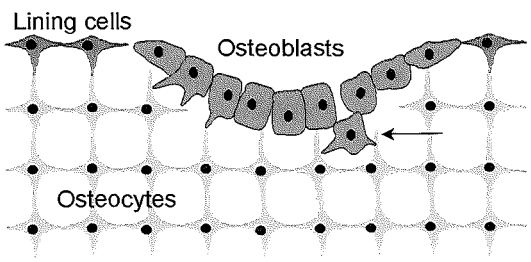

Figure 1.5: Schematical representation of incorporation of osteocytes in bone tissue. The osteoblast indicated by the arrow stays behind, is incorporated in the bone tissue and turns into an osteocyte.

The skeleton is continuously remodelled by the process just described. Every year, approximately 20% of the bone tissue is renewed [124]. The rate of renewal varies throughout the body [25]. In trabecular bone the rate of turnover varies from 10 to 30%/year, in cortical bone from 3 to 6% of the bone volume per year [65].

Besides repair of damage, bone remodeling enables the body to maintain calcium homeostasis* and to adapt the architecture of the skeleton to changes in external loads. When loads applied to the skeleton increase, osteoblasts will make more tissue than osteoclasts resorbed in order to increase bone mass, strength and stiffness [92]. When the loads decrease less bone tissue is needed to carry the loads and bone mass will decrease, by an increase in bone resorption and a decrease in bone formation. This last effect occurs for example during bed rest or spaceflight [179, 79].

The bone remodeling process also has its disadvantages. After peak bone mass has been reached at the age of 25-30 years, bone mass decreases slowly because osteoblasts make slightly less tissue than osteoclasts resorb. This is illustrated in

*Calcium homeostasis is the maintenance of a fairly constant level of calcium in the body. The skeleton is a reservoir of minerals, bone resorption frees the calcium from the bone tissue, so that it is available for other purposes.

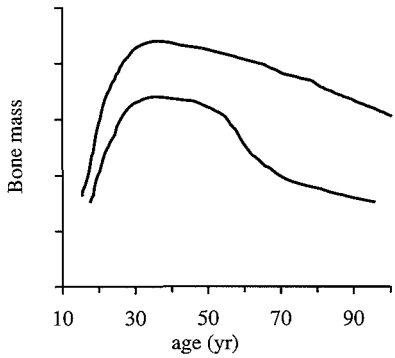

Figure 1.6: Changes in bone mass with age, in men and women.

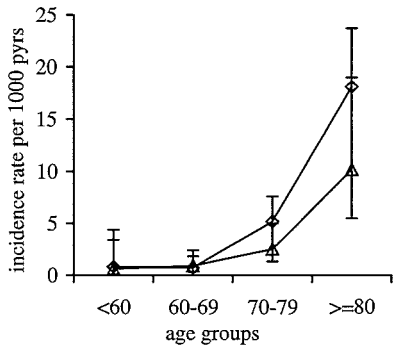

Figure 1.7: Increase in fracture incidence with age, in men (△)and women(◇) (graph from data presented in [37].)

figure 1.6, which shows the decrease in bone mass with age in men and women. On the macro scale, the cortex becomes thinner and the bone volume fraction in cancellous bone decreases. On the trabecular scale, trabeculae become thinner and plates are perforated. The thinning of structures in the cancellous bone increases the chance that trabeculae are breached by resorption cavities. It is believed that these breached trabeculae are not repaired, but removed by further osteoclastic resorption [108]. Trabeculae aligned in the main load bearing direction are mostly preserved, transversal trabeculae have a higher chance of being resorbed. This leads to an even larger loss of strength and stiffness, and an increase of fracture risk (see Fig.1.7).

It is clear that the changes in the skeleton with age are a result of the bone remodeling process, but it is not known exactly how the bone remodeling is regulated. Several hypotheses exist: damage, stress, strain and fluid flow are assumed to play a role [78, 20, 98, 86]. Increased remodeling in response to microdamage has been shown [5, 21, 104, 19], but not all remodeling is damage-related. A large part of all bone remodeling might not be targeted but random. Bone remodeling also plays a role in calcium homeostasis, for this purpose mechanical feedback is not needed [131].

When the bone remodeling loop is distorted, this can lead to large increases in bone mass or fast bone loss. For example, in postmenopausal osteoporosis, bone turnover is increased and bone loss is accelerated. The cancellous bone architecture becomes more anisotropic [29], transversal trabeculae are lost and the cortices get thinner. This reduces the strength of the bones and largely increases fracture risk.

Nowadays, anti-resorptive treatment is widely used in bone diseases in which bone remodeling is affected. The anti-resorptive agents act mainly via the osteoclasts and decrease bone resorption. Because bone resorption and formation are

coupled in the bone remodeling process, this results in a decrease in bone formation. The overall result is a decrease in the rate of bone turnover and a concomitant increase in the age of the bone tissue. In treatment of osteoporosis in large clinical trials the bone mineral density (BMD) as measured by DXA (Dual energy X-ray absorptiometry) increased 3-11% [50, 166]. The number of vertebral fractures was decreased up to 50% after 3-5 years [95, 50, 11, 138, 133]. The reductions in fracture risk were surprisingly high, considering the small increases in bone mineral density.

Concluding, the steps in the remodeling process are well described: bone resorption is followed by bone formation and subsequent mineralization of the new tissue. Damaged tissue is replaced by new tissue and the alignment of the trabeculae shows that mechanical signals play a role. The beneficial and the detrimental effects of bone remodeling are known, but it is not yet known if and how this process is regulated.

1.1 structure of this thesis

The aim of the research projects described in this thesis was to gain more insight in the regulation of bone remodeling and in the interactions between bone remodeling, architecture and bone tissue properties. The most striking changes during aging and osteoporosis take place in cancellous bone. For this reason, the research presented in this thesis focussed on bone remodeling in cancellous bone. We used computer modeling, finite element calculations and in vivo labeled bone specimens.

In the first study (**chapter 2**) a computer simulation model of the bone remodeling process in cancellous bone was made. The model mimics the process of bone remodeling in three dimensional models of cancellous bone tissue, made using x-ray micro computed tomography scans. The bone remodeling parameters resorption depth, number of resorption cavities and formation deficit were varied and the long term effects of the bone remodeling on stiffness and architecture were determined. Using this model, the effects of changes in the bone remodeling parameters on the cancellous bone architecture and stiffness were studied in computer models of human vertebral cancellous bone.

In the second study, described in **chapter 3** the mechanical consequences of bone loss and bone remodeling in cancellous bone were studied in detail. We used finite element models of human vertebral cancellous bone to investigate the distribution of external loads over the trabeculae in cancellous bone. Bone loss with aging was simulated and the changes in global stiffness and load distribution were determined. Besides this, we examined the stresses, strains and strain energy density in the vicinity of resorption cavities. These models give information about stresses and strains at trabecular level, which might play a role in the regulation of

the bone remodeling process.

Clinically, disorders of bone remodeling are frequently treated by suppressing the bone remodeling process. The anti-resorptive agents reduce bone turnover and increase bone mineral density (BMD) [31, 150, 177, 50]. Clinical trials have shown reductions in fracture risk which were larger than expected from the relatively small increases in BMD [32]. The model described in chapter 2 was modified, so that the number of resorption cavities, resorption depth and formation deficit could be changed during the simulation. Using the modified model, we simulated the changes in bone remodeling during the menopausal transition and subsequent anti-resorptive treatment, as described in **chapter 4**. Changes in bone mass and stiffness resulting from menopause and treatment were investigated. Specifically, we investigated the differences between three types of anti-resorptive drugs. Besides this we examined the differences between early and late started treatment. Bone mass and stiffness were compared at the start of the perimenopausal period and 20 years after the start of menopause.

In the third study described in this thesis the three dimensional distribution of remodeling sites in cancellous bone was investigated (**chapter 5**). Locations of bone apposition can be labelled in vivo with fluorochrome markers, which bind to calcium. When recently deposited osteoid mineralizes, the label is incorporated with the calcium in the tissue. These labels can then be visualized using fluorescence microscopy [93]. The 3D distribution of remodeling sites can not be investigated using other techniques currently used in bone research. Bone histology gives information about the locations of remodeling, but not about the 3D architecture. Micro-CT scans give information about the 3D architecture, but not about the locations of bone remodeling. The changes in cancellous bone with aging are known, but it is not known how these changes are created. Several scenarios are possible. For example, it is possible that resorption occurs more frequently on transversal trabeculae than on trabeculae aligned in the main load bearing direction. The formation deficit would then result in thinning of transversal trabeculae, while the aligned trabeculae are preserved. Another possibility is that resorption cavities are initiated on both aligned and transversal trabeculae, but that the formation deficit is smaller in aligned trabeculae because of larger stresses or strains in these trabeculae.

In order to study the distribution of bone remodeling sites, a setup for automated serial sectioning of bone specimens was built. This computer controlled setup consisted of a heavy duty sledge microtome, a fluorescence microscope and a digital camera. Bone specimens were embedded in black epoxy and serially sectioned in the setup. After each section, an image of the new top surface of the specimen was made, to make a three dimensional reconstruction of the bone specimen. The data set contained the three dimensional architecture of the cancellous bone and the locations of recent bone formation. These data sets were used to determine whether bone remodeling is initiated randomly throughout the structure,

or more on e.g. load bearing or transversal trabeculae (**chapter 5**).

The bone remodeling process does not only change the bone architecture, it also influences the properties of the bone tissue itself. Recently deposited bone tissue has a rather low mineral content, which increases as the tissue becomes older [64, 129]. A high turnover rate results in young tissue with a relatively low mineral content. A low turnover rate will result in older tissue, with a higher mineral content. It has been shown experimentally that the stiffness of bone tissue increases exponentially as the mineral content of the bone tissue increases [35]. In cancellous bone, the surface layer of the trabeculae is remodeled more frequently than the core of the trabeculae which is not reached by the resorption cavities [10, 16].

In the fifth study, described in **chapter 6**, we investigated the effect of this nonuniform mineral distribution on the global stiffness of cancellous bone. In order to do this, we made three different computer models of cancellous bone specimens. In these models, the mineral was distributed in three different ways over the trabeculae of the cancellous bone. In the first model, the mineral was distributed uniform, all elements had the same mineral content and stiffness. In the second model a thin surface layer had a lower mineral content and therefore also a lower stiffness, the thickness of this surface layer was varied. These models mimicked the in vivo mineral distribution. In the third model, a hypothetical mineral distribution, in which the surface layer had a higher mineral content than the core of the trabeculae was incorporated in the model. The global stiffness of these models was determined using finite element calculations. These simulations were used to determine whether the nonuniform distribution of the mineral over trabeculae is mechanically advantageous or not.

Differences in bone tissue properties are not only found within trabeculae, but also between young and old, healthy and diseased people [16, 18]. The average mineral content of bone tissue increases with age, which results in stiffer, but also more brittle bone tissue. It has been hypothesized, that the bone loss with increasing age is a result of malfunctioning of the bone cells [91]. According to that assumption the cells do not perceive changes in their environment, or they do not sent out the right signals anymore. The coupling between bone mass and the external loads is lost and bone stiffness decreases. In our sixth study (**chapter 7**), we hypothesized that the bone loss with age is not a result of malfunctioning of the bone cells, but of changes in the tissue properties with age. The increase in mineral content with age results in an increase in the stiffness of the bone tissue and a decrease in the deformation at cell level. The bone cells detect lower deformations and bone mass will decrease. In this chapter, we investigated the effect of changes in tissue stiffness on bone architecture, assuming that the bone cells act normally. We used finite element calculations, in which the bone architecture was adapted to the external loads. At locations where the strain was higher than a certain threshold, bone tissue was added to the surface of the trabeculae. Bone

tissue in which the strain was lower than a certain value was removed. These two threshold values are the boundaries of the so-called lazy zone: the range of strains that do not induce adaptation of the architecture. We investigated the changes in architecture resulting from changes in tissue stiffness and changes in the lazy zone.

The results of all these studies are put in a wider context and compared to existing knowledge on bone remodeling in the discussion. The studies in this thesis contribute to the unraveling of the bone remodeling process. However, they also make clear that there is a lot more to be done, before we really understand this complex biological system.

Chapter 2

A 3D simulation of age related remodeling in cancellous bone*

J.C. van der Linden
J.A.N. Verhaar
H. Weinans

*Reproduced from JBMR volume 16(4):688-96, 2001 with permission of the American Society for Bone and Mineral Research

2.1 Abstract

After peak bone mass has been reached, the bone remodeling process results in a decrease in bone mass and strength. The formation deficit, the deficit of bone formation compared to previous resorption, results in bone loss. Moreover, trabeculae breached by resorption cavities are probably not repaired. The contributions of these mechanisms to the total bone loss are unclear.

In order to investigate these contributions and the concomitant changes in trabecular architecture and mechanical properties, we made a computer simulation model of bone remodeling using micro-CT scans of human vertebral trabecular bone specimens. Up to 50 years of physiological remodeling were simulated. Resorption cavities were created, and refilled three months later. These cavities were not refilled completely, to simulate the formation deficit. Breached trabeculae were not repaired, loose fragments generated during the simulation were removed. Resorption depth, formation deficit and remodeling space were based on biological data.

The rate of bone loss varied between 0.3 and 1.1% per year. Stiffness anisotropy increased, morphological anisotropy (MIL) was almost unaffected. Connectivity density increased or decreased, depending on the remodeling parameters. The formation deficit accounted for 69-95%, breached trabeculae for 1-21% and loose fragments for 1-17% of the bone loss. Increasing formation deficit from 1.8 to 5.4% tripled bone loss but only doubled the decrease in stiffness. Increasing resorption depth from 28μm to 56μm slightly increased bone loss but drastically decreased stiffness. Decreasing the formation deficit helps to prevent bone loss, but reducing resorption depth is more effective in preventing loss of mechanical stiffness.

2.2 Introduction

The skeleton is continuously renewed in the remodeling process, which prevents accumulation of damage [19, 104] and adapts the bone architecture to external loads [55]. A side effect of this remodeling process is a gradual decrease of the bone volume after the peak bone mass has been reached, at approximately 30 years of age. This decrease is caused by the formation deficit, the deficit of osteoblast formation relative to osteoclast resorption [128]. In addition, more bone may be lost because trabeculae that are breached by resorption cavities are probably not repaired [127]. This bone loss and the concomitant changes in bone architecture decrease the strength and stiffness of the bone, and thereby increase the fracture risk.

Numerous studies have investigated the changes in the trabecular architecture with aging or as a result of diseases. In these studies parameters like trabecular thickness, trabecular spacing, connectivity and volume fraction have been determined in two and in three dimensions [70, 69, 116, 119]. Using fluorochrome-labeling techniques, remodeling parameters such as resorption, resting and refill period have been determined [48]. Furthermore, examples of breached trabeculae have been shown in SEM studies of trabecular bone specimens [108].

These studies have shown that bone is lost because of the formation deficit and breached trabeculae. However, the contributions of these mechanisms to the total bone loss are not known yet. The relation between the remodeling parameters measured in fluorochrome labeling studies and the changes in architecture determined in morphological studies is unclear. Moreover, it is not known what is more important in preventing or reducing bone loss using medicines: reducing resorption depth, or reducing the formation deficit. The formation deficit leads to thinner trabeculae, more breached trabeculae, and a lower BMD. A larger resorption depth will result in more breached trabeculae. The changes in architecture, however, depend on a combination of parameters, and can not be predicted easily.

In a few studies computer simulations have been used in order to assess the changes in trabecular thickness and the number of breached trabeculae that result from bone remodeling [90, 97, 136, 165]. These studies used simplified, two-dimensional models of the trabecular bone architecture. Recently, Tayyar et al. [163] performed a simulation in a simplified three-dimensional model of trabecular bone, using an artificial bar-plate model. In this model, resorption cavities were created in the middle of the 'trabeculae'. Using this model the authors determined contributions of the formation deficit and breached trabeculae and found that breached trabeculae accounted for 20 to 40 percent of the total bone loss, dependent on remodeling rate.

In this study we want to illustrate how bone remodeling parameters such as resorption depth, formation deficit, remodeling space and remodeling period affect bone loss, architecture and mechanical stiffness of trabecular bone. The re-

modeling process was studied using detailed three-dimensional models of human vertebral cancellous bone specimens made from micro-CT scans. We developed a three-dimensional computer simulation where resorption could take place everywhere on the surface of the trabeculae, mimicking in vivo remodeling. In our model bone is lost in three ways: the formation deficit results in a gradual loss of bone, breached trabeculae are not repaired and loose fragments created during simulated remodeling are removed. By varying the remodeling parameters, the effect of these parameters on the bone loss and bone architecture was investigated and the contributions of the formation deficit, breached trabeculae and loose fragments to the total bone loss were determined. In addition we examined the effects of remodeling and bone loss on mechanical stiffness and architectural parameters.

2.3 Materials and Methods

Specimens

The specimens used in this study were obtained from autopsy L4-vertebrae of three donors: two males, 37 and 77 years old, and one female: 80 years old. These were part of the European Union BIOMED 1 project "Assessment of Bone Quality in Osteoporosis". According to the donor data, these donors did not suffer any osteoporotic fractures. The specimens were micro-CT scanned (Scanco Medical, voxel size 14μm) and the reconstructions were binarized to obtain three-dimensional voxel models of $4 \times 4 \times 4$ mm trabecular bone, with cubic elements of $14 \times 14 \times 14\mu$m. The volume fractions of these specimens were 6.4% (female donor 80 years, F80), 11.8% (male donor 77 years, M77) and 12.9% (male donor 37 years, M37), resulting in computer models of 1.4 - 2.9 million brick elements.

Simulation of bone remodeling

The remodeling process was simulated in three steps. In the first step resorption cavities were created, randomly distributed over the surface of the trabeculae. The center elements of these hemi-spherical cavities were surface elements, here defined as elements with at least one face adjacent to marrow. The resorption depth was varied in the biologically relevant range [48]; resorption depths of 28, 42 and 56 μm were simulated. In the second step, a check for breached trabeculae was performed. Resorption cavities that breached trabeculae were not refilled. Breaching of a trabecula could be caused by one resorption cavity, or by more resorption cavities in the same trabecula. In the third step, all cavities that did not breach trabeculae were refilled. One or more surface elements in these cavities were not refilled in order to simulate the formation deficit. The formation deficit in the models was 1.8, 3.6 or 5.4% of a resorption cavity, which is in the range of measured biological values [54]. A two-dimensional representation of this simulation perfor-

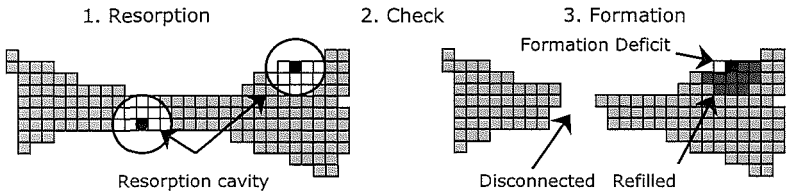

Figure 2.1: 2D representation of the simulation performed in 3D in this study.

med in three dimensions is shown in Figure 2.1. The three steps shown in Figure 2.1 were repeated to simulate the continuing process of physiological remodeling.

In each simulation cycle, new resorption cavities were created and old cavities were refilled. In our simulation, each simulation cycle corresponded to one month in real life. The cavities were refilled three simulation cycles after the resorption step, in the model the total time from the start of resorption to refill was assumed to be three months. The remodeling space, the volume occupied by resorption cavities, was 4% of the bone volume in all simulations. This results in a turnover of 16% per year, which corresponds to values found in histological studies of human bone [65].

During the simulation, loose fragments could be generated, if a trabecula was breached by resorption cavities at different locations. The loose fragments of bone, not connected to the main structure anymore, were removed from the model each 50^{th} simulation cycle. This removal of loose fragments was not performed each cycle, because it was a cpu-time consuming procedure. The difference in total bone loss between removing loose fragments each cycle and only each 50^{th} cycle was below 1% of the total bone loss, and therefore did not affect the results. This simulation of bone remodeling was performed on all three specimens. The combinations of remodeling parameters used in the simulations are shown in Table 2.1. Fifty years of remodeling were simulated in the model of the 37-year-old donor, 20 years of remodeling were simulated in the models of the 77 and 80-year-old donors. The amount of bone loss resulting from the three mechanisms of bone loss (formation deficit, breached trabeculae and loose fragments) was determined.

Morphological parameters

In order to investigate the influence of this simulated remodeling on the architecture, connectivity density and anisotropy were determined. Before calculating these parameters, the surface of the trabecular bone after simulated remodeling was smoothed, using 3D mathematical morphology software (Morph3D, R.A. Peters, Vanderbilt University). This was done to prevent the ruffled borders that resulted from the formation deficit in the simulation from influencing the morphological parameters. In Figure 2.2 some trabeculae are shown before and after smooth-

Table 2.1: Parameters used in the simulations of the remodeling process. The duration of the remodeling cycle was three months, the remodeling space 4% of the trabecular bone volume.

Variation of formation deficit			
Formation deficit		Resorption depth	
% of cavity	# elements	μm	# elements
1.8%	1	42	3
3.6%	2	42	3
5.4%	3	42	3
Variation of resorption depth			
Formation deficit		Resorption depth	
% of cavity	# elements	μm	# elements
5.4%	1	28	2
5.4%	3	42	3
5.4%	8	56	4

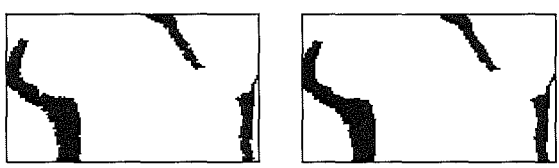

Figure 2.2: Some trabeculae from specimen F80, before and after the smoothing procedure carried out after simulated remodeling (Software: Morph3D, R.A.Peters, Vanderbilt University).

ing. Morphological anisotropy was determined as maximum divided by minimum value of the eigenvalues of the ellipsoid approximation of Mean Intercept Length (MIL). Connectivity density and MIL were determined using previously described methods [116, 119].

Mechanical properties

In order to investigate the effects of the simulated remodeling and changed morphology on the mechanical properties, the apparent stiffness of the specimens was calculated using finite element analyses. This was done for the original models, after 20 years of remodeling in specimens F80 and M77 and after 50 years of simulated remodeling in specimen M37. The datasets with elements of 14μm cubed were coarsened to datasets with elements of 42μm cubed. Previous studies have shown that elements of 40μm cubed are small enough to accurately calculate apparent stiffness of trabecular bone [169, 176]. Coarsened elements containing the

maximum number of 14μm bone elements (27 elements) were given a tissue modulus of 1000 MPa. The Young's Modulus of the coarsened elements was linearly related to the number of 14μm bone elements in the same volume in the original model. The tissue modulus in the finite element model was assumed to be uniform, isotropic and linearly elastic. Real bone matrix is not uniform, isotropic and linearly elastic, but good results for apparent stiffness of trabecular bone can be obtained using this approximation [82]. The global stiffness matrix was calculated by simulating six uniaxial strain cases in which homogeneous displacements were prescribed at the surfaces [175]. From this matrix, the best orthotropic representation of the global stiffness matrix was determined, using an optimization procedure [175]. The stiffness anisotropy was calculated as the maximum divided by the minimum of the stiffness in these orthotropic directions. The changes in stiffness due to simulated remodeling were determined.

2.4 Results

The formation deficit accounted for the major part of the bone loss. Bone loss caused by breached trabeculae became increasingly important with age, as the trabeculae became thinner and the probability of trabeculae being breached by a resorption cavity increased. After 45 years of simulated remodeling with a resorption depth of 42 or 56 μm and a formation deficit of 5.4% in the model of the specimen from the 37-year-old donor, a large part of the model was disconnected from the main structure, because of breached trabeculae, and the structure fell apart. Therefore, we did not include the results of these last simulation cycles in the results, further results from 50 years of simulated remodeling include only simulations with smaller formation deficits and shallower cavities.

The bone loss over 50 years of remodeling in the specimen from the 37-year-old donor varied between 16 and 47% in this simulation study, dependent on the remodeling parameters. Twenty years of simulated remodeling resulted in 6-23% bone loss in the two specimens from the 77 and 80-year old donors. We found that the formation deficit accounted for 69-95% of the bone loss, breached trabeculae for 1-21%, and loose fragments that were removed from the model for 1-17%, see Figures 2.3 and 2.4. The rate of bone loss varied between 0.3 and 1.1% per year.

Variation of resorption depth

Cavities of 28 or 42 μm in combination with a formation deficit of 5.4% resulted in all specimens in a rate of bone loss of 0.8% per year over the first 20 years of simulated remodeling. Apparently, these resorption depths are small compared to the trabecular thickness, so that almost no accelerated bone loss caused by breached trabeculae occurred (Fig.2.3, left and middle column). Cavities 56 μm deep resulted in faster bone loss, more trabeculae were breached, and more loose frag-

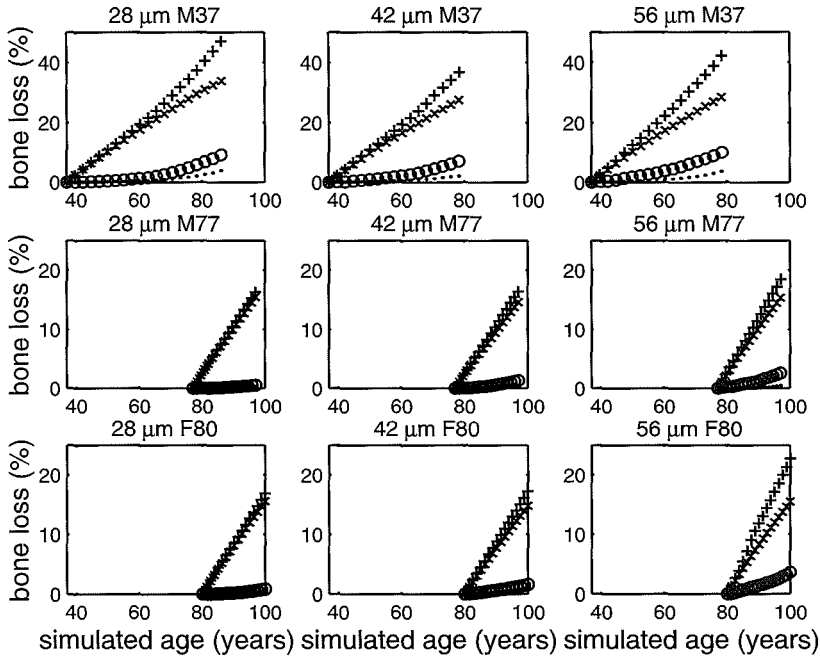

Figure 2.3: Bone loss with simulated age, expressed as a percentage of the original bone volume. Resorption depth was varied: the left, middle and right column show results for resorption depths of respectively 28, 42 and 56 μm. Formation deficit was 5.4% of a cavity, remodeling space 4% of the bone volume, remodeling duration 3 months. In the graphs the total bone loss (+), loss due to formation deficit (x), breached trabeculae (o) and loose fragments (•) are shown.

ments were generated (Fig.2.3, right column). This resulted in rates of bone loss of 0.9% per year in the specimens of the 37-year old and the 77-year old donor, and of 1% per year in the specimen from the 80-year-old, female donor. This difference is mainly caused by a larger amount of bone lost as a result of loose fragments, as can be seen in Figure 2.3. The rate of bone loss increased with simulated age, between simulated ages of 77 and 87 years the rate of bone loss in the specimen from the 37-year-old donor was 1.1% per year.

Variation of formation deficit

A larger formation deficit resulted in faster thinning of trabeculae, and thereby in a larger number of breached trabeculae. Bone loss with age as a result of a resorption depth of 42 μm, and varying formation deficit, is shown in Figure 2.4. The rate of bone loss depended largely on the formation deficit. A formation deficit of 1.8% of a cavity resulted in a rate of bone loss of 0.3% per year in all specimens. A formation deficit of 3.6% resulted in 0.5% bone loss per year in the specimen

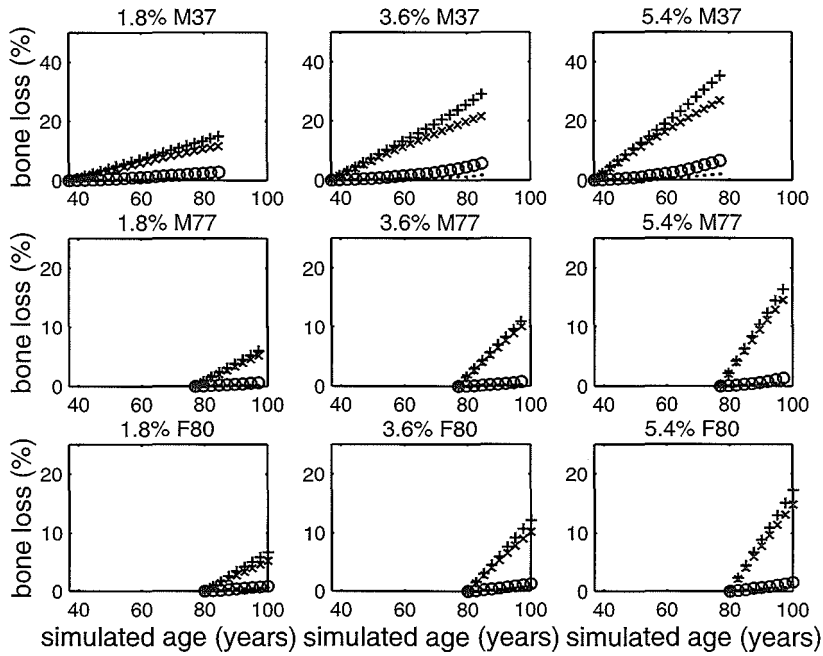

Figure 2.4: Bone loss with simulated age, expressed as a percentage of the original bone volume. Formation deficit was varied: left, middle and right columns show results for formation deficits of respectively 1.8, 3.6 and 5.4% of a cavity. Resorption depth was 42 μm, remodeling space 4%, remodeling duration 3 months. In the graphs the total bone loss (+), loss due to formation deficit (x), breached trabeculae (o) and loose fragments (•) are shown.

from the 77-year-old male donor, of 0.6% per year in both other specimens. A formation deficit of 5.4% resulted in an average rate of bone loss of 0.8% per year in all specimens.

Connectivity density

Connectivity density either increased or decreased, depending on the remodeling parameters. During remodeling plates are perforated, which increases connectivity density. Besides this, trabeculae are breached, which decreases connectivity density. The changes in connectivity density, resulting from the combined effect of these processes, are shown in Figure 2.5.

Mechanical properties

As expected, the specimen from the youngest, 37-year-old, donor had the highest apparent stiffness, in all directions. In all specimens, the maximal stiffness

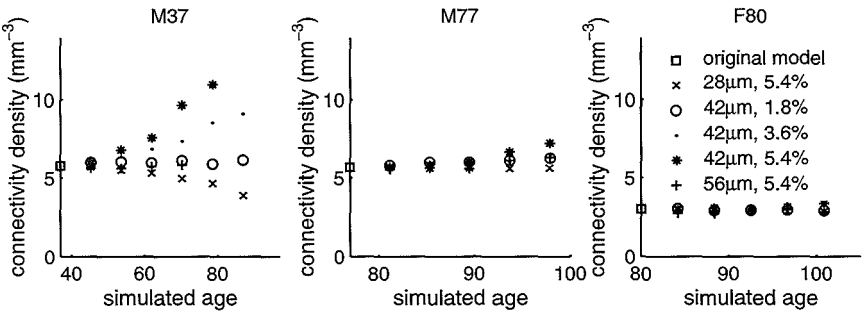

Figure 2.5: Change in connectivity density with simulated age. Resorption depth and formation deficit are indicated in the legend in the figure to the right.

in the orthotropic approximation was oriented within 7° of the superior-inferior direction. Fifty years of simulated remodeling resulted in a decrease in maximal stiffness of 22 to 64%, dependent on the remodeling parameters.

In transversal directions, the stiffness was decreased more, by 35 to 73%, as can be seen in Table 2.2. Twenty years of simulated remodeling in the specimen from the 80-year-old female donor resulted in a decrease of 9 to 33% in the direction of maximal stiffness. In the other directions the decrease was 18 to 46%. In the specimen from the 77-year-old male donor, the decreases were only 10 to 26% in the direction of maximal stiffness, and 14 to 39% in transversal directions. The direction of maximal stiffness did not change much as a result of the simulated remodeling, the maximal change was 4°. The apparent stiffness of the specimens before and after simulation of remodeling is shown in Table 2.2.

Mechanical and morphological anisotropy

The specimen from the youngest donor had the lowest morphological anisotropy, the specimen from the male donor of 77-year-old had the highest morphological anisotropy. This morphological anisotropy was almost unaffected by the simulated remodeling. The maximum value of MIL was oriented within 12° of the SI-direction for all specimens at all simulated ages, the minimum was oriented within 12° of the transversal plane.

The change in morphological anisotropy with simulated age is shown in Figure 2.6. Despite the small changes in morphological anisotropy the stiffness anisotropy showed an increase with simulated age. The stiffness anisotropy increased in all specimens as a result of the remodeling simulation, as can be seen in Table 2.2. The largest resorption cavities, of 56 μm, resulted in the largest decrease in stiffness, as well as the largest increase in stiffness anisotropy.

Table 2.2: Apparent stiffness and mechanical anisotropy of the three specimens. Apparent stiffness is shown in superior-inferior and transversal directions in MPa for the original models. Decrease in apparent stiffness is shown (in %) after 20 years of simulated remodeling in specimens F80 and M77, and after 50 years of simulated remodeling in specimen M37. Remodeling parameters resorption depth and formation deficit are shown in the table.

		Superior-Inferior	Transversal		anisotropy
M37	App. stiffness(MPa)	64.0	31.4	23.7	2.7
	Rem. parameters				
50 years of	28 μm, 5.4%	64%	73%	73%	3.6
simulated	42 μm, 1.8%	22%	35%	37%	3.3
remodeling	42 μm, 3.6%	38%	54%	52%	3.5
M77	App. stiffness(MPa)	55.2	24.8	15.3	3.6
	Rem. parameters				
20 years of	28 μm, 5.4%	20%	24%	25%	3.9
simulated	42 μm, 1.8%	10%	14%	16%	3.9
remodeling	42 μm, 3.6%	15%	19%	22%	3.9
	42 μm, 5.4%	21%	22%	29%	4.0
	56 μm, 5.4%	26%	33%	39%	4.4
F80	App. stiffness(MPa)	23.1	8.2	7.4	3.1
	Rem. parameters				
20 years of	28 μm, 5.4%	21%	26%	28%	3.5
simulated	42 μm, 1.8%	9%	18%	18%	3.4
remodeling	42 μm, 3.6%	16%	28%	24%	3.4
	42 μm, 5.4%	21%	30%	28%	3.4
	56 μm, 5.4%	33%	46%	41%	3.5

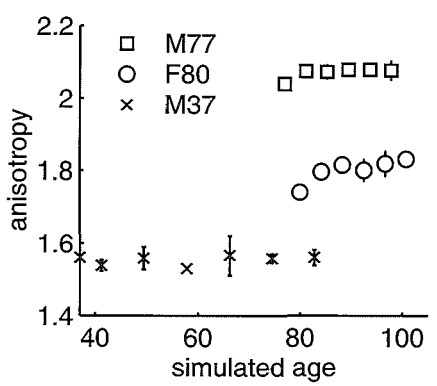

Figure 2.6: Morphological anisotropy versus simulated age, for all simulations shown in Figure 2.3 and 2.4. Mean and standard deviation are shown.

2.5 Discussion

The present simulation study provides a relationship between bone loss caused by the remodeling process in trabecular bone and the remodeling parameters that describe this remodeling process. In a three-dimensional simulation of the remodeling process resorption depth and formation deficit were varied, based on biological values. The contributions of thinning of trabeculae, breached trabeculae and loose fragments to the bone loss were quantified. The formation deficit accounted for 69-95% of the bone loss, breached trabeculae for 1-21%, and loose fragments that were removed from the model for 1-17%. The rates of bone loss were in the range of 0.3-1.1% per year, which is in good agreement with bone loss found in experimental studies [63, 96, 107].

It must be kept in mind, that in this simulation study the remodeling process is discretized: resorption cavities are either completely resorbed, or completely refilled. In reality the resorption and refill periods of the cavities last several weeks, a cavity has its maximum dimensions only during the reversal period, which is estimated to last approximately 9 days [48]. However, this discretization has no influence on the long-term effect of the simulated remodeling on the properties of the bone. Furthermore, because of the cubic elements in the model, the formation deficit can not be simulated as a thin surface layer with the present resolution. This results in a jagged surface of the trabeculae after decades of simulated remodeling. Therefore, the surface was smoothed before determination of architectural parameters. This smoothing does not affect the connectivity density, since no trabeculae are added or removed. However, a jagged surface would result in a large number of extra bone-marrow intercepts in a direction along the surface of the trabeculae. Smoothing of the surface results in a more accurate determination of morphological anisotropy determined by mean intercept length. Finally, after 45 years of simulated remodeling a large piece of the specimen of the 37-year-old donor was disconnected from the structure, resulting in a large sudden bone loss. This is a result of the small specimen size used in the simulation. A whole vertebra can not be cut in two by breaching only a few trabeculae. Moreover, if a number of trabeculae becomes very thin in vivo this will probably lead to a vertebral fracture before the structure can be cut in two parts by ongoing resorption.

We found that the formation deficit has a larger influence on the rate of bone loss than the resorption depth. This was an expected result, since increasing the formation deficit results directly in more bone loss, while increasing the resorption depth has only an indirect effect: trabeculae have a higher chance of being breached. Increasing the resorption depth from 28 to 42 μm, while keeping the other parameters constant, caused almost no change in the rate of bone loss. Increasing resorption depth from 42 μm to 56 μm resulted in 10% faster bone loss, while increasing the formation deficit from 1.8% to 3.6% of a cavity doubled the rate of bone loss. Increasing the formation deficit to 5.4% resulted in an extra in-

crease of 50 to 60% in the rate of bone loss. Therefore, it seems that in preventing bone loss, restoring the balance between osteoclastic resorption and osteoblastic formation is more important than reducing resorption depth. However, deeper cavities had a larger effect on mechanical properties. This can be explained by the large strain peaks at the bottom of deep resorption cavities [170]. Although cavities of 56μm and a formation deficit of 5.4% resulted in only 10% faster bone loss compared to cavities of 28 or 42 μm, mechanical stiffness decreased 25 to 50% more. These deep resorption cavities also caused the largest increase in stiffness anisotropy.

Connectivity density increased or decreased as a result of simulated remodeling, depending on the remodeling parameters. Trabeculae were breached, which decreased connectivity, and plates were perforated, which increased connectivity. Both these processes occur in vivo, but to the authors' knowledge, there is no experimental data showing an increase of connectivity with age. In contrast, all simulations of remodeling resulted in a decrease in the stiffness of the specimens. The values for connectivity density found in the present study are in the same range as in experimental studies in which connectivity density and stiffness of human trabecular bone specimens were determined [81]. In that experimental study a slight increase of connectivity density with decreasing stiffness was found for a constant bone volume. With increasing bone volume, a slight increase in connectivity density was found. The decrease in connectivity density with decreasing volume fraction in our study is in agreement with the experimental study [81], but the increase of connectivity density with decreasing volume fraction is in disagreement. Concluding, connectivity density alone can not be used as an indicator of stiffness of trabecular bone. However, loss of connectivity is irreversible, while thin trabeculae can thicken again as a result of antiresorptive treatment or increased mechanical loads. Therefore, connectivity density might be useful to get an indication of how much of the mechanical strength of trabecular bone can be regained after large amounts of bone have been lost [85].

An aspect that certainly plays a role in physiological remodeling, and that was not taken into account in the present simulation, is the role of mechanical loading. Numerous hypotheses exist about the way the loading influences the remodeling process. Disuse results in resorption of bone matrix [74], heavy use in apposition of bone [92]. In the present simulation the cavities were distributed randomly over the surface of the trabeculae. No stress, strain or damage distribution in the trabeculae was taken into account. At the moment, a 3D simulation of remodeling at the level of detail of the present study based on stress or strain criteria is unfeasible, but less detailed simulations have been performed [109]. However, as computer technology develops further, such a detailed simulation will probably be possible in the future.

The unloading of breached trabeculae is assumed to lead to a rapid resorption of the remaining struts in vivo [108]. In our simulations, breached, and therefore

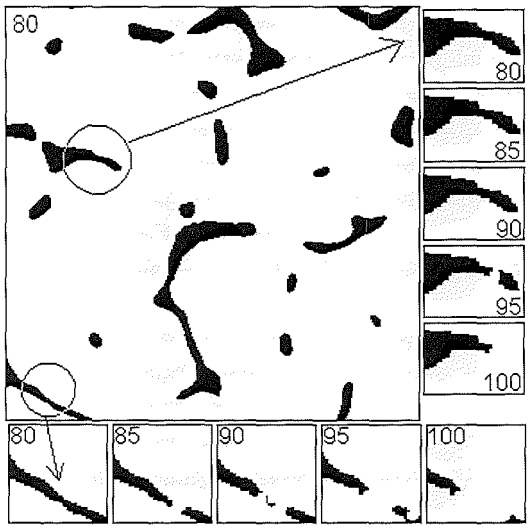

Figure 2.7: Effect of simulation of remodeling on bone structure, shown in one slice of the specimen from the 80-year-old female donor. The whole slice before simulated remodeling, at an age of 80 years, is shown. The details show the bone loss in two trabeculae. Simulated age is indicated in the figures.

unloaded trabeculae were not removed rapidly from the model. This does not influence the changes in stiffness anisotropy we found, because the remaining struts do not contribute to the stiffness of the specimen. However, if a strut was cut through, the loose fragment that was created in this way was removed from the model, resulting in a fast removal of the remaining struts (see Figure 2.7). Thus, although we did not include a stress or strain criterion in the model, like others did in two dimensions [78, 111], the struts remaining after breaching of trabeculae were removed relatively fast. In a previous simulation model of bone remodeling, performed in a simplified bar-plate model of trabecular bone [163], the whole 'trabecula' was removed when it was breached. In that study, the contribution of breached 'trabeculae' to the total bone loss was 20-40%. In our study, the contribution of breached trabeculae varied between 1 and 20%. The loose fragments in our study are also a result of breaching of trabeculae. If we combine the bone loss caused by breached trabeculae and the bone loss caused by loose fragments, this adds up to 20-30% of the total bone loss after 50 years of simulated remodeling in the specimen from the 37-year-old donor.

Although the morphological anisotropy stayed approximately constant during the simulation of normal physiological remodeling, we found an increase in stiffness anisotropy with age, in accordance with some experimental findings [61, 113]. This can be explained by the existing anisotropy of the specimens. During the

donors' life, the architecture was adapted to external loads. This resulted in specimens with thicker vertical trabeculae, and on average thinner horizontal trabeculae, shown by the initial anisotropy of the specimens. During the simulation, the thinner horizontal trabeculae have a larger chance of becoming breached by resorption cavities. If a trabecula was breached during the simulation, this trabecula did not contribute to the load bearing in the simulated mechanical test, but the remaining struts on both ends were still present in the model. The resolution of the models was high enough to detect the new intersections at the ends of the remaining struts [87], but this caused only small increases in morphological anisotropy. This explains the increase in stiffness anisotropy while the morphological anisotropy was almost unaffected.

In the present study, the remodeling parameters were kept fixed during the simulation. No increased resorption depth or increased remodeling space was included in the model, to study changes in bone remodeling in e.g. menopause or Paget's disease. However, these changes can be incorporated in the model, by changing remodeling parameters at a certain simulated age. This way, this simulation model can be used to evaluate e.g. anti resorptive drugs treatment.

Concluding, in the present study we estimated the contribution of the bone loss mechanisms formation deficit, breached trabeculae and loose fragments to the total bone loss. For this purpose, we made a simulation of the bone remodeling process in three-dimensional models of human vertebral trabecular bone. We used biologically relevant values as input for the remodeling parameters, and found rates of bone loss in the biologically relevant range. An increase in formation deficit caused a larger increase in rate of bone loss than an increase in resorption depth. However, deeper resorption cavities caused larger decreases in mechanical stiffness of the specimens.

2.6 Acknowledgements

The micro-CT scans of the vertebral specimens used in this study were kindly provided by Prof. P. Ruegsegger and were obtained as part of the European union biomed 1 project "Assessment of bone quality in osteoporosis". The authors wish to thank the Dutch National Computing Facilities Foundation (NCF) for computing facilities and A. Odgaard for providing the software used for calculating the morphological parameters. The contribution of Harrie Weinans has been made possible by a fellowship from the Royal Netherlands Academy of Arts and Sciences. Jacqueline van der Linden was supported by the Dutch Foundation for Research (NWO/MW).

Chapter 3

Mechanical consequences of bone loss in cancellous bone.*

J.C. van der Linden
J. Homminga
J.A.N. Verhaar
H. Weinans

*Reproduced from JBMR volume 16(3):457-65, 2001, with permission of the American Society for Bone and Mineral Research

3.1 Abstract

The skeleton is continuously renewed in the bone remodeling process. This prevents accumulation of damage, and adapts the architecture to external loads. A side effect is a gradual decrease of bone mass, strength and stiffness with age. We investigated the effects of bone loss on the load distribution and mechanical properties of cancellous bone, using three dimensional computer models of human cancellous bone.

Several bone loss scenarios were simulated. Bone matrix was removed at locations of high strain, of low strain and random throughout the architecture. Furthermore, resorption cavities and thinning of trabeculae were simulated. Removal of 7% of the bone mass at highly strained locations had deleterious effects on the mechanical properties, while up to 50% of the bone volume could be removed at locations of low strain before the structure collapsed. Thus, if remodeling would only be initiated at highly strained locations, where repair is likely needed, cancellous bone would be continuously at risk of fracture.

Thinning of trabeculae resulted in relatively small decreases in stiffness, the same bone loss caused by resorption cavities caused large decreases in stiffness and high strain peaks at the bottom of the cavities. This explains that a reduction in the number and size of resorption cavities in anti-resorptive drug treatment can result in large reductions in fracture risk, with small increases in bone mass. Strains in trabeculae surrounding a resorption cavity increased by up to 1000 microstrain, which could lead to bone apposition. These results give insight in the mechanical effects of bone remodeling and resorption at trabecular level.

3.2 Introduction

It is believed that the structure of cancellous bone adapts to external loads by modeling and remodeling processes, which result in an architecture well suited for its load bearing function [26, 55, 146]. In the remodeling cycle bone matrix is resorbed by osteoclasts, which make resorption cavities of 40 to 60 microns deep. In approximately 3 months these cavities are refilled with new bone matrix by osteoblasts. The formation and resorption phase are coupled so that the bone mass stays approximately constant during this continuing process of physiological remodeling [128]. Nevertheless, after the age of 30, the bone mass decreases slowly with age because there is a small deficit of osteoblast formation relative to osteoclast resorption. Moreover, disconnected trabeculae are probably not repaired [128]. In general, the amount of bone loss with aging in the spine and hip is in the order of 0.5% of the bone volume per year. The increase in resorption depth and activation frequency [49, 65] during menopause result in faster bone loss [2], as trabeculae are disconnected and plates are perforated. The decrease of bone mineral content (BMC) or bone mineral density (BMD) is the most important reason for reduced load bearing capacities of bone in elderly people [102]. However, the decrease in bone strength and increase in fracture risk can not be fully explained by the decrease of BMC or BMD [123]. This has resulted in a considerable interest in the architecture of cancellous bone, which could further explain the changes in the quality of the bone and the complementary increase in fracture risk.

Developments in three dimensional imaging have resulted in three dimensional quantification methods for the cancellous architecture [70, 69, 116, 119]. These methods have been used to gain a better understanding of the mechanical functioning of cancellous bone and to find relationships between the morphological parameters and mechanical properties such as strength and stiffness [61, 168]. Small changes in the architecture, which cause small changes in the morphological parameters, can considerably change the load distribution and thereby have a large effect on the mechanical properties and the fracture risk [60].

Bone remodeling causes changes in the architecture. After peak bone mass has been reached, bone is lost slowly, trabeculae become thinner and plates are converted to rods. Resorption cavities can have large effects on the properties of trabeculae. A resorption cavity with a depth of 40 - 60 μm can considerably deteriorate the strength of a trabecula with a thickness of approximately 100 μm. Failure of a trabecula results in increased loading of the surrounding trabeculae, which could lead to failure of the whole structure. Insight into the strain distribution in trabeculae could thus be useful in understanding mechanical aspects of bone loss and remodeling in cancellous bone and in predicting fracture risk. In cortical bone, strains can be measured in vivo, but in cancellous bone this is not possible [12, 22, 62, 152, 161].

The purpose of our work was to quantify the strain distribution in the trabeculae

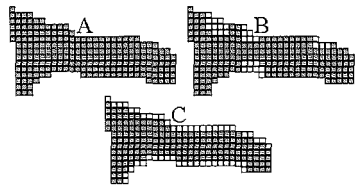

Figure 3.1: Two dimensional representation in one trabecula of the bone loss simulated in three dimensions in the 2^{nd} experiment. A: original model, gray elements are bone elements in the finite element model. B: bone loss by resorption cavities, white elements were removed in order to simulate the cavities. C: bone loss by thinning of trabeculae. White elements were removed from the model.

of cancellous bone, in order to estimate the mechanical effects of bone loss and bone remodeling. Using computer models that incorporate the full 3D architecture of cancellous bone we calculated the strains in individual trabeculae under normal physiological loading conditions. This enabled us to study how apparent level loading is resolved into tissue level deformations. Furthermore, we determined the changes in strain distribution and mechanical properties that resulted from bone loss by simulating various cases of bone loss in computer models. The results of these simulations show the mechanical effects of bone loss and remodeling at trabecular level.

3.3 Materials en methods

In this study we used 3D reconstructions of cancellous bone specimens, which were made using micro-CT scanning or serial sectioning. A specimen of 6 mm cubed from the proximal end of an autopsy human tibia was serially sectioned in slices of 20μm and digitized [117]. The 3D architecture was reconstructed in a computer model by converting the voxels to elements of 60μm cubed [175, 176]. The volume fraction of this specimen was 13.9%. Three specimens from the center of human vertebral bodies were reconstructed using a micro-CT scanner [39, 68]. The donors were two males, of 37 and 77-years-old (M37, M77), and one female, 80-years-old (F80). These datasets were coarsened to obtain finite element computer models of trabecular bone (4 mm cubed) with brick elements of 28μm cubed. The volume fractions of these specimens were 7.4%(F80), 13.4%(M37) and 8.9%(M77). The tissue material properties in the computer models were chosen isotropic with a Young's modulus of 5000 MPa and a Poisson's ratio of 0.3 [89, 176].

Using these finite element models several computer simulation experiments were performed in order to investigate the effects of bone loss on the strain distribution within the trabeculae. If a cancellous architecture is well suited for its load bearing function, the load will be distributed equally over all elements in the structure, resulting in a narrow strain distribution.

Worst case and best case scenario of bone loss.

The model of the cancellous bone specimen from the proximal tibia was loaded in the computer simulation in the Superior-Inferior direction, which corresponds to the in vivo loading axis. At the bottom face, displacements in the SI-direction were constrained, a displacement of -1 mm in the SI-direction was prescribed to the top face. Displacements in the side planes were suppressed for directions perpendicular to these planes. The strains in the trabeculae and the reaction force at the top surface were calculated using finite element analyses [176]. This reaction force was linearly related to the prescribed displacement and the Young's modulus of the cancellous bone tissue, because of the assumed linear elastic material properties. The strains were recalculated to correspond to a force of 18 N, which equaled an apparent stress of 0.5 MPa.

The maximal principal strains in the trabeculae were calculated. Changes in the maximal principal strain distribution as a result of bone loss were studied in three cases. First, a simulation of bone loss randomly distributed over the trabecular structure was performed. Second, bone was removed at locations of high strain and third, bone was removed at locations of low strain. With these simulations, insight into the influence of the location of bone loss on the deterioration of the mechanical properties of cancellous bone was obtained.

Bone loss caused by bone remodeling.

Although the previous simulation analyses may mimic potential stages of net bone loss, they certainly differ from the way in which bone is normally lost in vivo. The computer simulations in this second experiment mimicked both bone loss in resorption cavities, the direct effect of bone remodeling, and thinning of trabeculae, the long-term effect of remodeling with a formation deficit. In order to simulate the direct effect, resorption cavities were created in the three models of vertebral cancellous bone, randomly distributed over the surface of the trabeculae. The depth of these resorption cavities was 56 μm, which is in the biologically relevant range [47]. In 5 steps up to 20% of the bone volume was removed by creating resorption cavities.

In order to simulate long-term bone loss, trabeculae were thinned in 5 steps. Each step, more surface elements were removed from the trabeculae, until 20% of the bone volume was removed in the fifth step (see table 3.1). Thinning of trabeculae and creating of resorption cavities are illustrated in Figure 3.1.

A load of 8 N was applied to the finite element models in the SI-direction, which corresponds to the in vivo loading axis, as described in experiment 1. This load equaled an apparent stress of 0.5 MPa, which is in the physiologically relevant range [155]. The global stiffness matrix of the specimens was calculated in all phases of bone loss, by simulating three compressive and three shear tests in the finite element models. From this matrix, the Young's Moduli of the specimens in

Table 3.1: Volume fraction in five steps of bone loss by thinning of trabeculae or by resorption cavities

	V_f(%) (relative V_f[%])					
	F80		M37		M77	
Step no.	Cavities	Thinning	Cavities	Thinning	Cavities	Thinning
Original	7.4 (100)	7.4 (100)	10(100)	10 (100)	8.9 (100)	8.9 (100)
1	7.1 (96)	7.2 (97)	9.6 (96)	9.6 (96)	8.5 (96)	8.7 (97)
2	6.8 (92)	7.0 (95)	9.2 (92)	9.3 (93)	8.2 (92)	8.4 (95)
3	6.5 (88)	6.7 (91)	8.8 (88)	9.0 (90)	7.8 (88)	8.1 (91)
4	6.2 (84)	6.4 (86)	8.4 (84)	8.5 (85)	7.5 (84)	7.7 (86)
5	5.9 (80)	5.9 (80)	8.0 (80)	7.9 (79)	7.1 (80)	7.1 (80)

the three principal orthogonal directions were determined, using an optimization procedure [175]. In addition, the strain distributions in the original model and after 20% bone loss caused by resorption cavities or by thinning of trabeculae were determined and compared.

Resorption cavities in detail.

In this experiment, the effect of resorption cavities on the load distribution in the trabeculae was studied in more detail. One horizontal and one vertical trabecula were selected in the reconstruction of a vertebral body specimen (F80). Both trabeculae, located in the center of the reconstruction, had a rod-like shape and a diameter of approximately 120 μm. In the vertical trabecula, a resorption cavity was created. This cavity was made gradually deeper, until the trabecula was disconnected. In each step, the whole specimen was loaded in the SI-direction with a force of 8 N (0.5 MPa) in a finite element simulation, as described in experiment 1. The same experiment was performed in the horizontal trabecula. We investigated the changes in strain in the resorbed trabecula itself and the redistribution of the loads throughout the specimen that resulted from a resorption cavity in one trabecula.

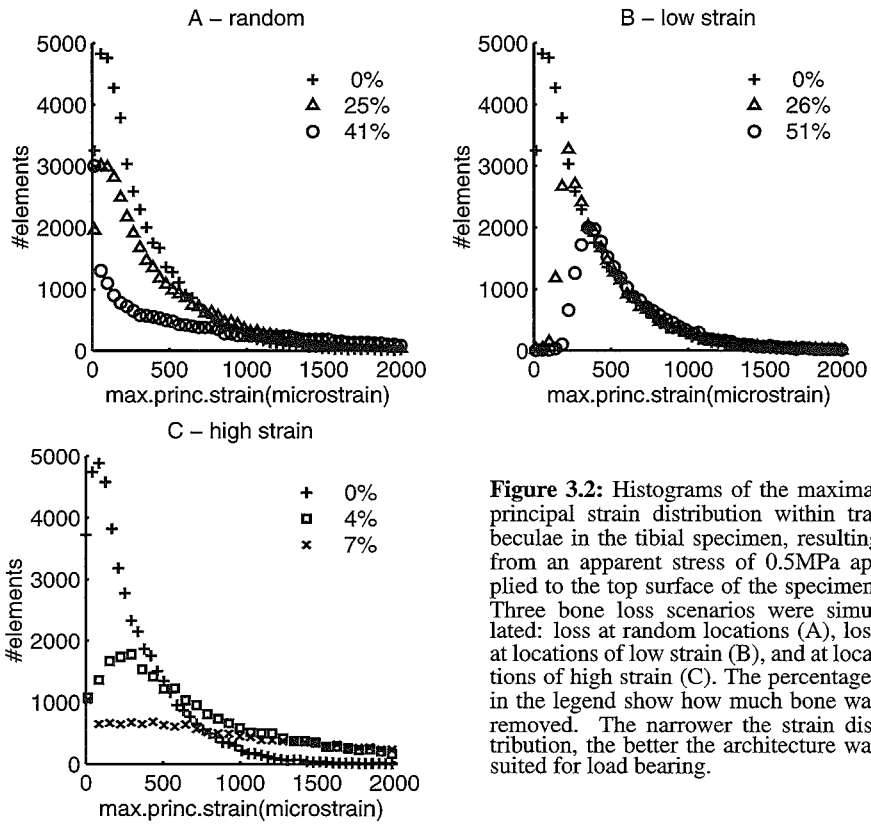

Figure 3.2: Histograms of the maximal principal strain distribution within trabeculae in the tibial specimen, resulting from an apparent stress of 0.5MPa applied to the top surface of the specimen. Three bone loss scenarios were simulated: loss at random locations (A), loss at locations of low strain (B), and at locations of high strain (C). The percentages in the legend show how much bone was removed. The narrower the strain distribution, the better the architecture was suited for load bearing.

3.4 Results

Calculated strain distributions in trabecular bone specimens.

A force of 18 N (0.5 MPa) on the top surface of the tibial specimen resulted in an apparent strain of 0.36% (3600 microstrain). In 90% of the elements the strain was lower than 700 microstrain, in most of these elements the strain was approximately 100 microstrain (Figure 3.2). This rather equal distribution of the load over the elements indicates that this specimen is well suited for its load-bearing function in the SI-direction. The same apparent stress applied to the vertebral specimen resulted in an apparent strain of 0.54% (5400 microstrain). In this specimen the strain in 90% of the elements was lower than 4300 microstrain, with most elements showing a strain of approximately 1000 microstrain (Figure 3.3C).

This wider strain distribution shows that the vertebral specimen had a lower stiffness, and a less efficient architecture. In this specimen, the applied stress might cause microdamage in a mechanical experiment in which a stress of 0.5 MPa is applied to the specimen [83].

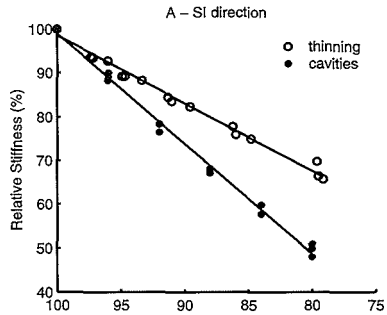

Figure 3.3: A: Change in maximum of apparent Young's Modulus resulting from bone loss by resorption cavities ($*$, E_{cav}) and by thinning of trabeculae ($\circ$, E_{thin}) in specimens M37, M77 and F80. Apparent Young's Modulus and relative volume fraction (V_f) of all specimens were normalized to 100% for the original specimens.
$E_{cav} = 2.5 * V_f - 152.5$ ($R^2 = 0.99$)
$E_{thin} = 1.5 * V_f - 55.0$ ($R^2 = 0.97$)

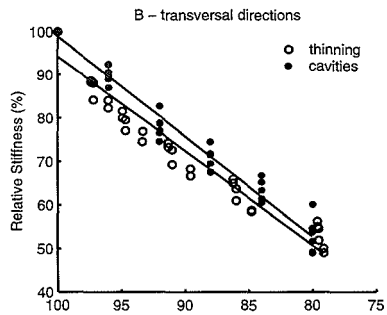

B: Change in apparent Young's moduli in transversal directions, resulting from bone loss by resorption cavities ($*$) or thinning of trabeculae ($\circ$).
$E_{cav} = 2.2 * V_f - 123.6$ ($R^2 = 0.94$)
$E_{thin} = 2.3 * V_f - 132.3$ ($R^2 = 0.97$)

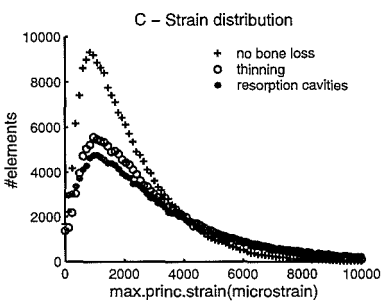

C: Histogram of the maximal principal strain distribution in a vertebral specimen (F80), resulting from an apparent stress of 0.5MPa, applied to the top surface of the specimen. The strain distribution is shown for the original configuration (no bone loss, $+$) and after removal of 20% of the bone volume, either by resorption cavities ($*$), or by thinning of trabeculae ($\circ$).

Worst case and best case scenario of bone loss

Randomly removing elements from the bone structure degraded the mechanical properties, the strain distribution flattened out significantly after removal of 25% of the bone volume. Up to 41% of the bone volume could be removed before the strain distribution became completely flat, indicating highly strained as well as almost unloaded elements in the structure (Figure 3.2A). The deterioration of the trabecular architecture depended largely on the location of the bone loss. Bone matrix removed at locations of low strains had a minor effect on the distribution, as shown in Figure 3.2B. Even after removal of 50% of the bone volume at locations of low strain, the distribution showed a narrow peak at 400 microstrain and almost no increase in the number of highly strained elements was found. In con-

Table 3.2: FE-calculated Stiffness of the three vertebral specimens in SI and transversal directions

Specimen	SI direction (MPa)	Transversal directions (MPa)	
F80	120	59	46
M37	212	82	51
M77	158	60	44

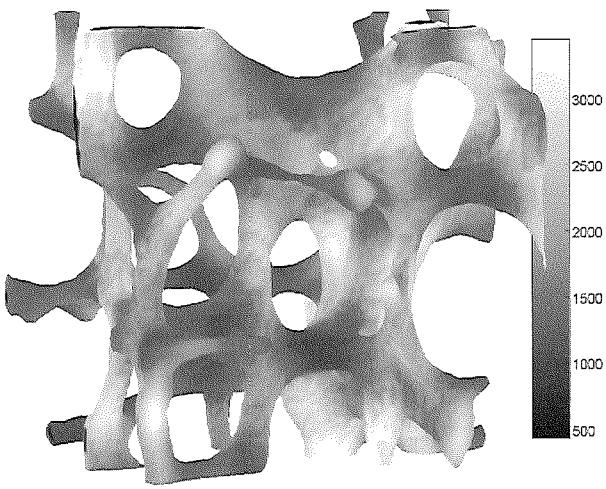

Figure 3.4: Central part ($2 * 2 * 2\text{mm}$) of specimen F80, showing the maximal principal strain distribution (in microstrain) over the trabeculae, resulting from an applied apparent stress of 0.5 MPa.

trast, removal of only 4% of the bone volume at locations of high strain caused a considerable change in the strain distribution and 7% loss resulted in a completely flattened strain distribution, and a 10 fold increase of the average strain (Figure 3.2C).

Bone loss caused by bone remodeling

The calculated stiffness of the three vertebral specimens is shown in table 3.2. Figure 3.4 shows the distribution of the maximal principal strain over the trabeculae in $2 \times 2 \times 2$ mm from the center of specimen F80. Resorption cavities caused a larger decrease in stiffness than thinning of trabeculae, especially in the SI-direction. Removal of 20% of the bone volume by resorption cavities decreased the apparent stiffness in the SI-direction by 50%, compared to a decrease of only 30% caused by thinning of trabeculae, as can be seen in Figure 3.3A. The difference between the

slopes of the regression lines was significant ($p < 0.001$). The difference between the decreases in stiffness in transversal directions caused by thinning of trabeculae or resorption cavities was not significant (Figure 3.3B). The lower stiffness that results from resorption cavities is reflected in the strain distribution within the trabeculae. Resorption cavities resulted in a wider strain distribution, and a lower peak at low strains (Figure 3.3C).

Resorption cavities in detail

The vertical trabecula in which the resorption cavity was created was compressed and bent in its original shape. The maximal strain in this trabecula was approx-

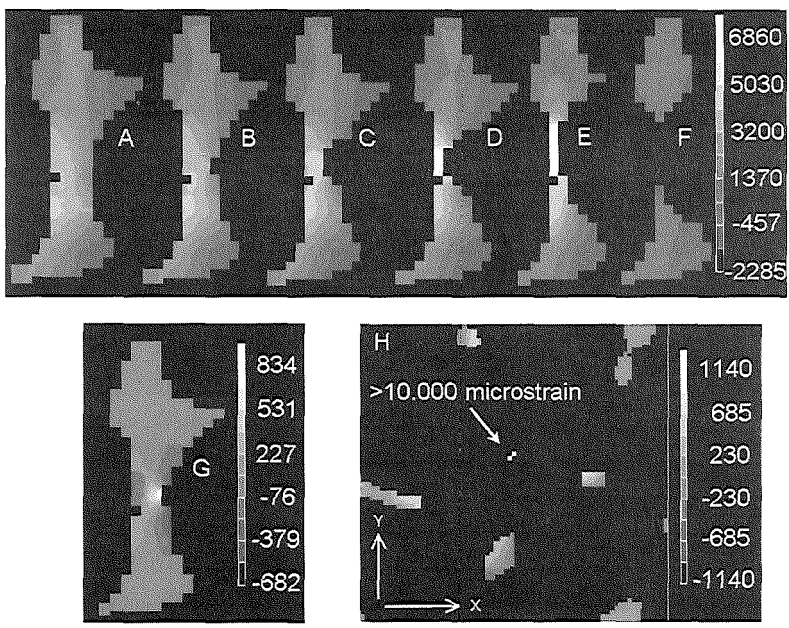

Figure 3.5: Resorption cavity in trabecula that was aligned with the main in vivo loading axis, in the middle of vertebral specimen F80. The thickness of this trabecula was approximately 120μm, resorption depth increased from A to F: A:0μm, B:28μm, C:56μm, D:84μm, E:84μm (wider cavity), F: disconnected. Figures A-F show strains in the superior-inferior direction, in microstrain. G: Changes in strain caused by the small cavity shown in figure B, in microstrain. A decrease in strain is shown in blue, an increase in yellow. H: One horizontal slice of the surroundings of the resorbed vertical trabecula, showing the difference in strain between the original configuration and figure E.

imately 4000 microstrain (Figure 3.5A). A small cavity as shown in Figure 3.5B caused an increase in strain of approximately 1000 microstrain at the bottom of the cavity, and a small decrease in strain near the rim of the cavity. These changes

in strain are shown in Figure 3.5G. With increasing resorption depth the strain in the resorbed trabecula increased further. The neighboring trabeculae gradually took over the load, and the load transferred through the resorbed trabecula decreased. In the 5th step (3.5E) extreme values, above 10,000 microstrain occurred in the resorbed trabecula. At this point, the load transferred through this trabecula was decreased by 25%. In step 6 (disconnection, Figure 3.5F) the strains in the surrounding trabeculae were approximately 1000 microstrain higher than in the original configuration (Figure 3.5H).

In the horizontal trabecula the strain in the initial configuration was significantly lower, the maximum value was only slightly higher than 1000 microstrain. The resorption cavity in this trabecula had only small effects, no extreme strain values were found. The strain in this trabecula doubled, and the load transferred through this trabecula decreased. The strain distribution in this trabecula with increasing resorption depth is shown in Figure 3.6. In the third step, the load trans-

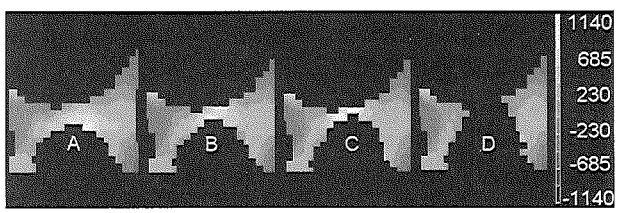

Figure 3.6: Resorption cavity in a horizontal trabecula, perpendicular to the main in vivo loading axis, in the middle of the vertebral specimen. The thickness of this trabecula was approximately 120 (m. Resorption depth increases from A to D: A: 0μm, B: 28μm, C: 56μm. In D the trabecula is disconnected. Strains in longitudinal direction in initial situation (A) and after several stages of resorption (B-D) are shown (in microstrain).

ferred through this trabecula was decreased by approximately 20%. However, the strains in the neighboring trabeculae were almost unaffected because the load transferred through this trabecula was 7 times smaller than the load transferred through the vertical trabecula.

3.5 Discussion

In this study we used computer simulation models to analyze how apparent level strains are resolved into local tissue level strains in trabecular bone specimens. Several bone loss scenarios were simulated in order to determine the changes in tissue level strains and mechanical properties. Although we have analyzed only a few specimens we assume that these reveal some general concepts. We used specimens from male and female donors of different ages, and these samples showed similar results.

The calculated tissue level strains were on average lower than the applied apparent strains, and in the same range as experimentally measured strains in cortical bone [6, 22]. This indicates that trabecular bone can deform heavily without high strains at the tissue level. Small amounts of bone loss at highly strained locations completely deteriorated the mechanical properties, while severe bone loss at locations of low strains (up to 50% of the bone volume) had only small effects. This shows that cancellous bone has a large safety factor for bone loss, as long as the bone is not lost at highly strained locations. Resorption cavities caused large local increases in strain and a redistribution of the load over the trabeculae. The load transferred through the resorbed trabecula was decreased by up to 25%, the strains in the surrounding trabeculae were increased by up to 1000 microstrain. Combining these results, we can conclude that resorption cavities at locations of high strain have deleterious effects on the stiffness of trabecular bone.

The models used in this study represented the three dimensional architecture of human cancellous bone, the elements were small enough to allow accurate calculation of global mechanical properties and strain distributions using cubic brick elements [75, 169, 174, 175, 176]. Since we investigated small deformations, the behavior of the bone matrix could be considered linear. However, matrix properties at the microstructural level, such as microdamage and the lamellar structure of the bone matrix, were not incorporated in our models. Therefore, the present computer models are only suited to investigate the effect of architectural changes. A disadvantage of the use of cubic elements is the jagged representation of the surface of the trabeculae. This may cause errors in the interpolated stresses and strains at the surfaces. However, since most of the strains in the cross-sectional views are internal values and because we have not found extreme gradients in the strain values near the surfaces of the trabeculae, we do not feel that the errors caused by the jagged surfaces substantially affected our findings.

Recently, a technique to determine strains in trabecular bone experimentally was developed [4]. X-rays or CT-scans of trabecular bone specimens are made in loaded and unloaded situation and the strains in the trabeculae are determined using texture correlation. The advantage of this method, compared to finite element models, is that no assumptions about the tissue mechanical properties have to be made. In finite element simulations changes in the architecture can easily be studied, by changing the architecture in the model. The strain values found with these techniques can not be compared directly, because different specimens were used. However, the output of both experiments is in the same range, and both techniques result in similar skewed strain distributions.

The finite element technique used in this study can be used to calculate strains in whole bones [174]. In the present study, we choose to calculate the strains in a smaller specimen, enabling the study of several bone loss scenarios within a reasonable amount of computing time. The strains found in the whole femur [174] were slightly lower than the strains found in the present study. This was probably

caused by the cortical shell around the trabecular bone that was included in the whole bone model. This shell might enable a more homogeneous distribution of the load over the trabeculae, resulting in a narrower strain distribution and a lower average strain.

The question has been raised in the literature why the small increases in bone mass that result from bisphosphonate, calcitonin or SERM treatment of osteoporotic patients result in large reductions of fracture risk [38, 147]. This reduction in fracture risk could not be explained by the small increases in bone volume of 5 to 8% after 1 to 3 years alone [71, 95, 180, 32]. Hence, it has been concluded that either the architecture improves considerably or the matrix tissue strength increases. Recently, the relation between increase in BMD and decrease in fracture risk was assessed using a compilation of data from a large number of studies [181]. A high correlation between increase in BMD and decrease in fracture risk was found. This supports the idea that the extra bone mass resulting from anti-resorptive treatment is deposited where it is mostly needed, so that a small increase in bone mass can largely reduce fracture risk.

In this study, we showed that resorption cavities caused large decreases in stiffness, and strain peaks at the bottom of the cavities. A decrease in the number of cavities would decrease the number of strain peaks, a decrease in depth of the cavities would decrease the strain at the bottom of the cavities. The known reduction in activation frequency and resorption depth that results from anti-resorptive treatment [153] results in smaller cavities, which are more widely separated. This could result in a rather large increase in the stiffness, and therefore also in strength of the bone [143], as can be concluded from the present finite element simulations.

Using the simulation results, we can gain insight into the influence of microdamage on bone remodeling. Increased bone resorption in damaged regions has been shown in cortical bone [21]. Under strenuous conditions, strains up to 5000 microstrain have been measured in animals and humans [6, 22]. From the calculated strain distributions in this study, we expect strains higher than 10,000 microstrain to occur in some trabeculae under strenuous conditions. These strain values can cause damage in the bone matrix [23]. If remodeling is induced by microdamage, this remodeling process would start by resorption of the damaged tissue by osteoclasts. In the first experiment we showed that removal of 4% of the bone volume at highly strained locations, which are likely the damaged regions, significantly deteriorated the structure. In normal physiology, approximately 15 to 20% of the trabecular bone is remodeled each year [65]. In combination with a duration of the remodeling cycle of 3 to 6 months, this yields that approximately 5% of the bone volume is undergoing remodeling at any timepoint [47, 56]. Thus, it seems unlikely that osteoclasts resorb only damaged tissue. The cancellous bone structure would be continuously at risk for failure. Furthermore, the remodeling rate of the vertical trabeculae would be higher, because strains in vertical trabeculae under physiological loading are higher than strains in horizontal trabeculae, as shown in

the present study. The formation deficit would result in thinning of the vertical trabeculae, with the horizontal trabeculae staying the same. In general, the opposite is found: the vertical trabeculae are conserved, while horizontal trabeculae are thinner, or even completely resorbed in old bone [106].

Another topic of great interest is the coupling between osteoclast resorption and osteoblast formation. At cellular level, osteoblasts control osteoclast activity by RANKL and its decoy receptor osteoprotegerin [184], but location specific coupling remains to be explained. Increases in strain at the bottom of a resorption cavity were shown in a simplified, cylindrical model of one trabecula [156]. If osteoblasts were activated by high strains, an automatic coupling would occur. In this study, we showed small increases in strain caused by a resorption cavity in a horizontal trabecula, in contrast to large increases in a vertical trabecula. A resorption cavity in a vertical trabecula also increased the strain in surrounding trabeculae (Figure 3.5H). This could induce bone formation on the surrounding trabeculae. This effect, apposition of bone matrix on trabeculae without previous resorption has been shown in experimental studies [46, 28]. This would decrease the load in the resorbed trabecula, and slow down the bone formation in the cavity. Thick trabeculae would become thicker and thin trabeculae might completely disappear, which is in agreement with histological findings [178]. In real bone, numerous resorption cavities play a role, leading to a more complex system [182]. Insight into this phenomenon could be obtained from finite element analyses in which bone remodeling is simulated as a dynamic feedback system [111, 157].

In conclusion, this study provides insight in the mechanical consequences of the bone remodeling process. This process is needed to maintain the trabecular architecture and to prevent damage accumulation, but it results in bone loss after peak bone mass has been reached. We have shown that the location of bone loss largely determines the mechanical consequences. From this we conclude that not all remodeling can be initiated at locations of high strains, the structure would be at risk for failure if all strained bone matrix was resorbed at the same time. These results support the idea that non-targeted remodeling, for e.g. calcium-homeostasis [130], plays a role in the remodeling process. The large fracture risk reduction that results from a small increase in bone mass in anti-resorptive treatment can be understood from the strain increase caused by resorption cavities. Deep resorption cavities cause extremely high strains in the resorbed trabeculae. These large local increases in strain could explain the location specific coupling between resorption and formation in the remodeling process. In addition the increased strain in the trabeculae surrounding a resorption cavity may induce bone formation on these trabeculae. The known decrease in osteoclast activity and cavity size that results from anti-resorptive treatment [153] will result in a drastic decrease of the strains at the bottom of the cavities, and a large increase in the stiffness of the bone. In this study we have shown that knowledge of the strain distribution at tissue level can help to explain the complex dynamics and mechanical effects of the bone

remodeling process.

3.6 Acknowledgements

The micro-CT scans of the vertebral specimens used in this study were kindly provided by Prof. P. Ruegsegger and were obtained as part of the European union biomed 1 project "Assessment of bone quality in osteoporosis" [39]. J.C. van der Linden was supported by the Dutch Foundation for Research (NWO/MW), the research of H. Weinans was made possible by a fellowship from the Royal Dutch Academy of Sciences (KNAW). Computing facilities were provided by the Dutch National Computer Facilities Foundation (NCF)

Chapter 4

A model at trabecular level to predict effects of anti-resorptive treatment after menopause*

J.C. van der Linden
J.A.N. Verhaar
H.A.P. Pols
H. Weinans

*submitted

4.1 Abstract

Anti-resorptive treatments are widely used to prevent osteoporotic fractures in men and women. Large clinical trials have shown vertebral fracture risk reductions up to 50%, resulting from relatively small increases of 3-8% in bone mineral density (BMD). In order to try to explain this large decrease in fracture risk we developed a computer model that mimics bone turnover in human vertebral cancellous bone during menopause and anti-resorptive treatment. This model links cell activity in trabeculae to changes in bone volume and mechanical properties of cancellous bone.

The predicted bone volume changes corresponded well to clinical BMD data. We found that the increased turnover during menopause must be transient, otherwise we can not explain the reduced rate of bone loss seen from 5 to 8 years after the start of the perimenopausal period.

We also compared the effects of anti-resorptive treatment started early and late. The long-term difference in bone volume between early and late treatment was only 2%. The difference in stiffness was considerably larger. Late treatment resulted in large increases in mechanical anisotropy of the cancellous architecture and decreases in transversal stiffness of up to 22%.

The effect of the incorporation of bisphosphonates in the tissue was small. After discontinuation of treatment bone was lost slower, but after 20 years the difference between the incorporated and the not incorporated drug was below 2% of the bone volume. This kind of simulation models may be used in the future to preclinically test new pharmaceuticals and treatment protocols and to predict long-term effects before patient data become available.

4.2 Introduction

Pharmacological agents that reduce bone resorption by osteoclasts are nowadays widely used in osteoporosis treatment. These anti-resorptive agents primarily increase bone mineral density (BMD) by reducing osteoclast activity and bone turnover [31, 150, 177]. In the first three years of treatment, fast increases in spinal BMD of 2-8% have been reported and ongoing slow increases up to 7 years after start of treatment have been shown [50, 166]. Anti-resorptive treatments reduced vertebral fracture risk by up to 50% [11, 50, 95, 133, 138]. This large reduction can, however, not be explained by the small increases in BMD [32].

The most important effects of anti-resorptive treatment take place in cancellous bone [144]. However, DXA and biochemical markers of bone turnover do not provide information about changes in architecture and stiffness of cancellous bone. More knowledge about the relation between the effects of anti-resorptive treatment at trabecular level and changes in global properties of cancellous bone could elucidate the large anti-fracture effects resulting from small increases in BMD.

In this study we used a computer model of cancellous bone remodeling, which we published previously [171]. This model uses three dimensional (3D) reconstructions of human cancellous bone created using micro-computed tomography (micro-CT) scans and remodeling parameters known from histology. The model links cellular activity at the trabecular level to changes in architecture and strength of cancellous bone. For the present study the model was extended, to enable simulation of menopause and anti-resorptive treatment. Small differences between treatments, of which it is difficult to predict the effect in patients, can be considered in detail in this model. Although simulations of the global effects of menopause on bone volume have been done [67, 112, 163, 164], this is (to our knowledge) the first simulation of postmenopausal bone loss and subsequent treatment that mimics bone resorption and formation in models of human cancellous bone that represent the 3D cancellous architecture. We simulated menopause and treatment with three types of anti-resorptive agents. Specifically, we compared the effects of treatment started early and late on bone volume and mechanical stiffness, which is highly correlated to strength of the bone. These models may be useful to preclinically test new pharmaceutical interventions and to predict treatment results many years before the patient data become available.

4.3 Methods

In order to develop our model we used a specimen from an autopsy L4-vertebra of a 37-year old donor. This donor was part of the European Union BIOMED1 project "Assessment of Bone Quality in Osteoporosis" and did not suffer any osteoporotic fractures. Using a micro-CT scanner (Scanco Medical, Zurich, Switzerland) a 3D reconstruction of the cancellous architecture was obtained (Fig.4.1a). This

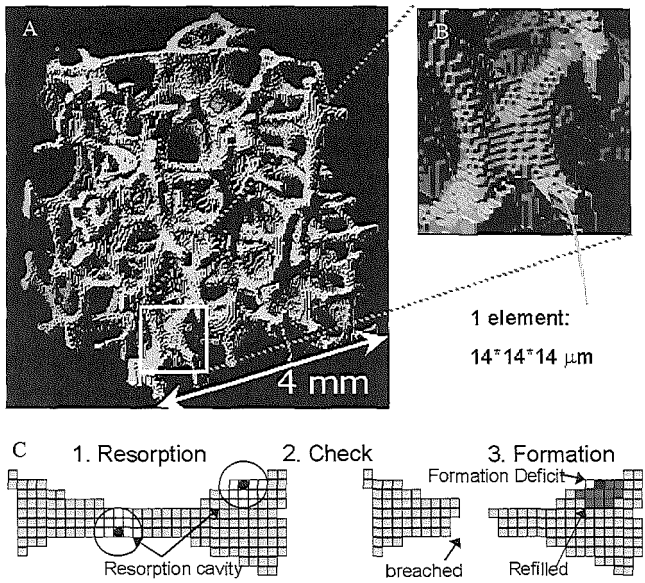

Figure 4.1: A: Three dimensional reconstruction of $4 \times 4 \times 4$ mm cancellous bone, made using a micro-CT scanner. B: Detail of the reconstruction shown in Figure A. All elements are cubes with a sidelength of 14μm. C: Two-dimensional representation of the three steps of the remodeling process performed in three dimensions in this study.

reconstruction was segmented to a model of $4 \times 4 \times 4$ mm cancellous bone, with cubic elements of $14 \times 14 \times 14\mu$m. The bone volume fraction was 12.9%.

We extended a previously presented model of bone remodeling [171] to simulate menopause and anti-resorptive treatment. In short: in step 1 spherical resorption cavities with a specified depth were created in a computer model of cancellous bone, randomly distributed over the surface of the trabeculae. In step 2 it was checked whether resorption cavities breached trabeculae. Cavities that breached a trabecula were not refilled, which resulted in permanent bone loss. All other cavities were refilled in step 3, except for one or more surface elements, which were removed from the model in order to simulate the formation deficit (Fig.4.1c). By repeating these three steps ongoing physiological remodeling was simulated.

In the extended model these remodeling parameters could be changed gradually during the simulation:

- the number of resorption cavities made by osteoclasts
- the depth of these cavities, called resorption depth
- the bone balance per cavity. A negative balance is called a formation deficit: osteoblasts make less bone than osteoclasts resorbed and bone is lost. A

positive bone balance we call a formation surplus: osteoblasts make more than osteoclasts resorbed and bone volume increases

Bone tissue deposited during simulated drug treatment was marked as drug-containing tissue, because it has been shown that bisphosphonates are mostly incorporated in active resorption cavities [154]. If the incorporated bisphosphonate decreased bone resorption, cavities made in bisphosphonate-containing tissue were less deep. The simulations were performed on an SGI Origin3800, 25 years of simulated remodeling took approximately 25 minutes of one CPU.

Development of model of menopause

The model of menopause was based on rates of bone loss and turnover of cancellous bone during the perimenopausal period from clinical and biological studies. This input was obtained from studies that used histomorphometry, bone remodeling markers in serum or urine and measurements of BMD and calcium balance.

Two histomorphometry studies showed that the bone formation rate in postmenopausal women was a factor 1.1 to 2 higher than in premenopausal women [65]. Several studies showed increases in bone remodeling markers over menopause, varying from 30 to 150 % [59, 135]. An increase in these markers indicates an increase in bone remodeling, but the exact changes in bone remodeling are not known [51]. Some studies showed elevated marker levels long after menopause, but the rate of bone loss decreases after the perimenopausal period [59, 135]. Measurements of calcium balance have shown that Ca resorption was increased more than Ca accretion in the first menopausal years, which corresponds to a negative bone balance and a larger formation deficit in the perimenopausal years [66].

Bone loss during the menopausal transition was determined using BMD measurements in a number of studies [101, 121, 134, 135]. Before menopause, these showed small bone losses, typically less than 1%/year. These studies showed that bone loss begins before the last menses and reaches a maximum during the perimenopausal period of 2.3 - 3.8%/year on average. After this fast loss, bone loss decreases and becomes very small during the 5th - 8th postmenopausal year, in one study not even significantly different from zero [101]. Finally, bone loss increases again to values similar to or slightly higher than the premenopausal bone loss rate. The rate of bone loss showed a wide biological variation. For example, the maximum rate of bone loss varied between 0.3 and 6% per year.

Using this information, we made a simulation model of menopause. We varied several parameters, as described in detail below, to investigate the sensitivity of the model to changes in these parameters. In order to explain how this model was developed, we included some intermediate results in this methods section. The model started with normal remodeling [171]. Remodeling space, the amount of bone resorbed but not yet replaced at any timepoint, was 4 or 6% of the bone volume [54, 126]. Resorption depth was 42μm [30], the formation deficit was

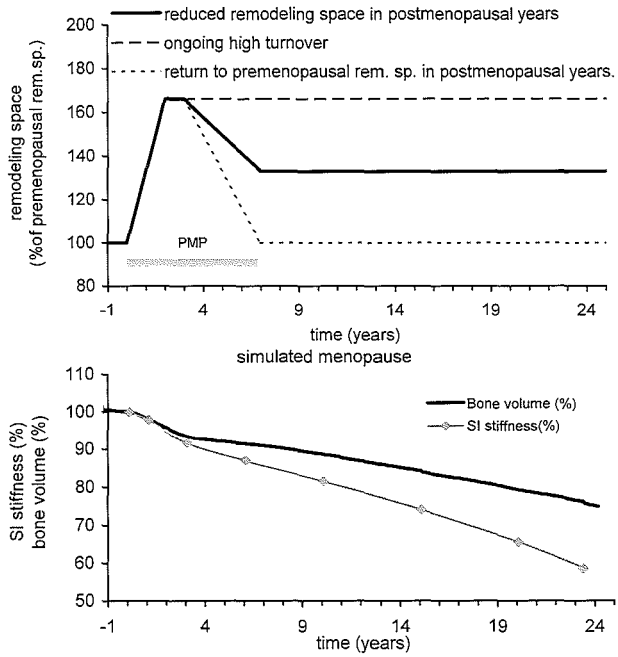

Figure 4.2: A. Change in the remodeling space during simulated menopause, in the case of an increase during the perimenopausal period (PMP in the figure) of 66%. B. Changes in bone volume and stiffness during simulated menopause according to the continuous line in Fig. A.

3.6% of a cavity [54]. This resulted in rates of bone loss in the premenopausal period of 0.6% (rem.sp.4%) and 1% (rem.sp.6%) of the bone volume per year. In order to simulate the increased remodeling rate during the perimenopausal years, we increased the remodeling space by 33, 66 or 100%, using the increases in bone remodeling markers as a guideline (Table 4.1).

Bone turnover was increased over a period of 2 years, because clinical studies showed that the rate of bone loss increases over a period of 2 to 3 years in the perimenopausal period [135] (see Fig.4.2a). Besides this, we increased the formation deficit during the perimenopausal years, in order to mimic the more negative bone balance during the perimenopausal years. The resulting rates of bone loss during the high turnover in the perimenopausal period are shown in table 4.1.

All these rates of bone loss are within the range of rates of bone loss measured in perimenopausal women [101, 121, 134, 135]. Ongoing turnover at the high remodeling rate (dashed line in Fig.4.2a), resulted in complete destruction of the bone architecture within 10 - 30 years. Although some bone marker studies showed elevated bone marker levels long after menopause [59, 135] the fast de-

Table 4.1: Rates of bone loss during the perimenopausal years. Premenopausal remodeling space was 4 or 6%, turnover in the perimenopausal period was increased as shown in the table. (rem.sp.=remodeling space, form.def.=formation deficit)

Premenopausal rem. sp.	4% of bone volume	6% of bone volume
Changes during	resulting rates of bone loss	
perimenopausal period	(% of bone volume/year)	
rem. sp. + 33%	1.25	2
rem. sp. + 66%	1.9	3
rem. sp. + 100%	2.5	4
rem. sp. + 33% and form.def. doubled	1.8	3
rem. sp. + 66% and form.def. doubled	2.6	4
rem. sp. + 100% and form.def. doubled	3.3	5

struction of the bone architecture is not in agreement with the BMD data, which showed a decrease in the rate of bone loss. Therefore, we decreased bone turnover in our simulation. The remodeling space was returned to the premenopausal value (Fig.4.2a, dotted line), or the remodeling space was decreased to a value in between the pre- and the perimenopausal remodeling spaces (Fig.4.2a, continuous line).

Again, all rates of bone loss resulting from these parameter settings were in the biological range. The simulation results show that input values for our simulation model in the biological range result in bone loss rates in agreement with BMD-studies. To simulate the effects of anti-resorptive treatment, we choose a model of menopause, which corresponded to the average rate of bone loss determined with BMD measurements during the perimenopausal period. We do not claim that the numbers used in this simulation correspond exactly to changes during the menopausal transition, we show that this simulation model, which is based on biological data, corresponds to rates of bone loss seen in clinical studies. The change in bone volume with age resulting from this menopause model is shown in Figure 4.2b. In this model, the premenopausal remodeling space was 4%, the remodeling space increased by 66% and the formation deficit doubled in the perimenopausal period.

The decrease in stiffness of the specimen in the load-bearing direction was calculated using finite element analyses [175]. The finite element-calculated stiffness is a good predictor of the strength of cancellous bone [77]. The stiffness of a material is a measure of its deformation under load. The stiffness can be determined in a compression test and is calculated as stress (force per unit of area) divided by strain (deformation in % of original size). In the finite element analysis a compression test is simulated and the stiffness of the bone is calculated numerically.

Simulation of anti-resorptive treatment

Using the model of menopause, we investigated the effects of three types of drugs on bone volume and stiffness of the cancellous bone. The effects of these drugs were based on the effects of anti-resorptive drugs described in literature, such as a decrease in resorptive activity of osteoclasts [154, 177], an anabolic effect on osteoblasts [84, 140] and a decrease in remodeling rate [177].

The first drug was incorporated in the bone tissue, as has been described for bisphosphonates [154]. Cavities made in drug-containing tissue were less deep. Besides this, the formation deficit was changed to a formation surplus and the number of cavities was decreased. The changes in remodeling during treatment are summarized in table 4.2. The second type of drug was not incorporated, as is the case in e.g. estrogen treatment. All cavities created during treatment with this drug were less deep, the number of cavities was decreased and the formation deficit was changed to a formation surplus, as shown in table 4.2. The third drug had a moderate effect on the bone remodeling, as is for example the case in raloxifene treatment. The decrease in number of cavities was only 25% and bone formation was equal to resorption. Five years of simulated treatment were started early (1 year after the start of the perimenopausal period), or late (10 years after the start of this period).

The effects of the treatment regimens on bone age, volume and stiffness were determined. For clarity, the three types of drugs will be called 'bisphosphonate', 'estrogen' and 'raloxifene' from here on. However, we do not claim that the changes in remodeling parameters in these simulations are exactly representative for bisphosphonate, estrogen and raloxifene treatment.

Furthermore, the simulation results were compared to clinical BMD data. Strictly speaking, these can not be compared directly. BMD, as measured by DXA, is an areal density of bone mineral content, in the simulations we determine bone volume. Anti-resorptive treatment reduces bone turnover, which results in an increase in the age of the tissue and in the mineral content [13] in a process called secondary mineralization. This secondary mineralization was not incorporated in our model. Therefore, the comparison of simulation results and BMD is only an indication, the increase in areal BMD in reality may be higher than the increase in bone volume computed in our model.

4.4 Results

Simulation of menopause

Using input parameters derived from biological data, we can simulate the bone loss during the menopausal transition in accordance with the bone loss seen in

Table 4.2: Remodeling parameters during and after simulated anti-resorptive treatment with a drug that was incorporated in the tissue ('bisphosphonate'), a drug that was not incorporated ('estrogen') and a drug with moderate effects('raloxifene').)

		Drug incorporated in tissue ('bisphosphonate')	Drug not incorporated in tissue ('estrogen')	Drug with moderate effects ('raloxifene')
During treatment	Resorption depth	Decreased for cavities in bisphosphonate-containing tissue (42 to 28μm)	Decreased for all cavities made during treatment (42to 28μm)	Decreased for all cavities made during treatment (42 to 28μm)
	#resorption cavities	-50%	-50%	-25%
	Formation surplus	+5%	+5%	0
After treatment	Resorption depth	Decreased for cavities made in bisphosphonate-containing tissue (42 to 28μm)	Returned to normal for all cavities (28 to 42 μm)	Returned to normal for all cavities (28 to 42 μm)
	#resorption cavities	Return to untreated	Return to untreated	Return to untreated
	Formation surplus	Return to untreated	Return to untreated	Return to untreated

BMD studies. Ongoing high turnover resulted in ongoing fast bone loss to such an extent that the bone architecture was destroyed within 30 years. A decrease in the excess remodeling space created in the perimenopausal period resulted in a postmenopausal rate of bone loss in accordance with clinical studies.

From these results we conclude that the remodeling rate reaches a maximum during the perimenopausal years and decreases thereafter. From our simulation we can not determine whether remodeling rate returns to the premenopausal remodeling rate or stays elevated, both resulted in rates of bone loss in the biological range. However, because most clinical studies indicate that the postmenopausal remodeling rate is higher than the premenopausal remodeling rate, we included this in our menopause model. The transient increase in turnover resulted in loss of 12% of the bone volume 10 years after menopause (Fig.4.2b). This is in the range of reported clinical data [121, 135]. In this simulation, the stiffness decreased 2% in the first year of high turnover and was decreased by almost 35% 20 years after the start of the perimenopausal period (Fig.4.2b).

Table 4.3: Increases in stiffness (in %) in the superior-inferior direction (SI) and transversal directions after 5 years of simulated estrogen (es), bisphosphonate (bis) or raloxifene (ral) treatment started early or late, compared to the untreated case.

	early			late		
	es	bis	ral	es	bis	ral
SI	14	14	7	13	13	6
transv.	26	26	15	20	18	11

Table 4.4: Difference between early and late treatment (in %) in stiffness 20 years after the start of the perimenopausal period.

	es	bis	ral
Stiffness SI	9	6	2
Stiffness transv.	22	15	8

Simulation of anti-resorptive treatment

Simulated estrogen treatment resulted in a fast increase in bone volume, up to 5% after 5 years of treatment. Simulated bisphosphonate and raloxifene treatment resulted in increases of 4 and 0.5%. The increase in bone mass was slower in the case of bisphosphonate treatment, because this drug only reduced resorption depth when it was incorporated in the tissue. Because of this, the effect became larger as more cavities were refilled during simulated treatment. Stopping simulated estrogen treatment resulted in faster bone loss than stopping simulated bisphosphonate treatment (Fig.4.3), because the bisphosphonates incorporated in the tissue still exerted a protective effect. This is in agreement with clinical data on spinal BMD [122, 158].

The increases in stiffness in the transversal directions were larger than in the main load bearing (superior-inferior) direction (Table 4.3). Between 1 and 10 years after start of menopause 9% of the bone volume was lost (Fig.4.2b). However, 20 years after the start of the menopausal transition the difference in bone volume

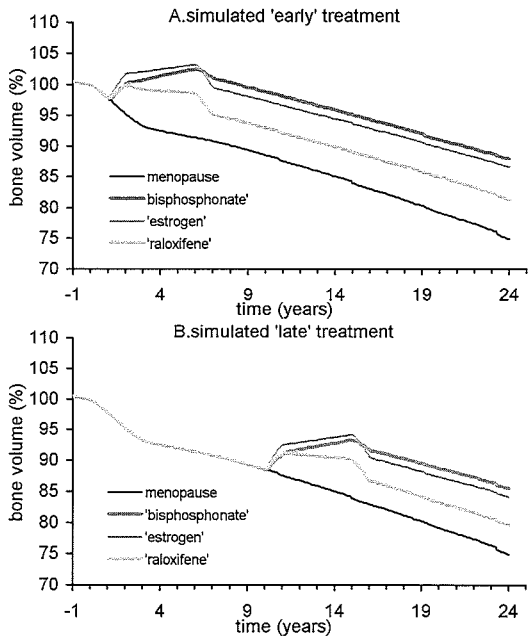

Figure 4.3: A: Effect on bone volume of three types of drugs, which resembled bisphosphonate, estrogen and raloxifene started 1 year after the start of the perimenopausal period. B: Effect on bone volume of the same three types of drugs as shown in Fig A, started 10 years after the start of the perimenopausal period.

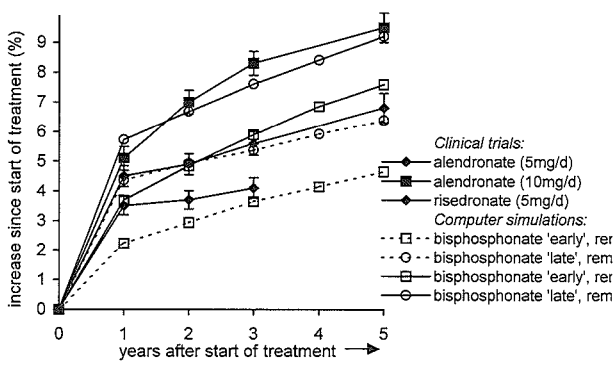

Figure 4.4: Comparison of clinical BMD measurements and simulation results. Shown is the increase relative to the bone mass at the start of treatment. (Alendronate data[166], risedronate data[52])

between early and late treatment was only 3% (Fig.4.3). The difference in stiffness was considerably larger, as shown in table 4.4.

The increases in bone volume in the simulations were in the range of increases in BMD seen in clinical studies. This is shown graphically for bisphosphonate treatment (Fig.4.4).

Simulated anti-resorptive treatment increased the mean age of the tissue by 9 to 13% 20 years after the start of the perimenopausal period.

4.5 Discussion

In this study, we developed a computer simulation model of human vertebral cancellous bone remodeling, which mimics bone turnover during menopause and anti-resorptive treatment. This model predicts changes in bone volume and global stiffness of cancellous bone based on biological input data. To our knowledge, this is the first computer model that incorporates remodeling parameters in 3D cancellous bone models to predict changes in bone volume, age and stiffness resulting from menopause and subsequent drug treatment.

The rate of bone loss resulting from the bone remodeling process depends on the remodeling space, the formation deficit and the duration of the remodeling cycle. These parameters are not exactly known, because they can not be measured directly in bone specimens. Instead, these parameters have been estimated by derivation from other, measurable, parameters [54, 126]. On the one hand, this is a limitation for computer simulation models, because estimated values must be used instead of directly measured values. On the other hand, this is exactly the power of this type of models: the estimated values can be incorporated in the simulation model, and by comparing the output of the model to changes observed in reality, it can be shown whether the parameter values were realistic. The changes in bone volume in our simulation model, which are in good agreement with biological data, indicate that the remodeling parameters we used were in the biologically relevant range.

We analyzed how sensitive our model was to changes in the remodeling parameters. Remodeling spaces of 3 to 6% resulted in changes in bone volume within the biologically relevant range, with remodeling spaces of 4 or 5% resulting in changes in bone volume according to the average BMD changes reported in literature. A variation in the periods over which the rate of turnover in our model was changed during the perimenopausal years had only small effects. Increasing bone remodeling over a period of 1, 2 or 3 years, and decreasing over a period of 3, 4 or 5 years resulted in variations of bone volume of less than 3% from 10 to 20 years after the start of the perimenopausal period. Obviously, the remodeling parameters that we used for the simulation model of menopause also affect the simulations of treatment. For example, increasing the formation deficit or the remodeling space

during simulated menopause changed the bone mass that could be reached during the anti-resorptive treatment. However, changing these parameters did not change our conclusions about the difference between the incorporated and the not incorporated drug, early and late treatment and the gain in stiffness in transversal and longitudinal directions.

According to our simulation model, the bone turnover rate decreases after the perimenopausal years. Previously, a decrease in turnover after menopause [44], as well as elevated turnover up to 40 years after menopause [59] have been shown. Our results show that ongoing high turnover would result in an unrealistic total destruction of the bone within 10-30 years after menopause. The decrease in turnover in our simulation resulted in changes in bone volume in agreement with BMD data from clinical studies [101, 121, 135]. Our simulations indicate that the reduced rate of bone loss 5 to 8 years after the start of the perimenopausal period is not a result of equal bone resorption and formation, but of a partial refilling of the excess remodeling space created during the perimenopausal period. In our model, postmenopausal turnover equal to the premenopausal remodeling rate, as well as postmenopausal turnover at a rate in between the pre- and the perimenopausal remodeling rate resulted in changes in bone volume in agreement with clinical BMD data. This might reflect the difference in turnover between subjects with normal bone loss and those who will develop osteoporosis [59].

Simulated anti-resorptive treatment resulted in changes in bone volume in agreement with clinical data [52, 166]. We showed increases in stiffness, which were larger than the increases in bone volume. Moreover, the anisotropy of the cancellous architecture changed: the transversal stiffness increased more than the stiffness in the main load bearing direction. In a fall, the bones are often not loaded in the main load bearing direction, but more in the transversal directions. Because stiffness and strength of cancellous bone are highly correlated [77] the large increase in transversal stiffness could contribute to the large anti-fracture effects of small increases in BMD. Moreover, the reduced turnover during treatment results in an increase in the average age and mineral content [13] of the bone tissue, which leads to a concomitant increase in stiffness [34]. In the simulations we determined the age of the bone tissue, but the relation between age and mineral content of bone tissue is not well known. Therefore, we presented the results as changes in bone volume, rather than BMD. A constant bone volume in our simulation model could correspond to a slow increase in BMD due to prolonged mineralization in reality. This would increase the stiffness of the cancellous bone even more than our model predicts.

Like all simulation models, this model is a simplification of reality. In reality resorption and refill of a cavity take several weeks, in the simulation cavities are either completely resorbed or completely refilled. This has, however, no effects on the long-term changes in bone volume and stiffness [171]. As input for our model we used a specimen from a male donor of 37 year to show that bone remodeling

and treatment can be simulated in our model. It has been shown that at this age there is no significant difference in vertebral cancellous bone volume fraction and mechanical properties between males and females [102, 107]. Besides this the effects on bone of anti-resorptive treatment in osteoporotic men and women are similar [166]. Furthermore, it has been shown that the differences between specimens in simulation outcome are rather small [171]. Finally, the effects of mechanical loads on the bone structure were not taken into account. Mechanical loading does affect bone remodeling, but the exact mechanisms are not known. A 3D simulation of bone remodeling as presented here, which also includes the effects of mechanical loads, is not feasible at the moment, but less detailed simulations and simulations in 2D have been performed [78, 109]. As computer technology develops further and the effect of loading on remodeling is better understood, such a detailed simulation will be possible in the future.

Most clinical studies have been performed in osteoporotic patients or in patients who were postmenopausal for at least 2 years [11, 50, 52, 166]. Here, we investigated the difference between treatment started 'early' and 'late' (1 and 10 years after the start of menopause). Late treatment resulted in an approximately 3% lower bone volume, a 2-9% lower stiffness in the main load bearing direction and an 8-22% lower stiffness in transversal directions than early treatment, 20 years after menopause. This indicates that late treatment can result in almost the same bone mass as early treatment, but irreversible loss of stiffness occurs. Furthermore, the long-term effect of incorporation of bisphosphonates in the bone tissue is small. Discontinuation of simulated bisphosphonate treatment resulted in a slower bone loss than discontinuation of estrogen treatment, but 20 years after menopause the difference in bone volume was less than 2%.

Heaney et al. [67] performed a mathematical fit of changes in remodeling to increases in BMD in alendronate treatment [95]. A decrease of 36-38% in newly created cavities and a positive bone balance of 1% of the bone volume per year resulted in a good fit. In this study, we showed that a reduction in number of cavities of 50% and a positive bone balance of 5% per cavity resulted in increases in bone volume in the range of increases in BMD in clinical studies (Fig.4.4). By varying the remodeling parameters, we could get a closer correspondence to the clinical results. However, our aim was not to make a fit to clinical data, but to develop a model that links bone remodeling at trabecular level to changes in global properties of cancellous bone and that enables comparison of different drug treatment protocols.

Taken together, the presented model mimics bone remodeling during menopause and anti-resorptive treatment, and predicts changes in bone volume in agreement with data from clinical follow-up studies. We found that the rate of bone turnover reaches a peak during the perimenopausal years and probably decreases thereafter. Estrogen treatment resulted in faster bone volume increases than bisphosphonate treatment, but on the long term the simulated effects of these agents were virtually

equal. However, during the first years after discontinuation of treatment, bisphosphonates incorporated in the tissue still exerted a protective effect. It might be possible to take advantage of this by applying intermittent treatment [145]. The presented model could be used as a guideline for the development of such treatment regimens. Moreover, simulation models of biological systems, like the one presented here, may be used in the future to predict the effects of drug treatments before patient data become available.

4.6 Acknowledgements

J.C. van der Linden was supported by the Dutch Foundation for Research (NWO/MW), the National Computing Facilities Foundation (NCF) provided computing time. The authors thank Prof. Peter Ruegsegger for providing the CT-scan data from the European Union project "Assessment of bone quality in osteoporosis".

Chapter 5

3D reconstruction of bone apposition

J.C. van der Linden
T. van Immerzeel
J.S. Day
J.A.N. Verhaar
H. Weinans

5.1 Abstract

Bone remodeling leads to changes in the cancellous bone architecture with age. Trabeculae become thinner, plates are perforated and some trabeculae are resorbed. The mechanisms by which these changes in architecture are created are not exactly known. For example, it is not known whether bone remodeling occurs more frequently on horizontal than on vertical trabeculae or maybe random throughout the structure.

In order to investigate this, we built a setup for three dimensional reconstruction of bone specimens, including the locations of recent bone apposition, which are labeled with fluorochrome labels. This setup consisted of a sledge microtome, a fluorescence microscope and a digital camera. The setup was automated by computer software and electronics.

Using this setup, we reconstructed 4 labeled dog vertebral bone specimens. We found that bone remodeling occurs slightly more on transversal trabeculae than on trabeculae aligned in the main load bearing direction, when the bone volume fraction is high. This might explain the changes in architecture with age: a more frequent remodeling of transversal trabeculae in combination with a formation deficit would lead to more thinning and loss of transversal than of aligned trabeculae.

5.2 Introduction

Disorders that affect the bone remodeling process can result in extremely high or low bone mass and changes in the architecture of cancellous bone. Moreover, even normal bone remodeling in healthy people results in a decrease of the bone mass with increasing age [107]. The osteoblasts make slightly less tissue than osteoclasts resorb, and trabeculae that are breached by resorption cavities are probably not repaired [108]. This leads to bone loss and an increase in anisotropy of the cancellous bone. Thin transversal trabeculae are resorbed, while trabeculae aligned in the load-bearing direction are mostly preserved. This is particularly clear if the bone mass is very low, like in osteoporosis [29].

It is clear that the changes in cancellous architecture result from the bone remodeling process, but the exact mechanism is not known. Several scenarios are possible. For example, it is possible that resorption occurs more frequently on transversal trabeculae than on trabeculae aligned in the main load bearing direction. This would result in thinning of transversal trabeculae by the formation deficit and almost no change in the aligned trabeculae. Another possibility is that resorption cavities are initiated on both aligned and transversal trabeculae, in combination with a smaller formation deficit in the aligned trabeculae because of higher stresses and strains in these trabeculae.

More knowledge on the spatial distribution of the resorption cavities in the cancellous architecture could elucidate the mechanisms that lead to the changes in cancellous bone with age. However, these questions can not be answered using techniques currently used in bone research. Using two dimensional sections of bone tissue labeled with fluorochromes, remodeling parameters have been determined in healthy and diseased bone biopsies in numerous studies. This technique gives information on the locations of bone remodeling, but not about the 3D cancellous architecture. Using micro-CT scans, three dimensional reconstructions of the bone architecture can be made, with resolutions up to 10 μm. This technique gives detailed information about the cancellous architecture, but not about the locations of fluorochrome labels.

In order to study the three dimensional distribution of bone remodeling, we made a setup for three-dimensional reconstruction of the bone architecture including fluorochrome labels. This setup consists of a sledge microtome, a fluorescence microscope and a digital camera. The computer-controlled setup automatically makes a stack of images from which we can reconstruct the 3D bone architecture including the locations of bone apposition.

The reconstructions can be used to study the spatial distribution of the apposition of new bone tissue in the cancellous architecture. Specifically, to investigate whether resorption cavities are distributed randomly over the surface of the trabeculae or located preferentially on vertical or horizontal trabeculae or on concave, convex or flat bone surfaces.

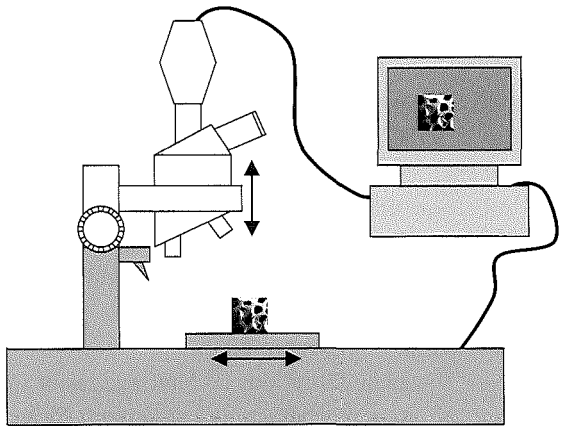

Figure 5.1: The computer controlled setup used in this study, consisting of a sledge microtome, a microscope and a digital camera.

5.3 Methods

The setup for automated sectioning was made using a sledge microtome (LKB 2259 Multirange Microtome), a fluorescence microscope (Nikon Optiphot 100S) and a digital camera (Coolsnap, RS Photometrics, 1392*1040 square pixels), as shown in figure 5.1.

The sledge with the bone specimen moves underneath the knife and a section of usually 10μm thick is made. The specimen moves back to the stop-position under the microscope and an image of the top surface of the block is made. This procedure is repeated until the desired number of images is made. The procedure is computer controlled, using Labview software (National Instruments) to control the camera and microtome. A linear potentiometer is used to measure the specimen position. This potentiometer is connected to the sledge with the specimen and the microtome. When the specimen is close to the desired stop position, the control over the sledge is switched automatically from the computer to an electronic circuit. This circuit enables real-time control of the sledge movement and stops the specimen at the desired position under the microscope. Using the electronic circuit, the stop position of the specimen could be reproduced within 5 μm.

The bone tissue and the labels can be distinguished in the same image. The tissue is autofluorescent, while calcein labels emit a brighter signal (see Fig. 5.2). When slices are used to study bone architecture and remodeling, the problem is that the slices are deformed. This problem does not occur when the images are made from the top surface of the block. However, the disadvantage of making images of the top surface of the block is that the light emitted from the labels shines

Figure 5.2: Image made from the top surface of the embedded bone specimen. left: original image, middle: segmented for bone, right: segmented for label.

through the bone tissue. Therefore, label in the bone tissue below the surface can be seen before it is actually sectioned.

We corrected for this effect using a deconvolution algorithm in Matlab (Matlab6, the Mathworks). As light shines through a material, the light intensity decreases exponentially:

$$I = I_0 \times t^n$$

Here, t is the fraction of the light intensity left after transmission through one slice of bone tissue (10μm in our setup). I_0 is the intensity of light emitted by the label and I is the intensity seen when a label that emits intensity I_0 is observed through n layers of bone tissue. The deconvolution algorithm starts in the bottom image, and subtracts the light emitted from label in this bottom layer from images on top of this layer. This is done for all the layers in the data set.

The result of this algorithm is shown in figure 5.3, for a phantom that was serially sectioned in the setup. This phantom was made of a piece of cortical cow bone, in which a hole with a diameter of 0.6 mm was drilled. The surface of the phantom was labelled with calcein green by immersing the phantom in a calcein green solution (10 mg calceinml) at room temperature for one hour. This phantom was sectioned as shown in Fig. 5.3. This figure shows the raw data and the data after deconvolution and segmentation.

To obtain the final data sets, the images were coarsened to obtain 3D data sets of $2.1 \times 2.8 \times 3$ mm consisting of cubic elements of 10 μm sidelength. Using a marching cubes algorithm in Matlab a smooth triangulated surface of the bone architecture was made, including the 3D locations of the labels in the bone.

Using the data sets thus obtained, we can investigate whether the resorption cavities were distributed randomly throughout the structure, or located preferentially on transversal or aligned trabeculae, or on convex, concave or flat surfaces. Here, we call the trabeculae which are oriented in the plane perpendicular to the main load bearing direction transversal trabeculae. Aligned trabeculae are the trabeculae which are aligned to the main load bearing direction. We use convex for

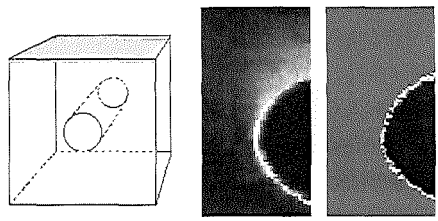

Figure 5.3: Left: phantom, made by drilling a hole in a bone specimen and labeling the surface with calcein green. Middle: reconstruction of phantom, made by serial sectioning, raw data. Right: segmented reconstruction after deconvolution to correct for the light shining through the bone tissue.

a surface that is created when a cavity is made in a plate of bone tissue, a concave surface is created when extra bone is added on a flat surface. The orientation of the trabeculae and the curvatures of the bone surface were determined using specially developed Matlab software, which used the surfaces triangles generated with the marching cubes algorithm as input.

The orientation of the trabeculae relative to the main load bearing direction was determined from the surface normals of the triangles in the trabecular surface. The algorithm that was used to determine the local surface curvatures was derived from a method described in literature.

5.4 calculation of local surface curvatures

The local curvature of a surface is characterized by two signed radii (r_1 and r_2). If we rotate a plane which contains the normal on the spot we find a largest and a smallest in magnitude. The two principal curvatures (κ_1 and κ_2 are the inverse of these radii ($\kappa_1 = \frac{1}{r_1}, \kappa_2 = \frac{1}{r_2}$). These are combined to determine the Mean curvature (H) and the Gauss curvature (K):

$$H = \frac{\kappa_1 + \kappa_2}{2} \qquad K = \kappa_1 \times \kappa_2 \tag{5.1}$$

Following Jinnai et al [80] we introduce area-averaged curvatures ($\hat{H}, \hat{K}$). According to [80], the area of a new continuous surface that is created by moving a surface with are S(0) outwards by a distance d is:

$$S(d) = S(0)(1 + 2\hat{H}d + \hat{K}d^2) \tag{5.2}$$

In our model, we do not have a continuous surface, but a triangulated surface generated using the marching cubes algorithm. We derived an algorithm to compute the curvatures based on the triangles of this triangulated surface.

The surface normal N of a triangle of which the corners are given by three vectors P_{1-3} is:

$$N = P_1 \times P_2 + P_2 \times P_3 + P_3 \times P_1 \tag{5.3}$$

The normalized surface normal is U:

$$\|N\| = \sqrt{N \cdot N} \qquad U = \frac{N}{\|N\|} \tag{5.4}$$

The surface of the triangle is:

$$s(0) = \frac{1}{2}\|N\| = \frac{1}{2}N \cdot U \tag{5.5}$$

D_{1-3} are the normals in the corners of the triangle, calculated from the normals of the surrounding triangles:

$$D = \frac{1}{n}\sum_{i=1}^{n} U_i \tag{5.6}$$

The vectors E_{1-3} have the same direction as D_{1-3} and point from the corners of the original triangle to the corners of a new triangle, which is created by moving the triangle outwards by a distance d:

$$E = d\frac{\|N\|}{N \cdot D}D = \frac{D}{D \cdot U}d \tag{5.7}$$

The surface s(d) of the new triangle is:

$$s(d) = \frac{1}{2}((P_1 + E_1) \times (P_2 + E_2) +$$

$$(P_2 + E_2) \times (P_3 + E_3) + (P_3 + E_3) \times (P_1 + E_1)) \cdot U \tag{5.8}$$

By performing the multiplications and substituting N, s(0) and E we can rewrite this to:

$$s(d) = s(0) +$$

$$\frac{d}{2}\left((P_2 - P_1) \times \frac{D_3}{D_3 \cdot U} + (P_3 - P_2) \times \frac{D_1}{D_1 \cdot U} + (P_1 - P_3) \times \frac{D_2}{D_2 \cdot U}\right).U +$$

$$\frac{d^2}{2}\left(\frac{D_1}{D_1 \cdot U} \times \frac{D_2}{D_2 \cdot U} + \frac{D_2}{D_2 \cdot U} \times \frac{D_3}{D_3 \cdot U} + \frac{D_3}{D_3 \cdot U} \times \frac{D_1}{D_1 \cdot U}\right) \cdot U \tag{5.9}$$

For the whole surface we sum over all triangles :

$$S(d) = S(0)+$$

$$\frac{d}{2}\sum\left((P_2 - P_1) \times \frac{D_3}{D_3 \cdot U} + (P_3 - P_2) \times \frac{D_1}{D_1 \cdot U} + (P_1 - P_3) \times \frac{D_2}{D_2 \cdot U}\right).U+$$

$$\frac{d^2}{2}\sum\left(\frac{D_1}{D_1 \cdot U} \times \frac{D_2}{D_2 \cdot U} + \frac{D_2}{D_2 \cdot U} \times \frac{D_3}{D_3 \cdot U} + \frac{D_3}{D_3 \cdot U} \times \frac{D_1}{D_1 \cdot U}\right) \cdot U \quad (5.10)$$

By comparing these last equations with equation 5.2 we see that we can calculate the average H and K from the triangulated surface:

$$2\hat{H} = \frac{1}{2S}\sum\left((P_2 - P_1) \times \frac{D_3}{D_3 \cdot U} + \right.$$

$$\left.(P_3 - P_2) \times \frac{D_1}{D_1 \cdot U} + (P_1 - P_3) \times \frac{D_2}{D_2 \cdot U}\right).U \quad (5.11)$$

$$\hat{K} = \frac{1}{2S}\sum\left(\frac{D_1}{D_1 \cdot U} \times \frac{D_2}{D_2 \cdot U} + \frac{D_2}{D_2 \cdot U} \times \frac{D_3}{D_3 \cdot U} + \frac{D_3}{D_3 \cdot U} \times \frac{D_1}{D_1 \cdot U}\right) \cdot U \quad (5.12)$$

However, the direction in which the corners of the triangles move when the surface is moved outwards by a distance d is not always determined. Initially a number of triangles intersects at one point, the common vertex of these triangles. If there is again one point of intersection after the triangles are moved outwards (parallel!) the direction in which the point moves is well defined. However, in general, more than three triangles intersect in a vertex. When these triangles are moved outwards, they do not intersect in one point anymore in most cases. The solution is a compromise in one sense or another: each triangle gets its own 'new' point or the new triangles are not exactly parallel to the original triangles. For this problem, we used a solution that others used before: we used surface weighted face normals. So N is used instead of U in equation 5.6 and if there are three or more surrounding triangles the set of equations is solved by the least square method. This results in the vertex normals D used in the formulas above. From equation 5.11 and 5.12 we can calculate the local mean (H) and gauss (K) curvatures:

$$H = \frac{1}{4s}\left((P_2 - P_1) \times \frac{D_3}{D_3 \cdot U} + (P_3 - P_2) \times \frac{D_1}{D_1 \cdot U} + (P_1 - P_3) \times \frac{D_2}{D_2 \cdot U}\right).U$$

$$K = \frac{1}{2s}\left(\frac{D_1}{D_1 \cdot U} \times \frac{D_2}{D_2 \cdot U} + \frac{D_2}{D_2 \cdot U} \times \frac{D_3}{D_3 \cdot U} + \frac{D_3}{D_3 \cdot U} \times \frac{D_1}{D_1 \cdot U}\right) \cdot U$$

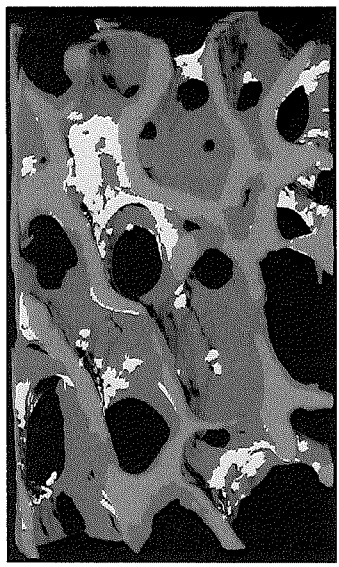

Figure 5.4: Reconstruction of cancellous bone architecture (dark grey), including the locations of the fluorochrome labels (light grey).

5.5 specimens

In this study we used four calcein labeled dog L1 vertebral bone specimens. The dogs received double calcein labelling according to a 2-12-2-5 schedule before sacrifice, as described in detail elsewhere [100]. We used specimens obtained from untreated dogs. The bone specimens were embedded in black epoxy resin (Epofix, Struers, colored black using araldite coloring paste from Ciba)[118].

5.6 Results

The serial sectioning process presented here is completely automated, slicing of 1 mm of bone in sections of 10μm thickness takes approximately 1 hour. Figure 5.4 shows part of a reconstruction of a dog vertebral cancellous bone specimen made using this setup.

Using these data sets, we determined the percentage of labelled surface, which was 18 ± 2 %. These percentages were slightly lower, but not significantly different from with the percentages of labelled surface in these dogs determined in the L3 vertebrae using 2D histology [99].

The percentage of labelled surface was slightly higher on the transversal tra-

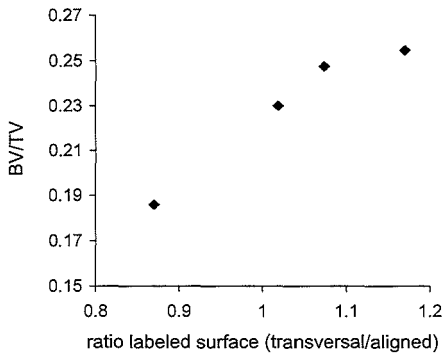

Figure 5.5: ratio of percentages labeled surface on transversal and aligned trabeculae vs BV/TV.

beculae than on trabeculae in the main load bearing direction in 3 of the 4 specimens. The ratio of labelled surface on transversal trabeculae and labelled surface on aligned trabeculae was related to the bone volume fraction, as shown in figure 5.5. In these specimens, we did not find a relation between the local surface curvature and the locations of the labels.

Concluding, bone remodeling is probably not initiated randomly throughout the architecture. Our results indicate that as long as the bone volume fraction is high, resorption is initiated slightly more frequently on transversal trabeculae. This could be regulated by stresses or strains in the trabeculae: these are lower in the transversal trabeculae than in the trabeculae in the main load bearing direction. If high stresses protect against resorption, resorption needed for e.g. calcium homeostasis might be initiated more on transversal trabeculae. Obviously, study of more specimens is needed to make more definitive conclusions about the regulation of bone remodeling.

5.7 Discussion

Bone remodeling leads to changes in architecture and mechanical properties of bone with increasing age. Especially in cancellous bone, the changes in bone volume, bone stiffness and strength with age can be large. Although it is known that these changes result from the bone remodeling process, it is not clear by what mechanism the observed changes are created. Knowledge about the three dimensional distribution of bone apposition in cancellous bone could elucidate this and thereby give insight in the mechanism by which bone remodeling changes the architecture of the bone.

In order to study this bone remodeling in three dimensions, we built a setup

to make reconstructions of the bone architecture including the locations of recent bone apposition. Mineralizing bone tissue can be labeled in vivo by fluorochrome labels that bind to calcium, given by intraperitoneal injections or orally. These labels are deposited in the bone tissue along with the calcium as the new bone tissue mineralizes. By reconstructing the locations of the labels in the bone, locations of recent new bone formation can be visualized. We have shown that it is possible to reconstruct both the bone architecture and the locations of fluorochrome labels incorporated in the mineral of the bone tissue from one set of images. The stacks of images were made using serial sectioning and fluorescence microscopy.

The use of micro-CT scanners has resulted in more insight in the changes in cancellous bone that occur with aging [68, 42]. As the resolution of this technique improves, probably even information about local mineralization can be obtained from the scan data. However, information about recent bone apposition and resorption in the remodeling cycle can at the moment not be obtained using these scanners. In the future, it will probably be possible to study the effects of bone remodeling with in vivo CT-scanners, but only in small animals like mice and rats. Using our setup, the architecture and the labels can be studied in three dimensions in biopsies from larger species as well.

Although the bone apposition sites are clearly labelled with fluorochrome markers, we can not detect bone resorption sites in our setup. It is generally accepted that bone resorption and formation are coupled in the bone remodeling process [128]. In the dogs used in this study, the growth plates were closed, so bone remodeling will be the dominant process, not bone modeling. It is therefore highly likely that the locations of bone formation that we find are previous bone resorption sites.

Using our setup, it will be possible to study normal bone remodeling, but also to gain more insight in the changes in bone remodeling that are caused by e.g. anti-resorptive treatment, in osteoporosis or osteoarthrosis. It is clear that bone remodeling is reduced during anti-resorptive treatment [177, 99, 166], but it is not known whether these treatments also change the spatial distribution of bone remodeling. Another application might be to look at the travelling of BMU's through the bone architecture. By using different colors of fluorochrome labels, bone apposition in subsequent weeks or months can be labelled and distinguished in the reconstructions [160]. Studying bone remodeling in three dimensions will certainly help to better understand the bone remodeling process in healthy organisms as well as during aging and pharmacological interventions.

5.8 Acknowledgements

The authors thank D. Burr (Indiana University school of medicine) for the dog specimens used in this study. Jacqueline van der Linden was supported by the Dutch Foundation for Research (NWO/MW).

Chapter 6

Trabecular bone's mechanical properties are affected by its non-uniform mineral distribution*

J.C. van der Linden
D.H. Birkenhäger-Frenkel
J.A.N. Verhaar
H. Weinans

*Reprinted from the Journal of Biomechanics: Volume 34(12):1573-80, 2001, with permission from Elsevier Science.

6.1 Abstract

The bone remodeling process takes place at the surface of trabeculae and results in a nonuniform mineral distribution. This will affect the mechanical properties of cancellous bone, because the properties of bone tissue depend on its mineral content.

We investigated how large this effect is by simulating several non-uniform mineral distributions in 3D finite element models of human trabecular bone. The mineral was distributed uniform, the surface layer had a higher mineral content than the core of the trabeculae or vice versa. The apparent stiffness of these models was calculated using finite element simulations. In the 'linear model' we assumed a linear relation between mineral content and Young's modulus of the tissue. In the 'exponential model' we included an empirical exponential relation in the model.

When the linear model was used the mineral distribution slightly changed the apparent stiffness, the difference varied between an 8% decrease and a 4% increase compared to the uniform model with the same BMD. The exponential model resulted in up to 20% increased apparent stiffness in the main load-bearing direction. A thin less mineralized surface layer (28μm) and highly mineralized interstitial bone (mimicking mineralization resulting from anti-resorptive treatment) resulted in the highest stiffness. This could explain large reductions in fracture risk resulting from small increases in BMD. The non-uniform mineral distribution could also explain why the bone tissue stiffness determined using nano-indentation is usually higher than the finite element determined stiffness.

We conclude that the non-uniform mineral distribution in trabeculae does affect the mechanical properties of cancellous bone and that the tissue stiffness determined using finite element modeling could be improved by including detailed information about mineral distribution in trabeculae in the models.

6.2 Introduction

The skeleton has an important load-bearing function. Therefore, numerous studies have quantified strength, stiffness and failure load of cortical and trabecular bone [27, 35, 83, 107, 141]. Besides experimental studies, finite element simulations have been used to calculate the stiffness of trabecular bone specimens.

The finite element simulations use 3D models of trabecular bone specimens made using micro-CT scans, MRI-scans or serial sectioning [75, 89, 120, 173]. These models accurately represent the three-dimensional architecture, but differences in material properties in the bone tissue* are usually not taken into account. The bone tissue is assumed to be uniform, isotropic and linearly elastic [75, 173]. Cancellous bone exhibits linear behavior for small deformations [83], but bone tissue has a lamellar structure, and is not isotropic. Furthermore, bone tissue is not uniform at the trabecular level: the bone remodeling process results in a nonuniform distribution of the mineral within the trabeculae. The surface layer of trabeculae is frequently renewed, but tissue in the middle of trabeculae (interstitial bone) can escape from this remodeling [10, 16], and become older than the surface layer. As new bone tissue mineralizes, approximately 70% of the mineral is deposited in a couple of days, but mineralization continues slowly for several more years [64, 129]. This results in a higher mineral content in the interstitial bone, compared to the surface layer. This non-uniform distribution has been shown with a variety of techniques [24, 40, 58, 115, 148], as illustrated in figure 6.1.

The distribution of the mineral over the trabeculae depends on the rate of bone turnover. A high turnover rate results in a large difference in mineral content between the interstitial bone and the surface layer. Anti-resorptive treatment results in less and shallower cavities, so that the difference in mineralization between the surface layer and the interstitial bone is small and the surface layer thin. It has been shown that the stiffness of bone tissue is exponentially related to the mineral content [35]. Therefore, besides differences in architecture between e.g. healthy and diseased bone, the mechanical properties might also be affected by differences in mineral distribution.

In trabeculae, the highly mineralized core is surrounded by a surface layer with a lower stiffness. This is in contrast with normal engineering practice, where I-beams and hollow pipes are used to obtain structures with a high (bending) stiffness combined with a low mass. However, in bridges and buildings failure must be prevented, while in trabeculae small cracks can be repaired as long as the trabeculae are not completely fractured. Furthermore, bone tissue with a high mineral content has a high stiffness, but a relatively low failure energy [34]. Therefore, the mineral distribution found in cancellous bone may be advantageous. The highly mineralized older bone is located in the middle [185], where deformations are

*In this chapter, 'bone tissue' is used to describe the material of which the trabeculae are made, including osteoid and mineralized matrix, but excluding bone marrow.

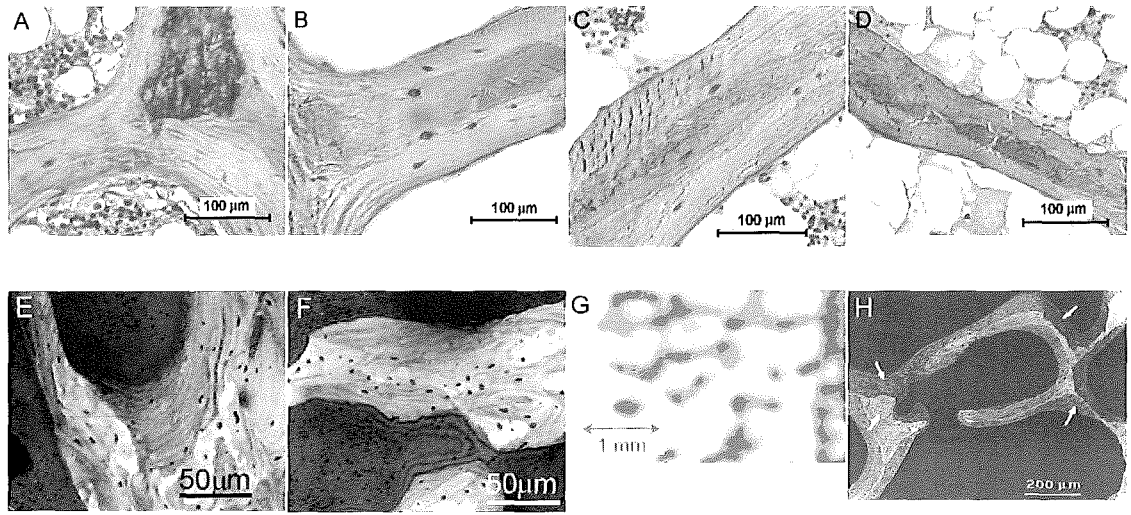

Figure 6.1: Non-uniform mineral distribution in trabecular bone, shown using several techniques. A-D: Human, thionine staining (high mineral content=dark staining). A: female, 58y, osteopetrosis. B, C: female, 77y, normal bone, D: male, 51y, normal bone. E, F: rat, tibia, scanning acoustic microscopy (SAM). High mineral content: light gray. (courtesy of C. Jorgensen, Aarhus University Hospital, Denmark). G: human, vertebra, female, 14y, Scanning small angle x-ray scattering (SAXS), high mineral content:black (Camacho et al., Bone 25(3)) H: minipig, rib, BSE-image (High mineral content: light gray) (Roschger et al., Bone 20(5))(G and H reprinted with permission from Elsevier Science)

smaller. Furthermore, this brittle bone is surrounded by a surface layer with a lower mineral content, which has better crack-stopping mechanisms.

The aim of this study was to investigate the influence of the non-uniform mineral distribution in trabecular bone on apparent stiffness in order to be able to estimate the effect of changes in this distribution caused by diseases or drug treatment.

6.3 Materials and Methods

The specimens used in this study were obtained from autopsy L4-vertebrae of three donors: two males, 37 and 77 years old, and one female: 80 years old. These were obtained as part of the European Union BIOMED 1 project "Assessment of Bone Quality in Osteoporosis". According to the donor data, these donors did not suffer any osteoporotic fractures. The specimens were scanned in a micro-CT scanner (Scanco Medical, voxel size 14μm, resolution 28μm). The reconstructions were segmented in order to obtain three-dimensional voxel models of $4 \times 4 \times 4$ mm cancellous bone, with cubic elements of $28 \times 28 \times 28\mu$m. The volume fractions of these specimens were 6.4% (female donor 80 years, F80), 11.8% (male donor 77 years, M77) and 12.9% (male donor 37 years, M37), resulting in computer models of 180,000 to 360,000 brick elements.

Using these datasets, we created various models with different mineral distributions. First, the mineral was distributed uniformly over the trabeculae. The mineral content of all elements was 0.4 g Ca/cm^3, which is in the biological range [9]. Second, the mineral distribution as observed in cancellous bone (see Figure 6.1) was simulated: the interstitial bone was given a high mineral content, with values of 0.44, 0.48 or 0.52 g Ca/cm^3 bone tissue. The surface layer of the trabeculae, which was either thin (28 μm) or thick 56 (μm), was given a lower mineral content, so that the mean mineral content of all elements was 0.4 g Ca/cm^3 bone tissue in all models. The mineral contents of the interstitial bone and of the surface layer are shown in table 6.1. Third, we created a hypothetical mineral distribution, in which the surface layer had a higher mineral content than the interstitial bone. The mean mineral content was again 0.4 g Ca/cm^3. This was only done for the case of the thin surface layer. In the case of the thick surface layer a mean mineral content of 0.4 g Ca/cm^3 could not be achieved without assigning negative mineral contents to the tissue in the middle of the trabeculae. The mineral contents of the interstitial bone and of the surface layer are shown in table 6.2. The different distributions would result in the same BMD in a DXA-scan. Figure 6.2 shows slices of the finite element models with simulated mineral distributions.

Assuming a linear relation between mineral content and Young's modulus, the

Table 6.1: Mineral content of interstitial bone ('Int bone') and surface layer (28 or 56 μm) of trabeculae in all three specimens for 4 different mineral contents in the interstitial bone, which has a higher mineral content than the surface layer, mimicking the in vivo mineral distribution.

		Surface layer					
	Int.	M37		M77		F80	
	Bone	28μm	56μm	28μm	56μm	28μm	56μm
Mineral	0.40	0.40	0.40	0.40	0.40	0.40	0.40
content	0.44	0.35	0.39	0.35	0.40	0.36	0.40
(gCa/cm^3)	0.48	0.29	0.39	0.31	0.39	0.32	0.39
	0.52	0.24	0.38	0.26	0.39	0.27	0.39

Table 6.2: mineral content of surface layer and interstitial bone of trabeculae in all three specimens for 4 different mineral contents of the surface layer, which is 28μm thick. The interstitial bone has a lower mineral content than the surface layer.

		Interstitial bone		
	Surface	M37	M77	F80
	layer	28μm	28μm	28μm
Mineral	0.40	0.40	0.40	0.40
content	0.44	0.37	0.36	0.36
(g Ca/cm^3)	0.48	0.34	0.33	0.32
	0.52	0.31	0.30	0.28

Young's modulus of each element (E_i) was calculated using this formula:

$$E_i = c * \frac{Ca_i}{Ca_{mean}}$$

Ca_i is the mineral content of the i^{th} element, Ca_{mean} is the mean mineral content of 0.4 g Ca/cm^3. The constant c in this linear model is 5 GPa, resulting in a Young's modulus of 5 GPa for elements with the mean mineral content of 0.4 g Ca/cm^3.

The global stiffness properties of the models were calculated using an element-by-element FE solver [176]. This solver was slightly modified, to allow for the assignment of different Young's moduli to the elements. In this method, six uniaxial mechanical tests (three compression and three shear tests) were simulated by applying homogeneous displacements at the surfaces. Each simulated test yielded one row of the global stiffness matrix of the specimen. Using an optimization

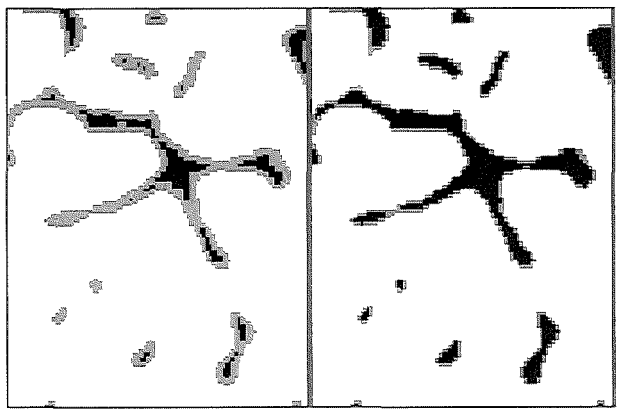

Figure 6.2: One slice of finite element model of donor M37, with a surface layer of either two elements (left) or one element (right). Marrow space is white, interstitial bone black, the surface layer is shown in gray. The surface layer was given either a lower (table 6.1) or a higher (table 6.2) mineral content than the interstitial bone.

procedure, the best orthogonal representation of the global stiffness matrix of the specimens was calculated [175]. From this matrix, we used the maximum apparent Young's modulus of the specimens, which was oriented within 6° from the superior-inferior direction of the specimens, and the Young's moduli in transverse directions, which were oriented within 6° from the transverse plane in all models. The direction of maximal stiffness was only slightly changed by changes in mineral distribution, the maximal change was 0.7°. The superior-inferior direction of the specimens corresponded to the main in vivo load bearing direction. The effect of the mineral distribution on the apparent stiffness of the specimens was determined.

Besides the linear relation between mineral content and Young's modulus, we also investigated the effect of an empirical exponential relation [35] on the apparent stiffness of the models mimicking the in vivo mineral distribution. By comparing the results of this exponential model to the previous linear model, the sensitivity of the calculated stiffness to the relation between mineral content and Young's modulus can be estimated. The Young's modulus of the elements was based on their mineral content, using a cubic relation:

$$E_i = c \times (\frac{Ca_i}{Ca_{mean}})^3 \tag{6.1}$$

Where E_i is the Young's modulus (MPa) of the i^{th} element, c is a constant (5 GPa), Ca_i is the mineral content of the i^{th} element, Ca_{mean} is the mean mineral content of the elements of the specimen (0.4 g Ca/cm^3). Using this formula, the Young's

Table 6.3: Mineral content of interstitial bone ('Int bone') and surface layer (28 or 56 μm) of trabeculae in all three specimens for 4 different mineral contents in the interstitial bone, which has a higher mineral content than the surface layer, mimicking in vivo mineral distribution.

		Surface layer					
	Int.	M37		M77		F80	
	Bone	28μm	56μm	28μm	56μm	28μm	56μm
Young's	5.00	5.00	5.00	5.00	5.00	5.00	5.00
modulus	6.66	3.24	4.76	3.45	4.88	3.58	4.91
(GPa)	8.64	1.95	4.54	2.26	4.75	2.47	4.81
	10.99	1.05	4.31	1.39	4.62	1.61	4.72

modulus of an element with the mean mineral content of 0.4 g Ca/cm^3 was 5 GPa. Table 6.3 shows the resulting tissue moduli for the interstitial bone and the surface layer, calculated using this formula in all three specimens.

The mineral distribution in the trabeculae also affects the way the loads applied to the bone are distributed over the trabeculae. We investigated the effect of the mineral distribution on the strain energy density distribution (SED) resulting from a uniaxial confined compression in the superior-inferior direction. An apparent stress of 0.5 MPa was applied to the top surface of the specimen. The bottom face was not allowed to move, elements in the side faces were not allowed to move perpendicular to these faces. The stress and strain in all elements in the model were calculated, and the strain energy density distribution was determined.

In an ideal structure, the load is distributed evenly over all the elements in the structure, resulting in a uniform SED distribution, and a narrow peak in the SED histogram. If a structure is not well suited for load bearing, some elements will be highly loaded, while others are almost not loaded, resulting in a wide SED distribution. By comparing SED distributions of the uniform and the nonuniform models, we can determine whether the nonuniform mineral distribution seen in cancellous bone is mechanically advantageous.

6.4 Results

The calculated apparent stiffness of the cancellous bone specimens was relatively independent of the mineral distribution when the linear model was used. The stiffness of the models that resembled the in vivo mineral distribution was somewhat lower than the stiffness of the uniform model. The maximal reduction in apparent stiffness was 8%. The models with a higher mineral content in the surface layer had a slightly higher apparent stiffness than the uniform model. The maximal increase was 4%.

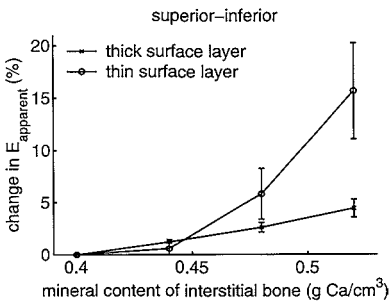

Figure 6.3: Change in apparent Young's modulus in superior-inferior direction as a function of the mineral content of the interstitial bone.

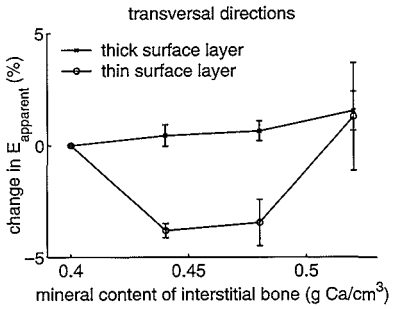

Figure 6.4: Change in apparent Young's Modulus in transversal directions as a function of the mineral content of the interstitial bone.

The apparent stiffness in superior-inferior direction of the models mimicking the in vivo mineral distribution was higher than the stiffness of the uniform model, when the exponential model was used (see Fig. 6.3). This stiffness increased when the mineral content in the middle of the trabeculae increased. The increase was larger in the case of the thin surface layer. The models with the thin surface layer had up to 20% (mean:15%) higher apparent stiffnesses in the main load bearing direction. The models with the thick surface layer showed smaller increases, the maximal increase was 5%.

In the transverse directions the nonuniform mineral distribution had smaller effects (see Fig. 6.4). The difference in apparent stiffness varied between a 4% decrease and a 1.5% increase, compared to the uniform models. The models with a thick surface layer showed a small increase in apparent stiffness with increasing mineral content in the interstitial bone. The models with the thin surface layer showed a decrease in apparent stiffness for a mineral content in the middle of the trabeculae of 0.44 and 0.48 g Ca/cm^3. For a mineral content of 0.52 g Ca/cm^3 in the interstitial bone the models with the thin layer showed an average increase in apparent modulus of 1.3%.

The higher stiffness in the superior-inferior direction of the models with a higher mineral content in the interstitial bone is a result of a more uniform distribution of the applied deformation energy over the elements. Figure 6.5 shows the SED-distribution of the elements in specimen M77 for the uniform model and the model with a thin surface layer and a mineral content in the interstitial bone of 0.52 g Ca/cm^3, which are the models with the lowest and highest apparent stiffness (see Figure 6.3). The model with the higher mineral content in the interstitial bone had a higher and narrower peak at low SED, and a 30% lower median SED value. This effect was similar for the other two specimens.

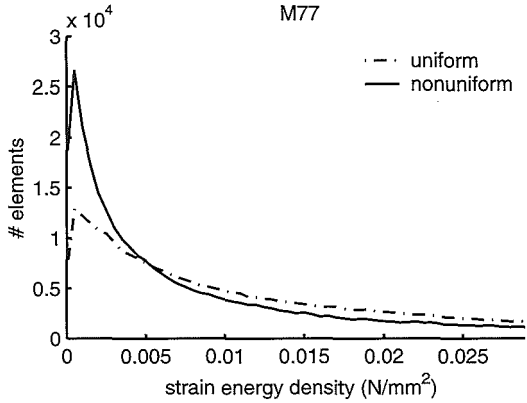

Figure 6.5: Strain energy density (SED) distribution of the elements in the model from the male donor of 77 years old, resulting from an applied stress of 0.5 MPa to the top surface of the specimen. The SED distribution of the uniform model is wider than the distribution of the nonuniform model with a mineral content of 0.52 g Ca/cm in the interstitial bone.

6.5 Discussion

The bone remodeling process results in a nonuniform mineral distribution in cortical and cancellous bone. In cancellous bone, the interstitial bone in the core of trabeculae has a higher mineral content than the surface layer. Since the stiffness of bone tissue depends on its mineral content [34], this non-uniform distribution will affect the apparent stiffness of cancellous bone. In order to determine how large this effect is we included non-uniform mineral distributions in finite element models of human trabecular bone. These non-uniform models represent the real bone better than the usually used uniform models [75, 173].

The mineral distribution had only a small effect on the apparent stiffness when a linear relation between mineral content and Young's modulus was assumed. Hypothetical mineral distributions with a high mineral content in the surface layer and a low mineral content in the interstitial bone resulted in higher apparent stiffnesses than the uniform model. The maximal increase was 4%. Models that mimicked the in vivo mineral distribution had a somewhat lower stiffness than the uniform model. The maximal decrease was 8%. This shows, that the mineral distribution in trabeculae is not advantageous when apparent stiffness is considered using the calculations in the linear model.

In this model, the mineral distribution within a rod (trabecula) does affect the bending stiffness, but has no effect on compression stiffness. The bending stiffness of a cylindrical rod ('trabecula') with a less mineralized surface layer as shown in table 6.1 can be up to 30% lower than the stiffness of a uniform rod with the

same mineral content. Therefore, the smaller effect of the mineral distribution on the apparent stiffness indicates that bending as well as compression occurs as the whole specimen is loaded. When the empirical exponential model is used, the decrease in stiffness of the surface layer is outweighted by the high stiffness of the interstitial bone. This results in an increase in the apparent stiffness compared to the uniform distribution, as determined using the finite element models.

In the present study we used a computer algorithm to create mineral distributions that resembled distributions seen in cancellous bone. The material properties in our models were nonuniform, but the tissue was still assumed to be isotropic and linearly elastic. Cancellous bone behaves linearly for small deformations [83], but trabecular bone tissue is not isotropic [151]. Both models, with surface layers of 28 and 56 μm thick, are simplifications of the real mineral distribution in cancellous bone. In real bone, the age of the bone packets made in the remodeling process varies, as well as their mineral content (see Fig.6.1). However, because remodeling takes place at the surface of trabeculae, the surface layer generally has a lower mineral content than the interstitial bone. Furthermore, it has to be kept in mind that the exponential relation was derived from experiments using cortical bone specimens [35]. Although it is very likely that a similar relation will be valid in cancellous bone tissue, this has yet to be verified.

It has been shown, that bone with a high mineral content has a relatively low failure energy. Bone tissue changes from ductile, for a low mineral content and low Young's modulus, to brittle, for a high mineral content and high Young's modulus [34]. In trabeculae, the highly mineralized interstitial bone provides a high compression stiffness. When cracks start in this tissue, the surface layer, which has a lower mineral content and better crack stopping mechanisms [185] prevents complete fracture of the trabeculae and repair of the damage is possible. In damaged trabeculae, it can be seen that the highly mineralized core contains microcracks, while the less mineralized surface layer maintains the mechanical integrity of the trabecula [57, 105].

In determining the stiffness of trabecular bone tissue, the nonuniform mineral distribution is usually not taken into account. For example in bending tests of individual trabeculae, the modulus is calculated assuming homogeneous material properties. Bending experiments resulted in Young's Moduli of 3-8 GPa [27, 88, 103]. In finite element simulations, the tissue modulus is determined by fitting the calculated apparent stiffness to the experimentally measured stiffness assuming homogeneous tissue properties. Good fits have been obtained with tissue moduli of 5 to 7 GPa [77, 89]. Kabel et al. found high correlations between calculated and measured stiffness using an 'effective isotropic tissue modulus' and concluded that inclusion of tissue level material properties is not necessary [82]. However, these high correlations do not prove that differences in tissue level properties do not affect apparent stiffness of cancellous bone. Moreover, the modulus found using finite element modeling is usually lower than the modulus found using ultrasound

and nanoindentation techniques, which yielded moduli of 8-20GPa [3, 73, 142, 151, 167, 187]. The nano-indentations are usually made in the highly mineralized core of the trabeculae, to avoid effects of the embedding resin [142]. This could explain the higher moduli found using this technique.

The stiffness of the models mimicking the real mineral distribution was up to 20% higher than the stiffness of the uniform model when the empirical exponential relation was used. The 20% increase was found in models with a Young's modulus of 11 GPa in the interstitial bone, which is twice as high as the modulus of the elements in the uniform model. If the tissue modulus were determined by fitting the simulation to a mechanical test, assuming homogeneous tissue, the stiffness of the interstitial bone tissue would be underestimated. As scanning techniques improve, higher resolutions and more detailed information can be obtained, e.g. by using synchrotron radiation (20). Including this information in finite element models might improve predictions of tissue properties of cancellous bone specimens.

In antiresorptive treatment, resorption cavities become shallower, resulting in thicker interstitial bone and a thin surface layer. If the treatment has an anabolic effect on osteoblasts, this will result in a thicker surface layer and an increase in bone volume. The present results show that highly mineralized interstitial bone and a thin surface layer results in a high apparent stiffness, even if the mineral content and the bone volume stay the same. In antiresorptive treatment, the amount of mineral in the bone can increase because of the reduced turnover [13]. This results in even more pronounced increases in stiffness and strength, which results in large reductions in fracture risk found in clinical studies [11].

Concluding, the nonuniform mineral distribution in trabeculae has an effect on the finite element calculated apparent stiffness, but the difference is not more than 20%. However, when trabecular tissue stiffness is determined by fitting simulation results to experimental tests assuming uniform tissue properties, the stiffness of the interstitial bone can be underestimated by a factor of 2. Furthermore, when the nonuniform mineral distribution is taken into account, the discrepancy between different ways of determining trabecular bone tissue modulus can be explained. Anti-resorptive treatment results in shallower cavities, and a thin less mineralized surface layer in combination with a highly mineralized core. The present results show that such a mineral distribution results in a high apparent stiffness. This could partly explain the high reduction in fracture risk resulting from only small increases in BMD. Finally, the enclosure of the highly mineralized interstitial bone by a less mineralized surface layer decreases the chance of complete fracture of trabeculae. While the effect of the mineral distribution on apparent stiffness is relatively small, the effect of this distribution on the toughness of the bone could be large.

6.6 Acknowledgements

The authors thank Peter Ruegsegger (University of Zurich, Switzerland) for providing the datasets of the trabecular bone specimens used in this study, Ton de Jong (department of pathology, Erasmus University Medical Center, Rotterdam) for preparing the thionine-stained samples and Claus Jorgensen (Aarhus University Hospital, Denmark) for the SAM-images. Jacqueline van der Linden is supported by the Dutch Foundation for Research (NWO/MW), the research of Harrie Weinans was made possible by a fellowship from the Royal Netherlands Academy of Arts and Sciences.

Chapter 7

Bone loss with age could be a side-effect of the ongoing mineralization of bone tissue*

J.C. van der Linden
J.S. Day
J.A.N. Verhaar
H. Weinans

*submitted

7.1 Abstract

With aging, bone architecture changes and bone mass, strength and stiffness decrease. In this paper, we hypothesize that the bone loss with age could be a result from changes in bone tissue* properties with age. As people get older, the average mineral content of their bone tissue increases. This results in a higher tissue stiffness and smaller deformations of the bones. In this paper, we assume that cells can detect local tissue deformation and adapt the cancellous architecture according to this information. Several authors have observed that bone architecture is adapted to external loads [55, 183]. High loads lead to increases of bone volume, small loads to bone loss [7, 79, 92].

We tested this hypothesis by using finite element simulations, in which the architecture of the cancellous bone was adapted to the applied external loads according to the 'mechanostat'. Bone tissue with a strain signal below a certain threshold was resorbed, a strain signal above a certain value induced bone formation. A strain signal in between these two boundaries, in the so-called 'lazy zone' did not induce any changes in bone architecture. We investigated the effect of the width of the lazy zone on bone mass, stiffness and architecture. Furthermore, we investigated the effect of an increase or decrease in trabecular tissue stiffness (while the lazy zone was not changed) on bone mass, stiffness and architecture.

We found that an increase in tissue stiffness led to bone loss and increased mechanical anisotropy. A decrease in bone tissue stiffness led to large increases in bone mass, resulting in an almost constant global stiffness in the main load bearing direction. Concluding, changes in trabecular tissue stiffness and deformation could affect bone mass and architecture during aging and in diseases. We showed that this mechanism can partly explain the bone loss with increasing age.

*Here, tissue is used for the mineralized tissue of which the trabeculae are made.

7.2 Introduction

With aging, the bone mass of the skeleton decreases. Cortices become thinner and more porous, trabeculae in the cancellous bone become thinner. Plates in the cancellous bone are perforated and some trabeculae are lost [1, 107]. This results in large decreases of the strength and stiffness of the skeleton. In extreme cases the skeleton becomes osteoporotic, which results in large increases in fracture risk. Recently, Lanyon and Skerry hypothesized that osteoporosis is a result of malfunctioning of the bone cells [91]. They assumed that the quality of the bones decreases because the bone cells do not react properly to stresses and strains any more in older people. This is a likely explanation, because the functioning of cells does degenerate with age.

However, this is not the only change in the skeleton with age. Most bone tissue is renewed frequently in the bone remodeling process, but some bone tissue escapes from this renewal and becomes older and more mineralized. For example, bone tissue in the middle of trabeculae is not reached by resorption cavities and becomes older than the surface layer of the trabeculae [10]. In cortical bone, old, highly mineralized osteons are found next to young osteons [132]. It has been shown, that the average mineral content of bone tissue increases as people get older [16, 17, 33, 64, 139]. Mechanical and indentation experiments have shown that the stiffness and microhardness of bone tissue increase as the mineral content of bone tissue increases [34, 72]. Assuming that the loads applied to the bone stay the same, a higher tissue stiffness results in smaller deformations.

In this paper, we assume that cells in the bone detect these smaller deformations in their vicinity and 'decide' that less bone is needed to carry the loads. We tested this hypothesis using a three dimensional bone remodeling simulation in which the cancellous architecture of human vertebral bone is adapted to external loads based on local deformations of the tissue. We examined the effects of the sensitivity of the bone cells and the properties of the bone tissue on the architecture, global stiffness and anisotropy of cancellous bone. In this model, the final architecture and stiffness of the specimen are determined by the reaction of the bone cells to their local environment.

7.3 Materials and methods

The specimens used in this study were obtained from autopsy L4-vertebrae of three donors: two males, 37 and 77 years old, and one female: 80 years old. These were obtained as part of the European Union BIOMED 1 project "Assessment of Bone Quality in Osteoporosis". According to the donor data, these donors did not suffer any osteoporotic fractures. The specimens were scanned in a micro-CT scanner (Scanco Medical, voxel size 14μm, resolution 28μm). The reconstructions were segmented in order to obtain three-dimensional voxel models of $4 \times 4 \times 4$ mm

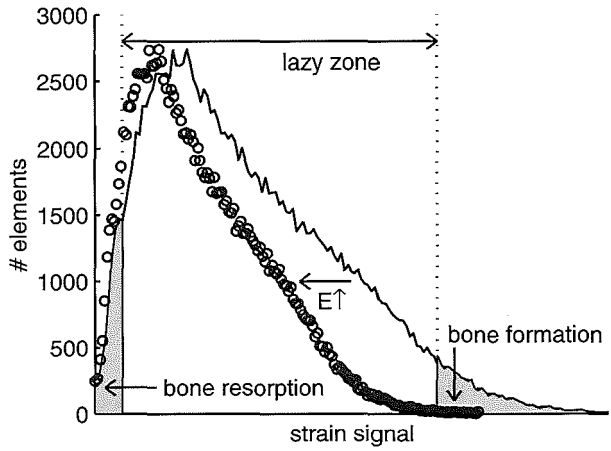

Figure 7.2: Illustration of the change in strain signal when the tissue stiffness increases. The arrow labeled '$E\uparrow$' indicates the shift when the tissue stiffness is increased.

10, 20 or 50%. The increased stiffness led to a decrease in deformation, which induced bone resorption because the signal in surface elements became lower than the lower boundary of the lazy zone (Fig.7.2). The architectures with the new bone tissue stiffness were adapted to the external loads and the bone volume, global stiffness and mechanical anisotropy of the resulting architectures were determined.

In order to fully investigate this mechanism of adaptation of the bone architecture to external loads according to a lazy zone, we also investigated the effect of a decrease in tissue stiffness on bone mass, architecture and global stiffness. We decreased the bone tissue stiffness with 10, 20 or 50%. These decreases also induced adaptation of the architecture, because deformation of the tissue increased, which led to bone apposition.

7.4 Results

The size of the region over which the strain signal was calculated had an effect on the final architecture. In the case of an increased tissue modulus, the difference in global stiffness in superior-inferior direction was less than 5%. In transversal directions, the difference between a region with a radius of 28 or 84 μm was less than 3%. A region of 140 μm, however, resulted in a 30% decrease in transversal stiffness. In the case of a decreased tissue modulus, the maximal difference in stiffness in superior-inferior direction was 20%, in transversal directions the maximal difference was 7% (Fig 7.3).

From these results we conclude that the effect of the size of this region is rather

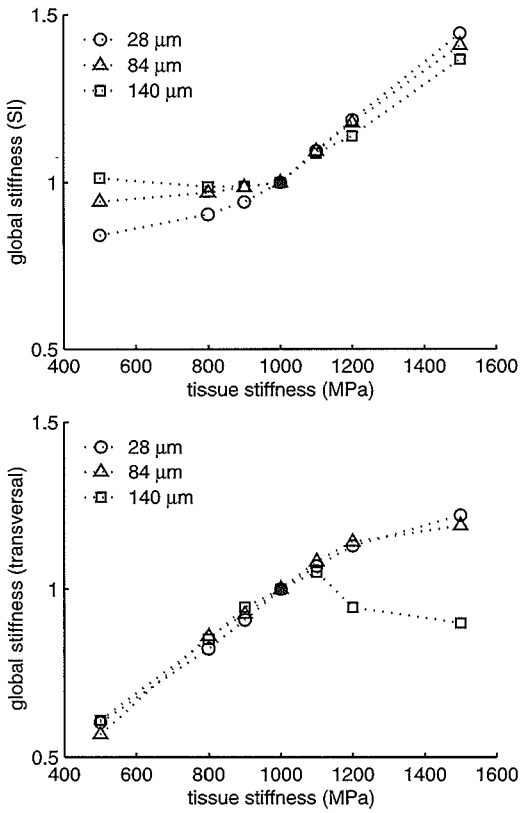

Figure 7.3: Effect of the size of the region over which the strain signal is calculated (the radius of the regions is shown in the legend)The global stiffness in the SI direction (top) and transversal directions (bottom), are shown for tissue stiffnesses ranging from 500 to 1500 MPa.

small, as long as the trabeculae are thicker than the radius of the region over which the signal is calculated. Radii of 28 or 84 μm resulted in similar results, 140 μm resulted in larger changes in architecture. In further simulations, we used a radius of 84 μm.

The width of the lazy zone had an effect on the equilibrium bone architectures: a narrow lazy zone resulted in a lower bone mass than a wide lazy zone (Fig 7.4a). Furthermore, the mechanical anisotropy resulting from a narrow lazy zone was higher (Fig 7.4b), because of a higher global stiffness in SI-direction and a lower stiffness in transversal directions (Fig. 7.4c).

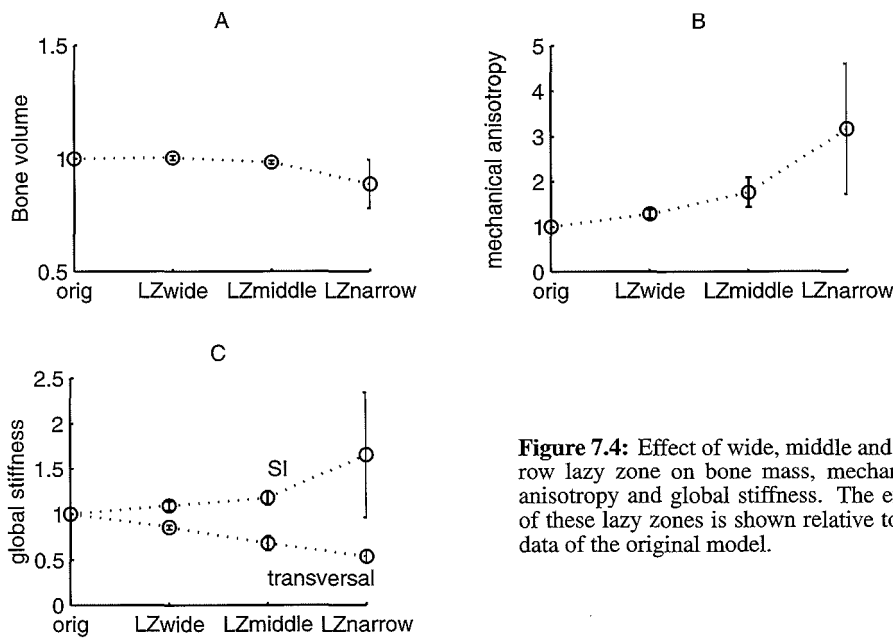

Figure 7.4: Effect of wide, middle and narrow lazy zone on bone mass, mechanical anisotropy and global stiffness. The effect of these lazy zones is shown relative to the data of the original model.

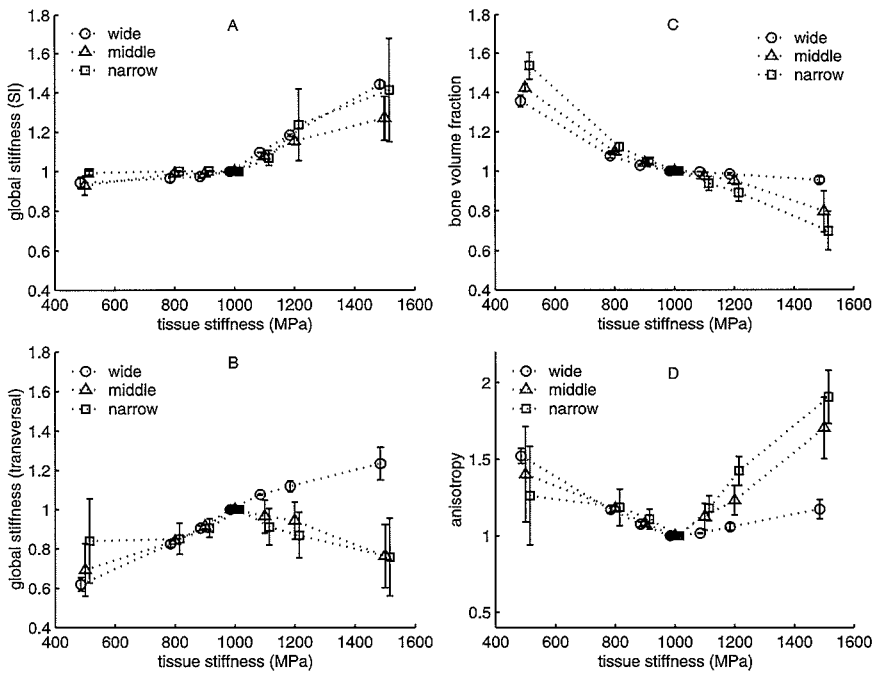

Figure 7.5: Global stiffness in SI and transversal directions (A and B), bone volume fraction (C) and mechanical anisotropy (D), relative to the data of the equilibrium models. Mean and standard deviation are shown of results of the three specimens. The data for the equilibrium models (E_{tissue} = 1000 MPa) of the wide, narrow and middle lazy zone are shown in black. The data points in the right halves of the graphs show the effect of an increase in tissue stiffness, the left halves show the effect of a decrease in tissue stiffness. Data points of the different lazy zones are shown next to each other, so that the errorbars do not overlap.

An increase in tissue stiffness, which simulated the increased tissue stiffness resulting from a higher mineral content, resulted in increases in global stiffness in the SI direction (Fig 7.5a). In transversal directions, a middle or narrow lazy zone resulted in a decrease in global stiffness (Fig 7.5b), a wide lazy zone resulted in increased stiffness. The increases in global stiffness were smaller than the increases in tissue stiffness, because the increase in tissue stiffness resulted in bone loss of 2 to 30% of the bone volume (Fig 7.5c). The increase in stiffness in superior-inferior direction was larger than the increase in transversal directions, which resulted in an increase in mechanical anisotropy (Fig 7.5d).

A decrease in bone tissue stiffness led to a large increase in bone mass, of up to 60% (Fig. 7.5c). This resulted in an almost constant global stiffness in SI-direction, despite the decrease in bone tissue stiffness (Fig. 7.5a). The global stiffness in transversal directions decreased (Fig.7.5b). The mechanical anisotropy increased, as shown in Fig 7.5d.

7.5 Discussion

In this paper we have tested whether bone loss with age could be a result of the ongoing secondary mineralization and the concomitant increase in tissue stiffness with age. We assumed that bone cells can detect the tissue deformation in their environment and adapt the bone architecture according to this information. We tested our hypothesis using finite element simulations of confined compression of cancellous bone specimens, mimicking the in vivo loading of the cancellous bone. In the simulations, the bone architecture was adapted to the external loads by adding bone in highly loaded regions and removing bone in only slightly loaded regions, according to the mechanostat theory.

We found that an increase in tissue stiffness led to an increase in mechanical anisotropy and up to 30% decrease in bone mass. The bone loss and the increase in anisotropy are in agreement with experimental data [43, 107]. However, we also found an increase in global stiffness, which is not in agreement with experimental tests. Two simplifications in the model contribute to this high global stiffness. First, we did not take the effects of microdamage into account, which might decrease the stiffness of highly mineralized bone tissue. Second, in our model the architecture is adapted to external loads, which are kept the same throughout the simulation. In reality, the loads applied to the skeleton decrease with age, because daily activity and muscle strength decrease with age. A decrease in loading results in decreased strains in the trabeculae and subsequent loss of bone mass and stiffness. Decreasing the applied external loads in our simulation would also lead to more bone loss and a lower global stiffness of the cancellous bone.

A decrease in tissue stiffness led to large increases in bone mass, up to almost 60%. These increases in bone mass resulted in an almost constant global stiff-

ness in the main load bearing direction, despite the decreased tissue modulus. In transversal directions, the global stiffness decreased with decreasing tissue modulus, the anisotropy of the architecture increased. The increase in bone volume is in agreement with experimental data. For example, in early osteoarthritis, a decreased tissue stiffness was found in combination with a high bone volume fraction [36]. Concerning anisotropy, data are conflicting. Some found an increase in anisotropy in an animal osteoarthritis model, others found decreases in anisotropy [45, 15] .

In our simulations, we increased the tissue modulus with 10, 20 or 50% and decreased the tissue modulus with the same percentages. Reductions in tissue modulus by up to 60% have been shown, for example in early osteoarthritis [36]. Therefore, the decreases in tissue stiffness we simulated are in the clinically relevant range. With aging, the mineral content of bone tissue has been shown to increase 5% on average [33]. Using an experimental exponential relation between tissue modulus and tissue stiffness [35], this would lead to an increase in tissue stiffness of 16%. Therefore, the increases in tissue stiffness of 10 and 20% are in the clinically relevant range. However, increases in tissue modulus of 50% do normally not occur. In anti-resorptive treatment, increases in mineralization of bone tissue up to 11% have been shown [13]. This will lead to a high stiffness. However, during anti-resorptive treatment, remodeling is decreased and therefore also the adaptation of the bone architecture.

An increase in tissue stiffness with 50% has the same effect on the strains in the tissue as a decrease in loading of 50%. The architecture that resulted from an increase in tissue stiffness with 50% is the same architecture that would result from a constant tissue stiffness and a decrease in loading of 50%. Therefore, the results of these simulations indicate what the effect of decreased loading with aging on architecture would be.

It has to be kept in mind that our finite element models calculate the global stiffness and strain distribution in the cancellous bone models, assuming that the bone tissue is homogeneous, linear and isotropic. In reality bone tissue has a lamellar structure and the bone tissue is not homogeneous. However, good results for the stiffness of cancellous bone specimens can be obtained using these approximations [77, 173]. The average mineral content of the bone tissue increases with age, but this mineral is not distributed uniformly over the trabeculae. The core of the trabeculae can escape renewal, and thereby become highly mineralized, while the surface layer of the trabeculae is more frequently renewed and has a lower mineral content. Furthermore, the effects of microdamage are not incorporated in our model. Because microdamage decreases the strength and stiffness of bone, this might lead to an overestimation of the global stiffness in the model.

This is more important in the highly mineralized models than in the models with a low mineral content and stiffness. A low mineral content and tissue stiffness is assumed to be a result of frequent remodeling of the tissue, so that micro-

damage can not accumulate. The high mineral content, however, is found in older bone tissue, which might have accumulated microdamage. Therefore, the global stiffness of the models with a high tissue stiffness might be overestimated. Besides this, bone tissue with a higher mineral content has less good crack stopping mechanisms and is more brittle [186]. Even if the stiffness is rather high, the work of fracture might be low, which increases the chance of fractures.

Another difference between our model and real bone adaptation, is that we adapted the cancellous architecture by gradually thinning and thickening trabeculae at the locations where the strain signal was not within the lazy zone. In reality, the adaptation occurs by over- or underfilling of resorption cavities. Once trabeculae are thin, the chance that trabeculae are breached by resorption cavities increases. Breached trabeculae will probably not be repaired [108], so that the stiffness and strength of the structure can decrease rather fast. This effect will lead to a rather fast decrease in global stiffness in transversal directions and a more pronounced increase in anisotropy than we found in this study [171].

It has been shown, that the cancellous architecture in the hip of hip fracture patients is more anisotropic than cancellous bone in healthy controls [29]. Our results show, that an increase in tissue stiffness leads to small decreases in bone mass, but rather large increases in anisotropy. These results could explain the increase in anisotropy in osteoporotics, if the bone tissue of osteoporotic patients were more highly mineralized than the bone tissue of healthy people. However, experimental data do not show large differences between normal and osteoporotic tissue. A slightly higher mineral content and a lack of collagen have been found in osteoporotic tissue [41, 8]. However, others found a slightly lower mineral content in osteoporotic patients [94]. In a study that compared finite element simulations to mechanical tests of osteoporotic and healthy people, the average bone tissue stiffness in the osteoporotic specimens was almost 10% higher than in control specimens, but this was not significant [76]. This indicates that at the tissue level, osteoporotic tissue might have a slightly higher stiffness, but the differences are too small to explain the extreme bone loss in osteoporosis. However, a slightly higher tissue modulus in combination with a narrow lazy zone might predispose for osteoporosis.

Taken together, changes in tissue modulus properties can partly explain changes in global bone properties with aging, and in bone diseases that change the bone tissue properties. With aging, the bone cells do their best to keep the tissue deformation in their environment more or less constant. This adversely results in bone loss, because the bone tissue stiffness increases. Of course, other factors can not be excluded, but the mechanism described here might play a role in the increases in subchondral bone volume in osteoarthritis and the gradual bone loss with age in all people.

Discussion

Bone tissue would be an ideal construction material: it contains collagen fibers for a high tensile strength and mineral crystals for a high compression stiffness. It is a living tissue: cells in the bone tissue adapt the bone architecture to external forces. High loading induces extra bone formation, disuse induces resorption of superfluous bone tissue. Moreover, small cracks in the tissue are repaired by the bone remodeling process.

However, this bone remodeling process also has disadvantages. With aging, bone architecture changes: bone mass decreases, the cortex becomes more porous, trabeculae become thinner and some trabeculae are lost. These changes are side effects of the bone remodeling process, but it is not exactly known how this process causes these changes in architecture. Several hypotheses exist: microdamage, stresses, strains and fluid flow are assumed to play a role [78, 20, 98, 86]. These factors are related to each other: for example, a change in tissue properties results in changes in the strains in the trabeculae. Bone remodeling changes the architecture and tissue properties and thereby the stresses, strains and fluid flows: the signals that probably regulate bone remodeling.

Bone remodeling could be distributed randomly throughout the bone tissue, it could be targeted to damage repair or it could be regulated by stresses or strains according to the mechanostat theory. These possibilities do not exclude each other; in vivo bone remodeling is probably a combination of these three types of bone remodeling.

In literature, it is under debate whether remodeling is targeted to microdamage or not. It is possible that bone remodeling is targeted to microdamage repair, but damage could also be repaired just because most bone tissue is replaced by random remodeling. Several authors have tried to estimate the contribution of damage-targeted remodeling to the total bone turnover. The estimated values vary widely: from histology in dog radii, it was estimated that 30% of the bone remodeling sites is targeted to microdamage [20]. Others used a mathematical model of cortical remodeling, in which they showed that it is possible that all remodeling in cortical bone is targeted to microdamage [98]. In cancellous bone, no estimates of targeted and non-targeted remodeling exist. However, because of the high turnover rate of cancellous bone, it is likely that the rate of cancellous bone turnover is higher than needed for damage repair [131].

According to the mechanostat theory, bone cells can detect the local stress or strain in the bone tissue and adapt the architecture according to this information. This theory can explain the change in cancellous architecture with age: the architecture becomes more aligned to the main load bearing direction, because more tissue is lost from transversal than from aligned trabeculae, in which stresses and strains are higher.

We asked ourselves whether mechanical feedback is needed for the changes in architecture with age in cancellous bone. In order to investigate this we simulated the whole remodeling cycle in cancellous bone in a computer simulation model

(chapter 2). We found changes in cancellous architecture similar to changes found in vivo, even though the bone remodeling sites were distributed randomly over the cancellous architecture in our model. From these simulations we conclude that mechanical feedback is not a prerequisite for the changes in cancellous bone with aging.

During growth, mechanical feedback might be more important. However, the architecture of cancellous bone is anisotropic the moment it is formed in the growth plate, the cancellous architecture is aligned to the main load bearing direction from the first start [162]. Therefore, mechanical feedback in bone remodeling is not needed to align the architecture to external loads.

However, we do not imply that bone remodeling is not affected by mechanical loading at all. The balance between bone resorption and formation depends on the external loads applied to the skeleton. It is known that during bed rest and space travel bone is lost and strenuous exercise, like e.g. weightlifting increases bone mass [74, 7, 92]. At trabecular level, stress or strain might also play a role. It is possible that resorption stops because of the large local increases in strain caused by resorption cavities (chapter 3). These same strain peaks might play a role in the coupling between resorption and formation [137, 156, 172].

Architectures similar to cancellous bone can be created from artificial meshes in computer models in which mechanical feedback is incorporated [78, 110]. In these models, adaptation of cancellous architectures to changes in external loads was also simulated. From these simulation models it was concluded that modeling of cancellous bone architecture according to mechanical feedback is a feasible concept. During e.g. fracture healing or when external loads change, this mechanical feedback probably plays a role. In an adult skeleton, where the architecture is adapted to more or less constant external loads this adaptive capacity is probably not used: random remodeling in our simulation resulted in changes in cancellous bone similar to in vivo changes.

It is possible to include mechanical feedback in our simulation model. This is not a matter of simply implementing the 'mechanical feedback rule' in the computer model, because the exact effect of mechanical loading on osteoclasts and osteoblasts activity is not known. However, the bone remodeling simulation could be used to verify hypotheses about the relation between local stress and strain and osteoclast and osteoblast activity. This might be useful to investigate effects of unloading and reloading of cancellous bone. Detailed models of bone remodeling, which include bone resorption and formation and mechanical feedback, might play a role in preclinical testing of e.g. anti-resorptive treatments in the future.

To investigate the three dimensional (3D) distribution of remodeling sites in cancellous bone, we built a setup to reconstruct the cancellous bone architecture including the locations of recent bone apposition (chapter 5). This computer controlled setup consisted of a sledge microtome, a fluorescence microscope and a

digital camera. The 3D architecture including the labels could be reconstructed from a stack of images. The cancellous architecture and the distribution of remodeling sites can not be investigated simultaneously with other techniques that are currently used in bone research. In studies that use fluorochrome labels, the locations of bone remodeling are known, but not the 3D architecture. Using micro-CT scans, the 3D architecture can be studied, but not the locations of the bone remodeling sites. In the future, it will probably be possible to study the effects of bone remodeling with in vivo CT-scanners, but only in small animals like mice and rats. Using our setup, the architecture and the labels can be studied in three dimensions in biopsies from larger species as well.

From the first 3D sectioning data from our setup we tend to conclude that bone remodeling is not completely random. In the investigated specimens, we found that the percentage of labeled surface was up to 20% higher on transversal trabeculae than on aligned trabeculae in specimens with a high bone volume fraction. From finite element simulations that simulate in vivo loading of cancellous bone we know that the strain in transversal trabeculae is lower than in aligned trabeculae (chapter 3), especially when the volume fraction is high. This indicates that bone remodeling is indeed affected by stresses or strains in the tissue. When the volume fraction is high, transversal trabeculae can be resorbed without largely decreasing the stiffness and strength of the cancellous architecture.

These 3D models of bone and fluorochrome labels open possibilities for further research. For instance, by combining finite element modeling with these models it can be investigated whether a relation between local stresses and strains in the bone tissue and bone remodeling exists. Another possibility is to investigate the effects of anti-resorptive treatment on bone remodeling. It is known that this treatment reduces the size and number of resorption cavities, but it is not known whether this treatment also affects the distribution of bone remodeling sites in the cancellous architecture. Furthermore, by using fluorochrome labels in different colors, the path of bone multicellular units over the trabecular surface could be followed.

In literature, it has been hypothesized that bone quality decreases with age because of degradation of the cells [91]. Although it is likely that bone cells in young and old people behave differently, this is not the only change in bone with increasing age. The bone tissue itself also changes, the average mineral content and tissue stiffness increase as people get older [139, 33, 17]. In chapter 7 we hypothesized that smaller tissue deformations, resulting from higher tissue mineralization and stiffness play a role in the bone loss with age. Using finite element models of bone, we showed that this is a feasible concept. Although bone loss with age is probably a result of multiple factors, the increase in tissue stiffness can partly explain the cancellous bone loss and the increase in anisotropy with age (chapter 7).

Finite element modeling was introduced some years ago to calculate the stiffness of cancellous bone specimens [176, 75]. Since then, this technique has been frequently used for this purpose. In the finite element models, it is generally assumed that the bone tissue is homogeneous, isotropic and linearly elastic. The tissue stiffness calculated this way is the 'effective tissue modulus': the modulus of the bone tissue including variations in tissue properties, cells and canaliculi. Because calculated stiffnesses correlated well with experimental test results, it has been concluded that more detailed incorporation of bone tissue properties is not necessary [82].

We thought that the non uniform material properties of trabecular tissue, especially the difference in mineralization and stiffness between the surface layer and the tissue in the middle of trabeculae, might have an effect on the global stiffness of cancellous bone. Therefore we investigated the effects of this non uniform mineral distribution in trabeculae on the global stiffness of cancellous bone (chapter 6). Bone tissue in the middle of thick trabeculae is not reached by resorption cavities and becomes older and more highly mineralized [10]. We found that the non uniform mineral distribution resulted in an up to 20% higher apparent stiffness than a uniform distribution (chapter 6). Therefore, the non uniform mineral distribution seems to be advantageous: the global stiffness is high because of the highly mineralized cores of the trabeculae, while the more elastic surface layer prevents complete fracture of trabeculae. This is in agreement with studies that showed damage in trabeculae: the microcracks were found in the highly mineralized core of the trabeculae [57, 105].

From the results of this study, we could explain a discrepancy between the bone tissue stiffness determined using finite element methods and using nanoindentation. The last method resulted in high values for the tissue stiffness [73, 142, 151, 167, 187]. Nano-indentation experiments are usually performed in in the middle of trabeculae, to avoid effects of the embedding resin. This implies that the nano indentations are made in the highly mineralized tissue, which has a high stiffness. When the tissue modulus is determined from finite element calculations assuming homogeneous tissue, the stiffness of the interstitial bone can be underestimated by up to a factor of 2 (chapter 6).

This shows, that it is worth while to make more detailed models, especially when improvements in CT-scanners and for example the use of monochromatic X-ray sources enables the construction of models with detailed density information.

In clinical trials of osteoporosis treatment, reductions in fracture risk were larger than expected from the small increases in bone mineral density [32]. Several anti-resorptive agents showed similar results: apparently, small increases in bone mineral density are sufficient to achieve large reductions in fracture risk [181]. In order to find an explanation for this, we simulated menopause and anti-resorptive treatment in cancellous bone (chapter 4). We found that small increases in re-

sorption depth resulted in rather large increases in strain below resorption cavities (chapter 3). The gain in stiffness resulting from simulated anti-resorptive treatment was larger in transversal directions than in the main load bearing direction (chapter 4). Taken together, the results from our simulations explain how the small increases in bone mineral density can result in large reductions in fracture risk. The bone stiffness in transversal directions is especially important in e.g. falls, when bones might fracture. The reduction in size and number of resorption cavities has rather small effects on the total bone mass, but the concomitant reduction in the number and intensity of the strain peaks will largely increase the strength and stiffness of the cancellous bone.

Obviously, good simulation results can not be obtained without input from the biological system. Most remodeling parameters have been determined from bone histology, but some parameters, like remodeling space and formation deficit can not be measured directly. These parameters are therefore estimated from other, measurable, parameters [54, 126]. On the one hand, this is a limitation of these computer simulations, the values of important parameters are not exactly known. On the other hand, this is exactly the power of these models: the estimated values can be included in the model and comparison of simulation results with clinical data shows whether the estimated values result in realistic output.

In this thesis, it was shown that the initiation of remodeling sites in age related remodeling is probably not regulated by mechanical feedback. Simulated random remodeling resulted in changes in architecture similar to changes seen in vivo, the existing anisotropy of the cancellous architecture increased 'automatically'. In the adult skeleton, the cancellous architecture is adapted to the external loads, which are more or less constant. Therefore, mechanical regulation of initiation of bone remodeling sites is not needed.

However, stress peaks below resorption cavities could play a role in coupling of resorption and formation and mechanical loading probably affects the bone balance; bone mass decreases with age, as activity and the loading of the skeleton decrease. We showed that this effect could be enhanced by an increase in mineral content and stiffness of bone tissue with age.

The results from the simulation studies described in this thesis give more insight in the interactions between remodeling, architecture and tissue properties. It must be kept in mind, that confirmation of a hypothesis in a simulation model does not exclude other possibilities. However, combination of this kind of models with 3D investigation of bone remodeling in labeled specimens and data from in vivo scanners will certainly result in a better understanding of bone remodeling.

Summary

The skeleton protects vulnerable organs like the heart and lungs, it provides lever arms for the muscles and it serves as a reservoir of minerals. The bone tissue is continuously renewed by the bone remodeling process, where bone tissue is resorbed by osteoclasts and replaced with new tissue by osteoblasts. This process enables the skeleton to adapt its architecture to changes in external loads, it plays a role in calcium homeostasis and it repairs microdamage.

This essential bone remodeling process also has disadvantages. After peak bone mass has been reached at the age of 25-30 years, bone mass decreases slowly because osteoblasts make slightly less tissue than osteoclasts resorb. This results in thinning of cortices and thinning and loss of trabeculae. This bone loss leads to an even larger loss of strength and stiffness and an increase in fracture risk.

It is not known how the bone remodeling process is regulated, but several hypotheses exist. Bone remodeling could be initiated randomly throughout the bones, it could be regulated by mechanical loading, by fluid flow or by damage in the tissue. In this thesis, interactions between bone remodeling, tissue properties and cancellous bone architecture were investigated. We used computer simulations, finite element calculations and in vivo labelled bone specimens. The most important changes in the skeleton during aging and osteoporosis take place in cancellous bone. Therefore, we focussed on bone remodeling in cancellous bone.

We developed a computer model to gain more insight in the effects of bone remodeling on the cancellous architecture (chapter 2). This model simulates the whole remodeling cycle in cancellous bone. Although this is not the first computer model of bone remodeling, it is the first model that uses three dimensional models of human cancellous bone and bone remodeling parameters known from histology. Like all models, our model is a simplification of reality (see section 2.5), but it mimics bone remodeling in cancellous bone closer than previously described models.

The random remodeling in our simulation model resulted in bone loss and increases in anisotropy of the cancellous bone, similar to changes seen in cancellous bone in vivo [107, 43]. This shows that the existing anisotropy in cancellous bone that is adapted to external loads will 'automatically' increase, even if the bone remodeling sites are distributed randomly over the trabecular surface. According to this simulation model, mechanical feedback is not a prerequisite for the increase in anisotropy seen with aging.

In a second study (chapter 3) the mechanical consequences of bone loss and bone remodeling were studied. We used finite element models to investigate the distribution of external loads over the trabeculae. The effects of resorption cavities and bone loss were investigated and the load distribution in the vicinity of resorption cavities was studied in detail. We found high peak stresses at the bottom of resorption cavities, which were higher in aligned than in transversal trabeculae[†].

[†]In this thesis, aligned trabeculae is used for trabeculae oriented in the main load bearing direction, transversal trabeculae are oriented in the plane perpendicular to the main load bearing direction.

We concluded that the high stress below resorption cavities could play a role in the coupling of bone resorption and formation. Stress peaks could induce bone formation by osteoblasts and they might prevent breaching of trabeculae by osteoclasts. Osteoblast activity could also be affected by the local stress in the resorption cavity. This might enhance the increase in anisotropy that was shown to result from random remodeling in the previous chapter.

In clinical trials of osteoporosis treatment, reductions in fracture risk were larger than expected from the small increases in bone mineral density [32]. In order to investigate how these small changes in bone mass can result in large decreases in fracture risk we simulated resorption cavities and anti-resorptive treatment in cancellous bone (chapter 3 and 4). We found that resorption cavities introduced large peak stresses, especially in aligned trabeculae (chapter 3). Furthermore, the gain in stiffness resulting from anti-resorptive treatment was larger in transversal directions than in the main load bearing direction (chapter 4). Taken together, these results explain how the small increases in bone mineral density can result in large reductions in fracture risk. The reduction in size and number of resorption cavities has rather small effects on the total bone mass, but the concomitant reduction in the number and intensity of the strain peaks will largely increase the strength and stiffness of the cancellous bone.

In order to investigate whether bone remodeling is initiated randomly throughout the architecture or not, the 3D distribution of bone remodeling sites in the architecture is needed. This 3D distribution can not be obtained using techniques currently used in bone research, like micro-CT scans and bone histology. Therefore, we built a setup to reconstruct the three dimensional cancellous architecture including the distribution of locations of recent bone apposition, as described in chapter 5. This setup consisted of a heavy duty sledge microtome, a fluorescence microscope and a digital camera. Locations of bone apposition were labelled in vivo using fluorochrome labels. The specimens were embedded in black epoxy, and serially sectioned in the setup. After each slice, an image of the new top surface of the epoxy block with the specimen was made. These images were combined into a three dimensional reconstruction of the cancellous bone, including the locations of the labels incorporated in the bone tissue.

Using this setup, we made three dimensional reconstructions of four labeled dog vertebral bone specimens (chapter 5). In these specimens, we found a higher percentage of labeled surface on transversal than on aligned trabeculae in specimens with a high bone volume. Finite element simulations of loading of cancellous bone have shown that the strain in transversal trabeculae is lower than in aligned trabeculae (chapter 3). This indicates that bone remodeling is indeed affected by stresses or strains in the tissue. When the volume fraction is high, transversal trabeculae can be resorbed without largely decreasing the stiffness and strength of the cancellous architecture.

Bone remodeling does not only change the cancellous architecture, it also af-

fects the tissue properties. Most bone tissue is replaced frequently, but some tissue can escape from remodeling and become older and highly mineralized. For example, the bone tissue in the middle of thick trabeculae is not reached by resorption cavities [10]. This affects the mechanical properties, because the stiffness of bone tissue increases as the mineral content increases [35]. In chapter 6 we investigated whether the non uniform mineral distribution in trabeculae is beneficial for its mechanical properties. In this study, the same amount of mineral was distributed in different ways over the trabeculae in finite element models. In the first model, the mineral distribution was uniform. In the second model, the surface layer of the trabeculae had a low mineral content, while the mineral content in the middle of the trabeculae was higher. This mimicked the in vivo mineral distribution. In the third model, the surface layer was highly mineralized, while the middle of the trabeculae had a lower mineral content. The stiffness of the bone elements was calculated from their mineral content, using a linear or an exponential model. The non-uniform distribution found in vivo resulted in a higher apparent stiffness than a uniform distribution. We concluded that the nonuniform mineral distribution that results from the bone remodeling process is advantageous. The highly mineralized middle of the trabeculae provides a high stiffness, while the surface layer, which has a lower mineral content and better crack stopping mechanisms, prevents complete fracture of trabeculae.

In literature, it has been hypothesized that the bone loss with age is a result of degradation of the cells [91]. Although it is likely that bone cells in young and old people behave differently, this is not the only change in bone with increasing age. As people get older, the average mineral content of their bone tissue increases [139, 33, 17]. Highly mineralized tissue has a high stiffness, which results in small deformations of the tissue under loading. In chapter 7 we hypothesized that a decrease in tissue deformations, resulting from higher tissue mineralization and stiffness play a role in the bone loss with age.

We tested this by simulated adaptation of a cancellous bone architecture to external loads in a finite element simulation (chapter 7). In the computer model, the tissue stiffness was varied to simulate changes in the mineral content of the bone tissue. We found that an increase in tissue stiffness resulted in bone loss and an increase in anisotropy. This is in agreement with changes in cancellous bone architecture with aging [43, 107]. A decrease in tissue stiffness resulted in large increases in bone mass and an almost constant global stiffness of the cancellous bone, despite the decrease in tissue stiffness. This high bone volume as a result of low tissue stiffness is in agreement with experimental findings in e.g. early osteoarthritis and rickets [36, 159]. Although bone loss with age is probably a result of multiple factors, the increase in tissue stiffness can partly explain the cancellous bone loss and the increase in anisotropy with age.

Samenvatting

Het skelet beschermt kwetsbare organen zoals het hart en de longen, het dient als hefboom voor de spieren en het fungeert als mineraal reservoir. Het botweefsel wordt constant vernieuwd door het botremodelleringsproces. Tijdens dit proces wordt botweefsel geresorbeerd door osteoclasten en wordt nieuw weefsel gemaakt door osteoblasten. Door dit proces kan de architectuur van het skelet worden aangepast aan veranderingen in de externe belasting, schade worden gerepareerd en de hoeveelheid calcium in het lichaam worden gereguleerd.

Dit proces heeft echter ook nadelen. Nadat de maximale botmassa is bereikt op de leeftijd van 25-30 jaar neemt de botmassa langzaam af, doordat osteoclasten net iets meer botmassa resorberen dan osteoblasten maken. Hierdoor worden de cortices dunner en gaan trabekels verloren. Dit botverlies leidt tot een afname van de sterkte en stijfheid van het skelet en een groter fractuurrisico.

Het is niet goed bekend hoe dit botremodelleringsproces wordt gereguleerd, maar er zijn wel een aantal hypothesen. Botremodellering zou random kunnen plaatsvinden, het zou geregeld kunnen worden door mechanische belasting, door vloeistofstroming of door schade in het botweefsel.

In dit proefschrift worden wisselwerkingen tussen botremodellering, weefseleigenschappen en de architectuur van trabeculair bot onderzocht. Hierbij zijn computer simulaties, eindige elementen modellen en in vivo gelabelde botpreparaten gebruikt. Omdat de belangrijkste veranderingen in het skelet met het ouder worden en bij osteoporose plaatsvinden in trabeculair bot, hebben we remodellering in trabeculair bot bestudeerd.

We ontwikkelden een computer model van botremodellering om meer inzicht te verwerven in de effecten van remodellering op de trabeculaire architectuur (hoofdstuk 2). In dit model wordt de hele remodelleringscyclus in trabeculair bot gesimuleerd. Hoewel dit niet het eerste model is dat botremodellering simuleert, is het wel het eerste model dat drie dimensionale modellen van menselijk trabeculair bot en remodelleringsparameters uit bothistologie gebruikt. Zoals alle modellen, is dit model een vereenvoudiging van de werkelijkheid (zie paragraaf 2.5), maar het benadert botremodellering in trabeculair bot dichter dan de eerder beschreven modellen.

De random remodellering in ons simulatiemodel resulteerde in botverlies en een toename in de anisotropie van het trabeculaire bot, zoals ook gebeurt in trabeculair bot in vivo [107, 43]. Hieruit blijkt dat de bestaande anisotropie van trabeculair bot automatisch toeneemt, zelfs bij random remodeling. Volgens dit simulatie model is mechanische terugkoppeling geen vereiste voor de veranderingen in architectuur met het ouder worden.

In de tweede studie (hoofdstuk 3) is de invloed van remodellering en botverlies op de mechanische eigenschappen van trabeculair bot onderzocht. Met eindige elementen modellen werd de verdeling van externe krachten over de trabeculaire architectuur berekend. Deze modellen werden gebruikt om resorptie lacunes en botverlies te simuleren en de spanningsverdeling rondom resorptie lacunes in de-

tail te bekijken. Resorptie lacunes veroorzaakten scherpe spanningspieken. Deze waren groter in trabekels in de richting van de grootste in vivo kracht dan in trabekels loodrecht hierop. Deze spanningspieken zouden een rol kunnen spelen in de koppeling tussen resorptie en formatie: ze zouden botaanmaak door osteoblasten kunnen stimuleren en kunnen voorkomen dat een resorptie lacune een trabekel doorsnijdt. De hoeveelheid bot die de osteoblasten maken zou ook kunnen afhangen van de spanning in de lacune. Dit zou de toename in anisotropie die gevonden werd in het vorige hoofdstuk kunnen versterken.

In klinische onderzoeken naar de behandeling van osteoporose waren de reducties in fractuur risico door kleine toenamen in botmassa groter dan verwacht werd [32]. Om dit te onderzoeken simuleerden we osteoporose en de behandeling daarvan in trabeculair bot (hoofdstuk 3 en 4). Resorptie lacunes veroorzaakten scherpe spanningspieken en de toename van de stijfheid van de trabeculaire architectuur was groter in de dwarsrichtingen dan in de hoofdrichting (hoofdstuk 4). Deze resultaten kunnen verklaren hoe de kleine toenamen in botmassa kunnen leiden tot een sterke reductie van het fractuurrisico. De afname in het aantal en de afmetingen van de resorptie lacunes heeft een tamelijk klein effect op de totale botmassa, maar de reductie in het aantal spanningspieken zal de trabeculaire structuur veel sterker maken.

Om te onderzoeken of botremodellering random plaatsvindt of gestuurd wordt door bijvoorbeeld mechanische belasting, is informatie over de drie dimensionale verdeling van remodeling nodig. Micro-CT scans en bot histologie, technieken die veel gebruikt worden in botonderzoek, geven hierover geen informatie. Daarom hebben we een opstelling gebouwd om de drie dimensionale botarchitectuur en de locaties waar recent nieuw bot werd aangemaakt te reconstrueren (hoofdstuk 5). Deze opstelling bestaat uit een slede microtoom voor harde weefsels, een fluorescentie microscoop en een digitale camera. Locaties waar bot werd aangemaakt werden in vivo gelabeld met fluorochrome labels, de preparaten werden ingebed in zwart epoxy. Van dit geheel werden coupes gesneden in de opstelling. Na iedere plak werd een opname gemaakt van de nieuwe bovenkant van het ingebedde preparaat, zodat uit al deze opnamen de drie dimensionale architectuur van het preparaat met de labels gereconstrueerd kon worden.

Met deze opstelling maakten we reconstructies van trabeculair bot uit 4 hondenwervels (hoofdstuk 5). In deze preparaten bevond zich meer label op de trabekels loodrecht op de richting van de grootste in vivo kracht dan op trabekels in de richting van deze kracht. Uit eindige elementen simulaties blijkt dat de vervorming van deze trabelekels loodrecht op de grootste in vivo kracht kleiner is dan in trabekels in de richting van deze kracht (hoofdstuk 3). Dit wijst erop dat remodellering beïnvloed wordt door mechanische belasting. In het bijzonder als de volume fractie hoog is, kan botweefsel van de trabekels loodrecht op de hoofdrichting geresorbeerd worden zonder dat de mechanische eigenschappen sterk achteruit gaan.

Botremodellering beïnvloedt niet alleen de trabeculaire architectuur, het heeft ook effect op de weefseleigenschappen. Het meeste botweefsel wordt regelmatig vervangen, maar er is ook botweefsel dat niet wordt vervangen, ouder wordt en daardoor steeds meer mineraal bevat. Zo wordt bijvoorbeeld het weefsel in het midden van dikke trabekels niet bereikt door resorptie lacunes [10]. Dit verandert de mechanische eigenschappen van het bot, omdat de stijfheid van het weefsel toeneemt wanneer de hoeveelheid mineraal in het weefsel toeneemt [35]. In hoofdstuk 6 onderzochten we of de niet uniforme mineraalverdeling in de trabekels gunstig is voor de mechanische eigenschappen van trabeculair bot.

In dit onderzoek werd een hoeveelheid mineraal op verschillende manieren over een computer model van trabeculair bot verdeeld. In het eerste model was de verdeling uniform. In het tweede bevatte de oppervlakte laag minder dan het midden van de trabekels, zoals in vivo ook het geval is. In het derde model bevatte de oppervlaktelaag meer mineraal dan het midden van de trabekels. De stijfheid van de elementen werd berekend uit de mineralisatie van de elementen, met behulp van een lineair of een exponentieel model. De niet uniforme verdeling die op de werkelijke in vivo verdeling leek resulteerde in een grotere stijfheid dan de uniforme verdeling. Deze verdeling lijkt dus gunstig te zijn. Het zwaar gemineraliseerde weefsel in het midden van de trabekels zorgt voor een grote stijfheid, terwijl de meer elastische oppervlaktelaag er voor zorgt dat de trabekels niet makkelijk breken.

In de literatuur is wel verondersteld dat het botverlies met de leeftijd het gevolg is van slecht functionerende botcellen in oudere mensen [91]. Hoewel dit een plausibele hypothese is, is dit niet het enige dat verandert in bot wanneer mensen ouder worden. De gemiddelde mineralisatie neemt ook toe, wat zorgt voor een grotere stijfheid van het weefsel [139, 33, 17]. Deze grotere stijfheid resulteert in kleinere vervormingen van het weefsel. In hoofdstuk 7 testten we de hypothese dat een afname in de vervorming van het botweefsel door een hogere mineralisatie en stijfheid van het botweefsel een rol speelt in het botverlies met het ouder worden.

Deze hypothese is getest door een trabeculaire structuur in een computer model aan te passen aan externe krachten (hoofdstuk 7). De weefselstijfheid werd gevarieerd om veranderingen in de mineraalinhoud van het weefsel te simuleren. Een hogere weefselstijfheid leidde tot botverlies en een toename in de anisotropie.

Deze resultaten zijn in overeenstemming met veranderingen in de trabeculaire botstructuur in vivo [43, 107]. Een verlaging van de weefselstijfheid resulteerde in een sterke toename van de botmassa en een daardoor bijna constante globale stijfheid van de architectuur. Deze hoge volumefractie is in overeenstemming met experimenteel gemeten waarden, bij bijvoorbeeld vroege artrose [36]. Het verlies van botmassa bij het ouder worden wordt waarschijnlijk door meerdere factoren veroorzaakt, maar de toename van de weefselstijfheid kan het botverlies en de veranderingen in architectuur gedeeltelijk verklaren.

References

[1] D. Agnusdei, R. Civitelli, and A. et al. Camporeale. Age-related decline of bone mass and intestinal calcium absorption in normal males. *Calcif Tissue Int*, 63(3):197–201, 1998.

[2] M.E. Arlot, E. Sornay-Rendu, and P. et al. Garnero. Apparent pre- and post-menopausal bone loss evaluated by dxa at different skeletal sites in women: The ofely cohort. *J Bone Miner Res*, 12(4):683–90, 1997.

[3] R.B. Ashman and J.Y. Rho. Elastic modulus of trabecular bone material. *J. Biomech.*, 21(3):177–81, 1988.

[4] B.K. Bay, T.S. Smith, D.P. Fyhrie, and M. Saad. Digital volume correlation: Three-dimensional strain mapping using x-ray tomography. *Experimental Mechanics*, 39(3):217–226, 1999.

[5] V. Bentolila, T.M. Boyce, and D.P. et al. Fyhrie. Intracortical remodeling in adult rat long bones after fatigue loading. *Bone*, 23(3):275–81, 1998.

[6] A.A. Biewener. Safety factors in bone strength. *Calcif Tissue Int*, 53(Suppl 1):S68–74, 1993.

[7] D.D. Bikle and B.P. Halloran. The response of bone to unloading. *J Bone Miner Metab*, 17(4):233–44, 1999.

[8] D.H. Birkenhaeger-Frenkel. A significant lack of collagen in osteoporotic bone. In C. Christiansen, J.S. Johansen, and B.J. Riis, editors, *International symposium on osteoporosis*, Osteoporosis, pages 443–445, Denmark, 1987. Norhaven A/S.

[9] D.H. Birkenhager-Frenkel, J.J. Groen, J.A. Bedier de prairie, and F.G.J. Offerijns. A simple physico-chemical method of assessment of osteoporosis. *Netherlands Journal of Nutrition*, 22(12):634–639, 1961.

[10] D.H. Birkenhager-Frenkel, A.L. Nigg, C.J. Hens, and J.C. Birkenhager. Changes of interstitial bone thickness with age in men and women. *Bone*, 14(3):211–6, 1993.

[11] D.M. Black, D.E. Thompson, and D.C. et al. Bauer. Fracture risk reduction with alendronate in women with osteoporosis: The fracture intervention trial. fit research group. *Journal of Clinical Endocrinology and Metabolism*, 85(11):4118–24, 2000.

[12] R.W. Blob and A.A. Biewener. In vivo locomotor strain in the hindlimb bones of alligator mississippiensis and iguana iguana: Implications for the evolution of limb bone safety factor and non-sprawling limb posture. *J Exp Biol*, 202(Pt 9):1023–46, 1999.

[13] G.Y. Boivin, P.M. Chavassieux, and A.C. et al. Santora. Alendronate increases bone strength by increasing the mean degree of mineralization of bone tissue in osteoporotic women. *Bone*, 27(5):687–94, 2000.

[14] A.L. Boskey. Mineralization, structure, and function of bone. In M.J. Seibel, S.P. Robins, and J.P. Bilezikian, editors, *Dynamics of bone and cartilage metabolism*, pages 153–164. Academic Press, San Diego, 1999.

[15] S.K. Boyd, R. Muller, and J.R. et al. Matyas. Early morphometric and anisotropic change in periarticular cancellous bone in a model of experimental knee osteoarthritis quantified using microcomputed tomography. *Clin Biomech (Bristol, Avon)*, 15(8):624–31, 2000.

[16] A. Boyde, J.C. Elliott, and S.J. Jones. Stereology and histogram analysis of backscattered electron images: Age changes in bone. *Bone*, 14(3):205–10, 1993.

[17] A. Boyde and S.J. Jones. Back-scattered electron imaging of skeletal tissues. *Metab Bone Dis Relat Res*, 5(3):145–50, 1983.

[18] A. Boyde, S.J. Jones, J. Aerssens, and J. Dequeker. Mineral density quantitation of the human cortical iliac crest by backscattered electron image analysis: Variations with age, sex, and degree of osteoarthritis. *Bone*, 16(6):619–27, 1995.

[19] D.B. Burr. Remodeling and the repair of fatigue damage. *Calcif Tissue Int*, 53(Suppl 1):S75–80; discussion S80–1, 1993.

[20] D.B. Burr. Targeted and nontargeted remodeling. *Bone*, 30(1):2–4, 2002.

[21] D.B. Burr, R.B. Martin, M.B. Schaffler, and E.L. Radin. Bone remodeling in response to in vivo fatigue microdamage. *J Biomech*, 18(3):189–200, 1985.

[22] D.B. Burr, C. Milgrom, and D. et al. Fyhrie. In vivo measurement of human tibial strains during vigorous activity. *Bone*, 18(5):405–10, 1996.

[23] W.E. Caler and D.R. Carter. Bone creep-fatigue damage accumulation. *J Biomech*, 22(6-7):625–35, 1989.

[24] N.P. Camacho, S. Rinnerthaler, and E.P. et al. Paschalis. Complementary information on bone ultrastructure from scanning small angle x-ray scattering and fourier-transform infrared microspectroscopy. *Bone*, 25(3):287–93, 1999.

[25] V. Carnevale, F. Dicembrino, and V. et al. Frusciante. Different patterns of global and regional skeletal uptake of 99mtc-methylene diphosphonate with age: Relevance to the pathogenesis of bone loss. *J Nucl Med*, 41(9):1478–83, 2000.

[26] D.R. Carter, T.E. Orr, and D.P. Fyhrie. Relationships between loading history and femoral cancellous bone architecture. *J Biomech*, 22(3):231–44, 1989.

[27] K. Choi, J.L. Kuhn, M.J. Ciarelli, and S.A. Goldstein. The elastic moduli of human subchondral, trabecular, and cortical bone tissue and the size-dependency of cortical bone modulus. *J. Biomech.*, 23(11):1103–13, 1990.

[28] J.W. Chow, A.J. Wilson, T.J. Chambers, and S.W. Fox. Mechanical loading stimulates bone formation by reactivation of bone lining cells in 13-week-old rats. *J Bone Miner Res*, 13(11):1760–7, 1998.

[29] T.E. Ciarelli, D.P. Fyhrie, M.B. Schaffler, and S.A. Goldstein. Variations in three-dimensional cancellous bone architecture of the proximal femur in female hip fractures and in controls. *J Bone Miner Res*, 15(1):32–40, 2000.

[30] J.E. Compston and P.I. Croucher. Histomorphometric assessment of trabecular bone remodelling in osteoporosis. *Bone Miner*, 14(2):91–102, 1991.

[31] F.P. Coxon, M.H. Helfrich, and R. et al. Van't Hof. Protein geranylgeranylation is required for osteoclast formation, function, and survival: Inhibition by bisphosphonates and ggti-298. *J Bone Miner Res*, 15(8):1467–76, 2000.

[32] S.R. Cummings, D.B. Karpf, and F. et al. Harris. Improvement in spine bone density and reduction in risk of vertebral fractures during treatment with antiresorptive drugs. *Am J Med*, 112(4):281–9, 2002.

[33] J.D. Currey. Changes in the impact energy absorption of bone with age. *J Biomech*, 12(6):459–69, 1979.

[34] J.D. Currey. Effects of differences in mineralization on the mechanical properties of bone. *Philos Trans R Soc Lond B Biol Sci*, 304(1121):509–18, 1984.

[35] J.D. Currey. The effect of porosity and mineral content on the young's modulus of elasticity of compact bone. *J. Biomech.*, 21(2):131–9, 1988.

[36] J.S. Day, M. Ding, and J.C. et al. van der Linden. A decreased subchondral trabecular bone tissue elastic modulus is associated with pre-arthritic cartilage damage. *J Orthop Res*, 19(5):914–8, 2001.

[37] C.E. De Laet, B.A. Van Hout, and H. et al. Burger. Hip fracture prediction in elderly men and women: Validation in the rotterdam study. *J Bone Miner Res*, 13(10):1587–93, 1998.

[38] D.W. Dempster. The contribution of trabecular architecture to cancellous bone quality [editorial]. *J Bone Miner Res*, 15(1):20–3, 2000.

[39] J. Dequeker. Assessment of quality of bone in osteoporosis–biomed i: Fundamental study of relevant bone. *Clin Rheumatol*, 13:S7–12, 1994.

[40] P. Derkx and D.H. Birkenhager-Frenkel. A thionin stain for visualizing bone cells, mineralizing fronts and cement lines in undecalcified bone sections. *Biotech Histochem*, 70(2):70–4, 1995.

[41] R.P. Dickenson, W.C. Hutton, and J.R. Stott. The mechanical properties of bone in osteoporosis. *J Bone Joint Surg Br*, 63-B(2):233–8, 1981.

[42] M. Ding and I. Hvid. Quantification of age-related changes in the structure model type and trabecular thickness of human tibial cancellous bone. *Bone*, 26(3):291–5, 2000.

[43] M. Ding, A. Odgaard, F. Linde, and I. Hvid. Age-related variations in the microstructure of human tibial cancellous bone. *J Orthop Res*, 20(3):615–21, 2002.

[44] P.R. Ebeling, L.M. Atley, and J.R. et al. Guthrie. Bone turnover markers and bone density across the menopausal transition. *J Clin Endocrinol Metab*, 81(9):3366–71, 1996.

[45] D.T. Edinger, K. Hayashi, and Y. et al. Hongyu. Histomorphometric analysis of the proximal portion of the femur in healthy dogs. *Am J Vet Res*, 61(3):268–74, 2000.

[46] R.G. Erben. Trabecular and endocortical bone surfaces in the rat: Modeling or remodeling? *Anat Rec*, 246(1):39–46, 1996.

[47] E.F. Eriksen. Normal and pathological remodeling of human trabecular bone: Three dimensional reconstruction of the remodeling sequence in normals and in metabolic bone disease. *Endocr Rev*, 7(4):379–408, 1986.

[48] E.F. Eriksen, F. Melsen, and L. Mosekilde. Reconstruction of the resorptive site in iliac trabecular bone: A kinetic model for bone resorption in 20 normal individuals. *Metab Bone Dis Relat Res*, 5(5):235–42, 1984.

[49] E.F. Eriksen, L. Mosekilde, and F. Melsen. Trabecular bone resorption depth decreases with age: Differences between normal males and females. *Bone*, 6(3):141–6, 1985.

[50] B. Ettinger, D.M. Black, and B.H. et al. Mitlak. Reduction of vertebral fracture risk in postmenopausal women with osteoporosis treated with raloxifene: Results from a 3-year randomized clinical trial. multiple outcomes of raloxifene evaluation (more) investigators [published erratum appears in jama 1999 dec 8;282(22):2124]. *Jama*, 282(7):637–45, 1999.

[51] D.R. Eyre. Biochemical basis of collagen metabolites as bone turnover markers. In J.P. Bilezikian, L.G. Raisz, and G.A. Rodan, editors, *Principles of bone biology*, pages 143–154. Academic Press, San Diego, 2001.

[52] I. Fogelman, C. Ribot, and R. et al. Smith. Risedronate reverses bone loss in postmenopausal women with low bone mass: Results from a multinational, double-blind, placebo-controlled trial. bmd-mn study group. *J Clin Endocrinol Metab*, 85(5):1895–900, 2000.

[53] H.M. Frost. Tetracycline-based histological analysis of bone remodeling. *Calcif Tissue Res*, 3(3):211–37, 1969.

[54] H.M. Frost. The pathomechanics of osteoporoses. *Clin Orthop*, 200:198–225, 1985.

[55] H.M. Frost. Bone "mass" and the "mechanostat": A proposal. *Anat Rec*, 219(1):1–9, 1987.

[56] H.M. Frost. Some effects of basic multicellular unit-based remodelling on photon absorptiometry of trabecular bone. *Bone Miner*, 7(1):47–65, 1989.

[57] D.P. Fyhrie and M.B. Schaffler. Failure mechanisms in human vertebral cancellous bone. *Bone*, 15(1):105–9, 1994.

[58] S.J. Gadeleta, A.L. Boskey, and E. et al. Paschalis. A physical, chemical, and mechanical study of lumbar vertebrae from normal, ovariectomized, and nandrolone decanoate-treated cynomolgus monkeys (macaca fascicularis). *Bone*, 27(4):541–50, 2000.

[59] P. Garnero, E. Sornay-Rendu, M.C. Chapuy, and P.D. Delmas. Increased bone turnover in late postmenopausal women is a major determinant of osteoporosis. *J Bone Miner Res*, 11(3):337–49, 1996.

[60] L.J. Gibson and M.F. Ashby. *Cellular solids. Structure and properties - second edition.* Cambridge solid state science series. Cambridge University Press, Cambridge, 1997.

[61] R.W. Goulet, S.A. Goldstein, and M.J. et al. Ciarelli. The relationship between the structural and orthogonal compressive properties of trabecular bone. *J Biomech*, 27(4):375–89, 1994.

[62] T.S. Gross, K.J. McLeod, and C.T. Rubin. Characterizing bone strain distributions in vivo using three triple rosette strain gages. *J Biomech*, 25(9):1081–7, 1992.

[63] H.J. Grote, M. Amling, and M. et al. Vogel. Intervertebral variation in trabecular microarchitecture throughout the normal spine in relation to age. *Bone*, 16(3):301–8, 1995.

[64] M. Grynpas. Age and disease-related changes in the mineral of bone. *Calcif Tiss Int*, 53(Suppl 1):S57–64, 1993.

[65] Z.H. Han, S. Palnitkar, and D.S. et al. Rao. Effects of ethnicity and age or menopause on the remodeling and turnover of iliac bone: Implications for mechanisms of bone loss. *J Bone Miner Res*, 12(4):498–508, 1997.

[66] R.P. Heaney, R.R. Recker, and P.D. Saville. Menopausal changes in bone remodeling. *J Lab Clin Med*, 92(6):964–70, 1978.

[67] R.P. Heaney, A.J. Yates, and 2nd Santora, A.C. Bisphosphonate effects and the bone remodeling transient. *J Bone Miner Res*, 12(8):1143–51, 1997.

[68] T. Hildebrand, A. Laib, and R. et al. Muller. Direct three-dimensional morphometric analysis of human cancellous bone: Microstructural data from spine, femur, iliac crest, and calcaneus. *J Bone Miner Res*, 14(7):1167–74, 1999.

[69] T. Hildebrand and P. Ruegsegger. A new method for the model-independent assessment of thickness in three-dimensional images. *Journal of microscopy*, 185(Pt1):67–75, 1997.

[70] T. Hildebrand and P. Ruegsegger. Quantification of bone microarchitecture with the structure model index. *CMBBE*, 1(1):15–23, 1997.

[71] S. Hizmetli, H. Elden, and E. et al. Kaptanoglu. The effect of different doses of calcitonin on bone mineral density and fracture risk in postmenopausal osteoporosis. *Int J Clin Pract*, 52(7):453–5, 1998.

[72] R. Hodgskinson, J.D. Currey, and G.P. Evans. Hardness, an indicator of the mechanical competence of cancellous bone. *J Orthop Res*, 7(5):754–8, 1989.

[73] C.E. Hoffler, K.E. Moore, and K. et al. Kozloff. Heterogeneity of bone lamellar-level elastic moduli. *Bone*, 26(6):603–9, 2000.

[74] M.F. Holick. Perspective on the impact of weightlessness on calcium and bone metabolism. *Bone*, 22(5 Suppl):105S–111S, 1998.

[75] S.J. Hollister, J.M. Brennan, and N. Kikuchi. A homogenization sampling procedure for calculating trabecular bone effective stiffness and tissue level stress. *Journal of Biomechanics*, 27(4):433–44, 1994.

[76] J. Homminga, B.R. McCreadie, and T.E. et al. Ciarelli. Cancellous bone mechanical properties from normals and patients with hip fractures differ on the structure level, not on the bone hard tissue level. *Bone*, 30(5):759–64, 2002.

[77] F.J. Hou, S.M. Lang, and S.J. et al. Hoshaw. Human vertebral body apparent and hard tissue stiffness. *J. Biomech.*, 31(11):1009–15, 1998.

[78] R. Huiskes, R. Ruimerman, G.H. van Lenthe, and J.D. Janssen. Effects of mechanical forces on maintenance and adaptation of form in trabecular bone. *Nature*, 405(6787):704–6, 2000.

[79] M. Inoue, H. Tanaka, and T. et al. Moriwake. Altered biochemical markers of bone turnover in humans during 120 days of bed rest. *Bone*, 26(3):281–6, 2000.

[80] H. Jinnai, H. Watashiba, and T. et al. Kajihara. Surface curvatures of trabecular bone microarchitecture. *Bone*, 30(1):191–4, 2002.

[81] J. Kabel, A. Odgaard, B. van Rietbergen, and R. Huiskes. Connectivity and the elastic properties of cancellous bone. *Bone*, 24(2):115–20, 1999.

[82] J. Kabel, B. van Rietbergen, and M. et al. Dalstra. The role of an effective isotropic tissue modulus in the elastic properties of cancellous bone. *J. Biomech.*, 32(7):673–80, 1999.

[83] T.M. Keaveny, X.E. Guo, and E.F. et al. Wachtel. Trabecular bone exhibits fully linear elastic behavior and yields at low strains. *Journal of biomechanics*, 27(9):1127–36, 1994.

[84] G. Khastgir, J. Studd, and N. et al. Holland. Anabolic effect of estrogen replacement on bone in postmenopausal women with osteoporosis: Histomorphometric evidence in a longitudinal study. *J Clin Endocrinol Metab*, 86(1):289–95, 2001.

[85] J.H. Kinney and A.J. Ladd. The relationship between three-dimensional connectivity and the elastic properties of trabecular bone. *J Bone Miner Res*, 13(5):839–45, 1998.

[86] J. Klein-Nulend, J.G. Sterck, and C.M. et al. Semeins. Donor age and mechanosensitivity of human bone cells. *Osteoporos Int*, 13(2):137–46, 2002.

[87] M. Kothari, T.M. Keaveny, and J.C. et al. Lin. Impact of spatial resolution on the prediction of trabecular architecture parameters. *Bone*, 22(5):437–43, 1998.

[88] J.L. Kuhn, S.A. Goldstein, and K. et al. Choi. Comparison of the trabecular and cortical tissue moduli from human iliac crests. *J Orthop Res*, 7(6):876–84, 1989.

[89] A.J. Ladd, J.H. Kinney, D.L. Haupt, and S.A. Goldstein. Finite-element modeling of trabecular bone: Comparison with mechanical testing and determination of tissue modulus. *J Orthop Res*, 16(5):622–8, 1998.

[90] C.M. Langton, T.J. Haire, and P.S. et al. Ganney. Dynamic stochastic simulation of cancellous bone resorption. *Bone*, 22(4):375–80, 1998.

[91] L. Lanyon and T. Skerry. Postmenopausal osteoporosis as a failure of bone's adaptation to functional loading: A hypothesis. *J Bone Miner Res*, 16(11):1937–47, 2001.

[92] J.E. Layne and M.E. Nelson. The effects of progressive resistance training on bone density: A review. *Med Sci Sports Exerc*, 31(1):25–30, 1999.

[93] T.C. Lee, T.L. Arthur, L.J. Gibson, and W.C. Hayes. Sequential labelling of microdamage in bone using chelating agents. *J Orthop Res*, 18(2):322–5, 2000.

[94] B. Li and R.M. Aspden. Composition and mechanical properties of cancellous bone from the femoral head of patients with osteoporosis or osteoarthritis. *J Bone Miner Res*, 12(4):641–51, 1997.

[95] U.A. Liberman, S.R. Weiss, and J. et al. Broll. Effect of oral alendronate on bone mineral density and the incidence of fractures in postmenopausal osteoporosis. *N Engl J Med*, 333(22):1437–43, 1995.

[96] S. Majumdar, H.K. Genant, and S. et al. Grampp. Correlation of trabecular bone structure with age, bone mineral density, and osteoporotic status: In vivo studies in the distal radius using high resolution magnetic resonance imaging. *J Bone Miner Res*, 12(1):111–8, 1997.

[97] R.B. Martin. On the significance of remodeling space and activation rate changes in bone remodeling. *Bone*, 12(6):391–400, 1991.

[98] R.B. Martin. Is all cortical bone remodeling initiated by microdamage? *Bone*, 30(1):8–13, 2002.

[99] T. Mashiba, T. Hirano, and C.H. et al. Turner. Suppressed bone turnover by bisphosphonates increases microdamage accumulation and reduces some biomechanical properties in dog rib [see comments]. *J Bone Miner Res*, 15(4):613–20, 2000.

[100] T. Mashiba, C.H. Turner, and T. et al. Hirano. Effects of suppressed bone turnover by bisphosphonates on microdamage accumulation and biomechanical properties in clinically relevant skeletal sites in beagles. *Bone*, 28(5):524–31, 2001.

[101] G. Mazzuoli, M. Acca, and D. et al. Pisani. Annual skeletal balance and metabolic bone marker changes in healthy early postmenopausal women: Results of a prospective study. *Bone*, 26(4):381–6, 2000.

[102] R.W. McCalden, J.A. McGeough, and C.M. Court-Brown. Age-related changes in the compressive strength of cancellous bone. the relative importance of changes in density and trabecular architecture. *J Bone Joint Surg Am*, 79(3):421–7, 1997.

[103] P.L. Mente and J.L. Lewis. Experimental method for the measurement of the elastic modulus of trabecular bone tissue. *J. Orthop. Res.*, 7(3):456–61, 1989.

[104] S. Mori and D.B. Burr. Increased intracortical remodeling following fatigue damage. *Bone*, 14(2):103–9, 1993.

[105] S. Mori, R. Harruff, W. Ambrosius, and D.B. Burr. Trabecular bone volume and microdamage accumulation in the femoral heads of women with and without femoral neck fractures. *Bone*, 21(6):521–6., 1997.

[106] L. Mosekilde. Age-related changes in vertebral trabecular bone architecture–assessed by a new method. *Bone*, 9(4):247–50, 1988.

[107] L. Mosekilde. Sex differences in age-related loss of vertebral trabecular bone mass and structure–biomechanical consequences. *Bone*, 10(6):425–32, 1989.

[108] L. Mosekilde. Consequences of the remodelling process for vertebral trabecular bone structure: A scanning electron microscopy study (uncoupling of unloaded structures). *Bone Miner*, 10(1):13–35, 1990.

[109] M. Mullender, B. van Rietbergen, P. Ruegsegger, and R. Huiskes. Effect of mechanical set point of bone cells on mechanical control of trabecular bone architecture. *Bone*, 22(2):125–31, 1998.

[110] M.G. Mullender and R. Huiskes. Proposal for the regulatory mechanism of wolff's law. *J Orthop Res*, 13(4):503–12, 1995.

[111] M.G. Mullender, R. Huiskes, and H. Weinans. A physiological approach to the simulation of bone remodeling as a self- organizational control process. *J Biomech*, 27(11):1389–94, 1994.

[112] R. Muller and P. Ruegsegger. Analysis of mechanical properties of cancellous bone under conditions of simulated bone atrophy. *J Biomech*, 29(8):1053–60, 1996.

[113] P.H. Nicholson, X.G. Cheng, and G. et al. Lowet. Structural and material mechanical properties of human vertebral cancellous bone. *Med Eng Phys*, 19(8):729–37, 1997.

[114] P.J. Nijweide, E.H. Burger, J. Klein Nulend, and A. van der Plas. The osteocyte. In J.P. Bilezikian, L.G. Raisz, and G.A. Rodan, editors, *Principles of bone biology*. Academic Press, San Diego, 2001.

[115] K.J. Obrant and R. Odselius. Electron microprobe analysis and histochemical examination of the calcium distribution in human bone trabeculae: A methodological study using biopsy specimens from post-traumatic osteopenia. *Ultrastruct Pathol*, 7(2-3):123–31, 1984.

[116] A. Odgaard. Three-dimensional methods for quantification of cancellous bone architecture. *Bone*, 20(4):315–28, 1997.

[117] A. Odgaard, K. Andersen, F. Melsen, and H.J. Gundersen. A direct method for fast three-dimensional serial reconstruction. *J Microsc*, 159(Pt 3):335–42, 1990.

[118] A. Odgaard, K. Andersen, and R. et al. Ullerup. Three-dimensional reconstruction of entire vertebral bodies. *Bone*, 15(3):335–42, 1994.

[119] A. Odgaard and H.J. Gundersen. Quantification of connectivity in cancellous bone, with special emphasis on 3-d reconstructions. *Bone*, 14(2):173–82, 1993.

[120] A. Odgaard, J. Kabel, and B. et al. van Rietbergen. Fabric and elastic principal directions of cancellous bone are closely related. *J. Biomech.*, 30(5):487–95, 1997.

[121] H. Okano, H. Mizunuma, and M. et al. Soda. The long-term effect of menopause on postmenopausal bone loss in japanese women: Results from a prospective study. *J Bone Miner Res*, 13(2):303–9, 1998.

[122] B. Orr-Walker, D.J. Wattie, M.C. Evans, and I.R. Reid. Effects of prolonged bisphosphonate therapy and its discontinuation on bone mineral density in post-menopausal osteoporosis. *Clin Endocrinol (Oxf)*, 46(1):87–92, 1997.

[123] S.M. Ott. When bone mass fails to predict bone failure. *Calcif Tissue Int*, 53(Suppl 1):S7–13, 1993.

[124] S.M. Ott. Theoretical and methodological approach. In J.P. Bilezikian, L.G. Raisz, and G.A. Rodan, editors, *Principles of bone biology*, pages 231–241. Academic Press, San Diego, 2001.

[125] A.M. Parfitt. Quantum concept of bone remodeling and turnover: Implications for the pathogenesis of osteoporosis. *Calcif Tissue Int*, 28(1):1–5, 1979.

[126] A.M. Parfitt. The psychiological and clinical significance of bone histomorphometric data. In *Bone histomorphometry: Techniques and interpretation*, pages 143–223. CRC Press, Boca Raton, FL, 1983.

[127] A.M. Parfitt. Age-related structural changes in trabecular and cortical bone: Cellular mechanisms and biomechanical consequences. *Calcif Tissue Int*, 36(Suppl 1):S123–8, 1984.

[128] A.M. Parfitt. The cellular basis of bone remodeling: The quantum concept reexamined in light of recent advances in the cell biology of bone. *Calcif Tissue Int*, 36(Suppl 1):S37–45, 1984.

[129] A.M. Parfitt. The composition, structure and remodeling of bone: A basis for the interpretation of bone mineral measurements. In J.Dequeker, editor, *Bone mineral measurement by photon absorptiometry*, pages 9–28. Leuven University Press, Leuven, 1988.

[130] A.M. Parfitt. Problems in the application of in vitro systems to the study of human bone remodeling. *Calcif Tissue Int*, 56(Suppl 1):S5–7, 1995.

[131] A.M. Parfitt. Targeted and nontargeted bone remodeling: Relationship to basic multicellular unit origination and progression. *Bone*, 30(1):5–7, 2002.

[132] J.B. Phelps, G.B. Hubbard, X. Wang, and C.M. Agrawal. Microstructural heterogeneity and the fracture toughness of bone. *J Biomed Mater Res*, 51(4):735–41, 2000.

[133] H.A. Pols, D. Felsenberg, and D.A. et al. Hanley. Multinational, placebo-controlled, randomized trial of the effects of alendronate on bone density and fracture risk in postmenopausal women with low bone mass: Results of the fosit study. foxamax international trial study group. *Osteoporos Int*, 9(5):461–8, 1999.

[134] J.M. Pouilles, F. Tremollieres, and C. Ribot. The effects of menopause on longitudinal bone loss from the spine. *Calcif Tissue Int*, 52(5):340–3, 1993.

[135] R. Recker, J. Lappe, K. Davies, and R. Heaney. Characterization of perimenopausal bone loss: A prospective study. *J Bone Miner Res*, 15(10):1965–73, 2000.

[136] J. Reeve. A stochastic analysis of iliac trabecular bone dynamics. *Clin Orthop*, 213:264–78, 1986.

[137] J. Reeve. A role for mechanical strain in the preservation of trabecular number (letter to editor). *JBMR*, 17(8):1555, 2002.

[138] J. Reginster, H.W. Minne, and O.H. et al. Sorensen. Randomized trial of the effects of risedronate on vertebral fractures in women with established postmenopausal osteoporosis. vertebral efficacy with risedronate therapy (vert) study group. *Osteoporos Int*, 11(1):83–91, 2000.

[139] S.A. Reid and A. Boyde. Changes in the mineral density distribution in human bone with age: Image analysis using backscattered electrons in the sem. *J Bone Miner Res*, 2(1):13–22, 1987.

[140] G.G. Reinholz, B. Getz, and L. et al. Pederson. Bisphosphonates directly regulate cell proliferation, differentiation, and gene expression in human osteoblasts. *Cancer Res*, 60(21):6001–7, 2000.

[141] J.Y. Rho, R.B. Ashman, and C.H. Turner. Young's modulus of trabecular and cortical bone material: Ultrasonic and microtensile measurements. *J. Biomech.*, 26(2):111–9, 1993.

[142] J.Y. Rho, T.Y. Tsui, and G.M. Pharr. Elastic properties of human cortical and trabecular lamellar bone measured by nanoindentation. *Biomaterials*, 18(20):1325–30, 1997.

[143] J.C. Rice, S.C. Cowin, and J.A. Bowman. On the dependence of the elasticity and strength of cancellous bone on apparent density. *J Biomech*, 21(2):155–68, 1988.

[144] B.L. Riggs and L.J. Melton. *Osteoporosis: Etiology, diagnosis, and treatment, 2nd ed.* Lippincott-Raven, Hagerstown, MD, USA, 2 edition, 1995.

[145] B.J. Riis, J. Ise, and T. et al. von Stein. Ibandronate: A comparison of oral daily dosing versus intermittent dosing in postmenopausal osteoporosis. *J Bone Miner Res*, 16(10):1871–8, 2001.

[146] G.A. Rodan. Bone mass homeostasis and bisphosphonate action. *Bone*, 20(1):1–4, 1997.

[147] E.J. Roldan and J.L. Ferretti. How do anti-osteoporotic agents prevent fractures? *Bone*, 26(4):393–6, 2000.

[148] P. Roschger, P. Fratzl, K. Klaushofer, and G. Rodan. Mineralization of cancellous bone after alendronate and sodium fluoride treatment: A quantitative backscattered electron imaging study on minipig ribs. *Bone*, 20(5):393–7, 1997.

[149] W. Roux. *Der kampf der theile im organismus.* Engelmann, Leipzig, 1881.

[150] D.J. Rowe, L.A. Etre, M.J. Lovdahl, and D.J. Pietrzyk. Relationship between bisphosphonate concentration and osteoclast activity and viability. *In Vitro Cell Dev Biol Anim*, 35(7):383–8, 1999.

[151] M. Roy, J.Y. Rho, T.Y. Tsui, and G.M. Pharr. Variation of young's modulus and hardness in human lumbar vertebrae measured by nanoindentation. *Advances in Bioengineering*, BED-33:385–386, 1996.

[152] C.T. Rubin and L.E. Lanyon. Dynamic strain similarity in vertebrates; an alternative to allometric limb bone scaling. *J Theor Biol*, 107(2):321–7, 1984.

[153] R.G. Russell, M.J. Rogers, and J.C. et al. Frith. The pharmacology of bisphosphonates and new insights into their mechanisms of action. *J Bone Miner Res*, 14 Suppl 2:53–65, 1999.

[154] M. Sato, W. Grasser, and N. et al. Endo. Bisphosphonate action. alendronate localization in rat bone and effects on osteoclast ultrastructure. *J Clin Invest*, 88(6):2095–105, 1991.

[155] M.J. Silva, T.M. Keaveny, and W.C. Hayes. Load sharing between the shell and centrum in the lumbar vertebral body. *Spine*, 22(2):140–50, 1997.

[156] T.H. Smit and E.H. Burger. Is bmu-coupling a strain-regulated phenomenon? a finite element analysis. *J Bone Miner Res*, 15(2):301–7, 2000.

[157] T.S. Smith, R.B. Martin, M. Hubbard, and B.K. Bay. Surface remodeling of trabecular bone using a tissue level model. *J Orthop Res*, 15(4):593–600, 1997.

[158] J.L. Stock, N.H. Bell, and 3rd et al. Chesnut, C.H. Increments in bone mineral density of the lumbar spine and hip and suppression of bone turnover are maintained after discontinuation of alendronate in postmenopausal women. *Am J Med*, 103(4):291–7, 1997.

[159] T. Sugiyama, T. Taguchi, and S. Kawai. Adaptation of bone to mechanical loads. *Lancet*, 359(9312):1160, 2002.

[160] T.C. Sun, S. Mori, and J. et al. Roper. Do different fluorochrome labels give equivalent histomorphometric information? *Bone*, 13(6):443–6, 1992.

[161] S.M. Swartz, J.E. Bertram, and A.A. Biewener. Telemetered in vivo strain analysis of locomotor mechanics of brachiating gibbons. *Nature*, 342(6247):270–2, 1989.

[162] E. Tanck, J. Homminga, G.H. van Lenthe, and R. Huiskes. Increase in bone volume fraction precedes architectural adaptation in growing bone. *Bone*, 28(6):650–4, 2001.

[163] S. Tayyar, P.S. Weinhold, and R.A. et al. Butler. Computer simulation of trabecular remodeling using a simplified structural model. *Bone*, 25(6):733–9, 1999.

[164] J.S. Thomsen, L. Mosekilde, R.W. Boyce, and E. Mosekilde. Stochastic simulation of vertebral trabecular bone remodeling. *Bone*, 15(6):655–66, 1994.

[165] J.S. Thomsen, L. Mosekilde, and E. Mosekilde. Quantification of remodeling parameter sensitivity–assessed by a computer simulation model. *Bone*, 19(5):505–11, 1996.

[166] R.P. Tonino, P.J. Meunier, and R. et al. Emkey. Skeletal benefits of alendronate: 7-year treatment of postmenopausal osteoporotic women. phase iii osteoporosis treatment study group. *J Clin Endocrinol Metab*, 85(9):3109–15, 2000.

[167] C.H. Turner, J. Rho, and Y. et al. Takano. The elastic properties of trabecular and cortical bone tissues are similar: Results from two microscopic measurement techniques. *J. Biomech.*, 32(4):437–41, 1999.

[168] D. Ulrich, B. van Rietbergen, A. Laib, and P. Ruegsegger. The ability of three-dimensional structural indices to reflect mechanical aspects of trabecular bone. *Bone*, 25(1):55–60, 1999.

[169] D. Ulrich, B. van Rietbergen, H. Weinans, and P. Ruegsegger. Finite element analysis of trabecular bone structure: A comparison of image-based meshing techniques. *J Biomech*, 31(12):1187–92, 1998.

[170] J.C. van der Linden, J. Homminga, J.A.N. Verhaar, and H. Weinans. Mechanical consequences of bone loss in cancellous bone. *J Bone Miner Res*, 16(3):457–65, 2001.

[171] J.C. van der Linden, J.A. Verhaar, and H. Weinans. A three-dimensional simulation of age-related remodeling in trabecular bone. *J Bone Miner Res*, 16(4):688–96, 2001.

[172] J.C. van der Linden, J.A.N. Verhaar, and H. Weinans. A model of skeletal remodeling should (but does not currently) include mechanical feedback (answer to letter to editor). *JBMR*, 17(8):1556, 2002.

[173] B. Van Rietbergen, S. Majumdar, and W. et al. Pistoia. Assessment of cancellous bone mechanical properties from micro-fe models based on micro-ct, pqct and mr images. *Technol Health Care*, 6(5-6):413–20, 1998.

[174] B. Van Rietbergen, R. Muller, and D. et al. Ulrich. Tissue stresses and strain in trabeculae of a canine proximal femur can be quantified from computer reconstructions. *J Biomech*, 32(4):443–51, 1999.

[175] B. Van Rietbergen, A. Odgaard, J. Kabel, and R. Huiskes. Direct mechanics assessment of elastic symmetries and properties of trabecular bone architecture. *J. Biomech.*, 29(12):1653–7, 1996.

[176] B. Van Rietbergen, H. Weinans, R. Huiskes, and A. Odgaard. A new method to determine trabecular bone elastic properties and loading using micromechanical finite-element models. *J. Biomech.*, 28(1):69–81, 1995.

[177] S. Vedi and J.E. Compston. The effects of long-term hormone replacement therapy on bone remodeling in postmenopausal women. *Bone*, 19(5):535–9, 1996.

[178] A. Vesterby, H.J. Gundersen, F. Melsen, and L. Mosekilde. Normal postmenopausal women show iliac crest trabecular thickening on vertical sections. *Bone*, 10(5):333–9, 1989.

[179] L. Vico, P. Collet, and A. et al. Guignandon. Effects of long-term microgravity exposure on cancellous and cortical weight-bearing bones of cosmonauts. *Lancet*, 355(9215):1607–11, 2000.

[180] E. Vignot and P.J. Meunier. Effects of raloxifene on bone loss and fracture risk in the menopausal woman. *Contracept Fertil Sex*, 27(12):858–60, 1999.

[181] R.D. Wasnich and P.D. Miller. Antifracture efficacy of antiresorptive agents are related to changes in bone density. *J Clin Endocrinol Metab*, 85(1):231–6, 2000.

[182] H. Weinans and P.J. Prendergast. Tissue adaptation as a dynamical process far from equilibrium. *Bone*, 19(2):143–9, 1996.

[183] J. Wolff. Das gesetz der transformation der knochen (translated as 'the law of bone remodeling' by p.maquet and r.furlong, 1986, springer-verlag, berlin. *Hirchwild*, 1892.

[184] H. Yasuda, N. Shima, and N. et al. Nakagawa. A novel molecular mechanism modulating osteoclast differentiation and function. *Bone*, 25(1):109–13, 1999.

[185] P. Zioupos and J.D. Currey. The extent of microcracking and the morphology of microcracks in damaged bone. *Journal of Materials Science*, 29:978–986, 1994.

[186] P. Zioupos and J.D. Currey. Changes in the stiffness, strength, and toughness of human cortical bone with age. *Bone*, 22(1):57–66, 1998.

[187] P.K. Zysset, X.E. Guo, and C.E. et al. Hoffler. Elastic modulus and hardness of cortical and trabecular bone lamellae measured by nanoindentation in the human femur. *J. Biomech.*, 32(10):1005–12, 1999.

Dankwoord

De kaft zit erom, 't is klaar. Dit boekje zou er niet geweest zijn zonder een aantal mensen in de vakgroep en daarbuiten. Bovendien geeft zo'n boekje meteen de kans om deze mensen zwart op wit te bedanken, dus bij deze:

Harrie Weinans en Jan Verhaar wil ik bedanken omdat ze mij 4 jaar geleden hebben aangenomen, hoewel ik toen nog nauwelijks wist wat een osteoclast was, laat staan dat die met een osteoblast samenwerkt in een proces dat remodelering heet. Intussen heb ik over die botbiologie een hoop bijgeleerd, ik hoop dat we met de combinatie van biologie en techniek nog veel leuke en interessante ontdekkingen zullen doen.

Bij het leren begrijpen van de biologische processen heb ik veel gehad aan de uitleg van de 'biologen' in de groep: Franci, Holger, Gerjo en Irene, bedankt voor al jullie uitleg van biologie voor techneuten. Verder wil ik Judd en Erwin bedanken voor de leuke discussies, jullie kritische commentaar, slimme ideeën en lekker eten. En natuurlijk Justus, Jarno, Michiel, Nicole, Olivier, Pieter, Erik, Teun, Nienke, Inesz, Fabienne, Wendy, Petra, Koen en Barbara voor de goede sfeer, van hard werken via tafeltennis op de gang tot keek van de week.

Huib Pols wil ik bedanken voor zijn belangstelling voor en enthousiasme over de 'computational biology', en voor zijn kritische, maar altijd opbouwende commentaar op mijn werk. Dorie Birkenhäger, dankjewel voor het delen van je grote kennis over bot en de afwijkingen die daarin voorkomen. Cor, bedankt voor het altijd heel snel maken van al die kleine onderdeeltjes voor mijn opstelling, Joop, bedankt voor het uitlenen van soldeerbouten, voltmeters etc., toen de orthopedie die nog niet had.

Hiernaast wil ik een aantal mensen buiten het lab bedanken: natuurlijk mijn vader en moeder, die ervoor gezorgd hebben dat ik kon gaan studeren, en die het in tegenstelling tot een hoop andere mensen volkomen logisch vonden dat dat aan een technische universiteit was. Karin en Sabine, leuk dat jullie mijn Paranimfen zijn! Michiel, dankjewel voor alles en de rest. Mirjam, Erik, Olav, Marco, Remco en alle anderen die dit begrijpen: ik hoop nog vaak uien en wontons met jullie te eten en samen te vieren dat de zomertijd weer wintertijd wordt.

List of Publications

- J van der Kuur, B Korevaar, M Pols, JC van der Linden, BJ Thijsse, 1997 Argon-Surface Interactions in IBAD-Deposited Molybdenum Films. In: Barber JC et al. (ed.) Materials Research Society Proceedings, vol. 504, 1999, Boston, pp 57-62.
- JC van der Linden, LJ Seijbel, BJ Thijsse 1999 Early stages of IBAD-film growth: Differences between (100) and polycrystalline Mo substrates. Nucl. Instr. and Meth. in Phys. Res. B 148:98-103
- JC van der Linden, J Homminga, JAN Verhaar, H Weinans, 2001 Mechanical consequences of bone loss in cancellous bone. J Bone Miner Res 16(3):457-65.
- JC van der Linden, JAN Verhaar, H Weinans, 2001 A three-dimensional simulation of age-related remodeling in trabecular bone. J Bone Miner Res 16(4):688-96.
- JC van der Linden, JAN Verhaar, H Weinans, 2001 Trabecular bone's mechanical properties are affected by its non-uniform mineral distribution. Journal of Biomechanics 34(12):1573-1580
- JS Day, M Ding, JC van der Linden, I Hvid, DR Sumner, H Weinans, 2001 A decreased subchondral trabecular bone tissue elastic modulus is associated with pre-arthritic cartilage damage. J Orthop Res 19(5):914-8
- JC van der Linden, JAN Verhaar, HAP Pols, H Weinans, A simulation model at trabecular level to predict effects of anti-resorptive treatment after menopause, submitted
- JS Day, M Ding, P Bednarz, JC van der Linden, T Mashiba, T Hirano, CC Johnston, DB Burr, I Hvid, DR Sumner, H Weinans, Does secondary mineralization affect the Young's Modulus of trabecular bone matrix after bisphosphonate treatment? A case for the negative, submitted.
- JC van der Linden, JAN Verhaar, H weinans, 3D reconstruction of bone apposition, to be submitted
- JC van der Linden, JS Day, JAN Verhaar, H Weinans, Bone loss with age could be a side-effect of the ongoing mineralization of bone tissue, submitted
- JC van der Linden, H. Weinans, Computer simulations of cancellous bone remodeling, In: The Skeleton - Biochemical, Genetic and Molecular Interactions in Development and Homeostasis, in press.

Curriculum vitae

4 oktober 1974	geboren in Vlaardingen
1986-1992	VWO, Chr.sg. Groen van Prinsterer te Vlaardingen
1992-1997	Studie Technische natuurkunde, Technische Universiteit Delft. Afstudeerwerk verricht bij de groep fysische kristallografie - vaste stoffysica bij Prof.dr.ir. F. Tuinstra en Dr.ir.P. Scholte: 'Initiële groei van germanium op silicium, onderzocht met scanning tunneling microscopie en lage energie electronen diffractie'
1997-1998	Onderzoek naar defecten in dunne opgedampte metaallagen, met THDS (thermal helium desorption spectrometry). Faculteit Materiaalkunde, TU-Delft.
1998-2002	Promotie onderzoek verricht aan de Erasmus Universiteit, afdeling orthopedie bij Dr.ir. H. Weinans en Prof.dr. J.A.N. Verhaar. Het resultaat hiervan is dit proefschrift: 'Interactions between remodeling, architecture and tissue properties in cancellous bone.'
heden	werkzaam als postdoc op het orthopedisch onderzoekslab van het Erasmus MC en de groep structural optimization and computational mechanics van de faculteit Ontwerp, Constructie en Productie van de TU-Delft.